Mechanism of Cytoskeleton Modification by Histone Methyltransferase SETD2

by

Sarah E. Kearns

A dissertation submitted in partial fulfillment
of the requirements for the degree of
Doctor of Philosophy
(Chemical Biology)
at the University of Michigan
2021

Doctoral Committee:

Professor Michael Cianfrocco, Co-Chair
Professor Kristen Verhey, Co-Chair
Professor Yali Du
Professor Ryoma Ohi
Professor Jayakrishnan Nandakumar

Sarah E. Kearns

skearns@umich.edu

ORCID iD: 0000-0001-5640-909X

Dedication

To all the lobsters: may your eleven protofilament microtubules be thoroughly considered.

To my family and friends: none of this would be possible without you.

Acknowledgements

All the work that follows would not be possible without all the hard work of the admin and staff: Anna Mapp, Bruce Palfey, Zhaohui Xu, Laura Howe, Traci Swan, Traci Carulli, AJ Dziak, Cathy Andrews, and the staff who keep our glassware, facilities, and work environments safe and clean. I also must thank my funding sources because they financially supported me and my project the past five years, and it's great that our country supports science and education: Graduate Assistance in Areas of National Need Fellowship (P200A150164) and Chemical Biology Interface Training Grant from the NIH (5T32GM008597-22).

Thank you to my Ph.D. advisors Mike Cianfrocco & Kristen Verhey for letting me join and work in their lab. You both took a huge risk on me when I was switching labs, and I am honored to work with both of you. You've both supported and given me the space to figure out myself and work life balance, revitalized my love of science, and taught me how to be a good person and careful researcher. To Kristen, I admire your way of thinking and the careful way you ask questions and think about science. To Mike, it's been a privilege to be your first student, to see your ideas evolve and watch the lab grow, and to work with you and learn from you (and for the zuccs). Thank you both for trusting me with new projects, for being patient with me through difficult moments, and encouraging my growth.

Thank you also to my committee members Puck Ohi, JK Nandaumar, and Yali Dou. It's rare that I look forward to giving a presentation and public speaking, but I was always excited to get your ideas and feedback about my project and enjoyed our kind and considerate discussions.

My biggest recommendation to incoming graduate students is to vibe check the lab environment before joining because the people and the space will be with whom and where a lot of time is spent. It's the people you'll come to rely on when things get confusing and tough, and the people you'll celebrate accomplishments with. They are your colleagues, mentors, mentees, but most of all friends. Because I switched labs before being co-mentored, I must first and foremost thank Rob Fick and Lindsey Mortitz from the Trievel lab for teaching me all about methyltransferases, perseverance, and how to find the strength to overcome obstacles. Since I've

been co-mentored, this means that I have twice as much fun with double lab mates in the Cianfrocco and Verhey labs over the years: Somaye Badiyan, Tony Ludlam, Jen Cash, Emily Eberhardt, Mike Schost, Zhenyu Tan, Lily Hahn, Yilai Li, Lynne Blasius, Yang Yue, Martin Englke, Jeremey Welsch, Alison Boss, Breanne Budaitis, Archie Geng, Jesse Cisneros, Andy Poulos, Kristin Schimert, and Nnaemeka Unaegbu. They are all a constant source of inspiration, support, encouragement, and energy at the bench or digitally on Slack/Zoom. Martin and Tony in particular helped me get started in the labs and had so much patience as I learned cell culture techniques. I could count on Emily or Breanne to be extra with, and for talking things out during strange hours of the day. When experiments weren't working, Tony, Somaye, or Lynne always had the answer. When it came time to relax and celebrate, Jen and Kristin knew how to organize bonfires and happy hours, respectively and get everyone together. It's the moments in between experiments that are my fondest memories, cracking jokes and memes, making conference friends, and having fun on "Science Saturdays." Thank you all for the honor of working with and becoming good friends.

The third floor of the Life Science Institute in particular has been an amazing place to work, not just because of the core equipment and fancy building, but because of the people, especially: Elyse Petrunak, Jen Meagher, Sumit Bandakar, Tyler Beyett, Jen Bohn, Tyler McCullough, Mike Rankin, Shero Lao, and Nick Burke. Thank you all for vibin' in the kitchenette and taking coffee breaks with me. A reiterated thank you to Tyler for mentorship during lab transitions, showing me how to do cell culture, and to think like a scientist while having an eye of a photographer.

I would also like to thank everyone who has collaborated and helped drive my projects. At UMich, Venky Basrur and Sarah Haynes of the Proteomics Center; Min Su, Amy Bondy, Laura Koepping, and Chris Lilienthal in the cryoEM suite, and the Microtubule Super Group involving the Cianfrocco, Ohi, Verhey, Sept, DeSantis labs. Especially Min brought a lot of laughter and learning to each microscope session and challenged me to know my stuff. Additionally, I thank Cheryl Walker of the Baylor College of Medicine, and Frank Mason and Kim Rathmell of Vanderbilt. Their cellular data laid the groundwork for a lot of my thesis project, and their authentic excited energy during collaborator meetings was really endearing. And Mark Herzik who, with Mike, is making a cool cryoEM education platform and let me be a part of it. I can't wait to see this project grow.

My love of science and research came from the amazing faculty and teachers at Rochester Institute of Technology. Their combination of accessible and engaging academic rigor made me both understand and appreciate the complexity of the world, while seeking answers through research and derivation. I cannot thank Eric West, David Ross, Andre Hudson, Carl Lutzer, David Anderson, and Suzanne O'Handley enough for all their support, letting me research or TA with them, and learn so much about physics, mathematics, and biochemistry. Especially my research advisor Moumita Das, who suffered through so many of my terrible practice talks while still encouraging me to present our work at local and national conferences, continues to be a role model as a woman in science who taught me so much about perseverance and keeping personality in research.

While science and research have defined much of my time as a graduate student, science communication and its associated community helped me grow into the person I am and the interests I've cultivated. I'd been involved with an organization, MiSciWriters, which seeks to train graduate students and postdoctoral fellows in writing and editing science writing for the general public, since my third week of graduate school, so it's been amazing to watch it grow over the four years of my involvement with the group. As such, I must thank Irene Park who let me join the team as a very inexperienced writer, and subsequently all the other leadership members I've had the pleasure of working with: Whit Froehlich, Kristina Lenn, Emily Glass, Alyse Krausz, Melissa Englund, Muyu Situ, Ellen Brennen, Zena Lapp, Attabey Rodríguez-Benitez, and Isabel Colon-Bernal. MiSciWriters also helped start the first inaugural Communicating Science Conference in Michigan (ComSciCon-MI). Chairing this event helped push me into roles I never thought I could play in the scicomm world and made me appreciate all the skills and talents that everyone I got to work with has, certainly the attendees and invited guests, but especially my fellow leadership team the first year: Stephanie Deppe, Jess Chen, Jess Cote, Andrew McAllister, Gizem Kurt, and Attabey. Thank you all so much for coming together and believing we could make something impactful and lasting within the midwestern scicomm community, it's been so exciting to see it grow each year. The science writing community in Ann Arbor is also teaming with energy and support with many meetups and discussions going on throughout the year. In particular, a small scrappy group including former and current Ann Arbor-ites meets monthly to workshop pieces, giving pluses and polishes on drafts. This group, involving Jimmy Brancho, Sara Talpos, Liz Wason, Kevin Boehnke, and Alex Taylor, have become great friends and mentors.

I also must thank my friends who have stuck by my side and supported me, even though I'm terrible at responding to texts, returning calls, and making plans that I'm not always at least 15 minutes late to. Graduate school is tough, and I've definitely not kept in well enough touch with all of you, but I cannot thank Rosa Vasquez, Garrett Johnson, Alex Clark, Kelly Mack, Mandy and Kory Qvigstad, Emily Thurnherr, and Matt Carson enough for keeping me sane, going adventures in the world, and making tons of laughter and delicious bakes. Rosa-and-Sarah day mojitos have become a key tradition for improving morale, while having deep conversations about improving our lives. Writing meetups with Garrett were also something I always looked forward to, even though we did more chatting than writing, but honestly all the better. Emily has been my most grounding friend since undergrad and I cannot stress how amazing, and wholesome she is. Matt and his extroverted personality brought a lot of joy while I lived in Boston, and continues to bring fun, obscure car references, and smiles over periodic roommate video calls. Also, thank you to my amazing neighbors, Beth and Steve, that shared fresh garden crops and soups with me, and showed me what it means to be a good neighbor. Additionally, the community at the Emmanuel Lutheran Church gave hope, and welcomed my doubting heart into their presence with open arms and have helped me keep trying to find faith in Him. I promise that I'll keep praying and searching.

The biggest acknowledgements, thanks, and gratitude for my family: my mom, my dad, my sister Amelia, my stepdad Tim, and most of all my best friend Aidan. Thank you all for coming to visit me throughout my time at UMich. Especially my mom and dad for supporting me through thick and thin, and listened to me explain my work with earnest curiosity even if they didn't understand what I was saying. I'm thankful my dad brought me to see a UMich football game so I could actually understand the "go blue" spirit. Thanks to my mom and sister for also convincing me to adopt a cat, Louis, he provided great fun, company, and snuggles. For too much of my life, especially during (grad) school, I undervalued the support and love of family, but thank you for being there when I did end up reaching out and sharing with me your love and support. Thank you to Aidan especially for supporting me and us when things were really tough, for accepting my experimental bakes, for all the adventures, and for pushing and inspiring me to be better. I'm so thankful for all the ways you lightened my heart and sharing so much of your life with me. Lastly, thank you to all my friends, family, and community for all of your support, this life would not be possible without each and every one of you that've made an impact.

Table of Contents

List of Figures

List of Appendices

List of Abbreviations, Acronyms, and Symbols

αTAT: α-tubulin acetyltransferase
αTubK40me3: α-tubulin lysine 40 trimethylation
αTub1B/βTub3: recombinant single isotype tubulin
ΔαTubCTT: Tail-less α-tubulin
cryoEM: cryogenic electron microscopy
CTD: C-terminal domain (RNA Polymerase II)
CTF: contrast transfer function
CTT: C-terminal tail (tubulin)
DNA: deoxyrobinecleic acid
GMPCPP: guanosine 5'-(beta,gamma-methylene)-diphosphate
GTP: guanosine triphosphate
H3K36me3: histone 3 lysine 36 trimethylation
    Other abbreviations have similar structure and refer to other histones, lysines, or methylation states
KIF: Kinesin motor
KMT: lysine methyltransferase
MAP: microtubule associated protein
K_M: Michaelis-Menten constant
LatA: Latrunculin, actin polymerization inhibitor
PTM: post-translational modification
RNA Pol II: RNA polymerase II
SAH: S-adenosyl homocysteine (product of methyl transfer)
SAM: S-adenosyl methionine (methyl donor)
TIRFM: total internal reflective fluorescence microscopy
tSETD2-FLAG: truncated SETD2 enzyme (1418-2564) with C-terminal FLAG affinity tag
TTLL: tubulin tyrosine ligase like

Abstract

In order for the busy and crowded cell to have a semblance of organization, it leverages a complex and dynamic network of polymers, the cytoskeleton, to provide structure and serve as molecular roads for cargo transport. Two main polymer systems, microtubules and actin filaments, provide long- and short-range transport, respectively. Additionally, microtubules form the mitotic spindle and primary cilia, while actin filaments are critical for cell migration and muscle contraction. How cytoskeletal elements have such diverse functional roles is in part due to post-translational modifications, where specific chemical modifications signal for protein interactions and particular motor protein motility. For example, tubulin methylation is only found on mitotic spindles, the microtubule-based bipolar structure that separates chromosomes during cell division and is enzymatically added by SETD2. SETD2 canonically modifies histones, specifically histone 3 at lysine 36, and is the only enzyme that can tri-methylate this residue.

Knock-out of SETD2 results in histone- and/or microtubule-dependent genetic instability leading to cancer-driving mitotic defects like multipolar spindles and micronuclei formation. Mutations in SETD2 are implicated in cancer, most commonly in the kidney cancer clear cell renal cell carcinoma (ccRCC), with SETD2 mutations occurring in 10-15% of all ccRCC cases. Thus far, the role of SETD2 in cancer has only been studied in a histone methylation context, but the contribution of cytoskeletal methylation remains unclear. Studies using tumor cells from ccRCC patients demonstrated that when the level of the SETD2 gene product is less than normal (haploinsufficiency), there is a loss of tubulin methylation and genomic instability, whereas total SETD2 inactivation results in a loss of histone methylation. This stepwise model for the loss of SETD2 functionality describes histone and tubulin methylation at the gene level but does not describe the enzymatic regulation of SETD2 amongst its substrates biochemically. Moreover, specific ccRCC mutations have a differential impact on either histone or tubulin methylation in cells, where a R2510H mutation, found in a domain important for regulating protein-protein interactions of SETD2 (the Set2 Rpb1 Interacting SRI domain), retains histone methylation but

not tubulin methylation. As such, there remains a significant realm of tubulin-dependent processes that drive ccRCC pathologies that remain unexplored.

In this study, I used *in vitro* biochemical reconstitution with recombinant proteins to determine how SETD2 recognizes and methylates tubulin in addition to actin. By exploiting known tubulin-targeting agents, I found that SETD2 preferentially methylates the dimeric form of tubulin over microtubule polymers and, using recombinant single-isotype tubulin, I demonstrated that methylation is restricted to lysine 40 of alpha-tubulin. Moreover, by introducing pathogenic mutations into SETD2 to probe the recognition of histone and tubulin substrates, I found that particular mutations within the SRI domain tune histone and tubulin methylation by regulating protein-protein interactions with tubulin or RNA Polymerase II. Lastly, I found that tubulin substrate recognition requires the negatively-charged C-terminal tail of alpha-tubulin. Curiously, the SRI domain does not play a similar regulatory role with actin substrate suggesting an alternative recognition site, but our collaborative work found that actin methylation by SETD2 is necessary for cell motility and actin dynamics at the cell periphery. Future studies into tubulin and actin chemical modifications are required to understand the nuanced interactions and crosstalk amongst histone, tubulin, and actin chemical codes in cells and their implications for cancer and disease progression.

Chapter 1: Introduction

1. 1 Cytoskeletal networks in cells

Cellular processes are extremely diverse and complicated, yet essential for life. The wide range of tasks that each individual cell carries out, either in isolation or in collections of tissues and organisms, must be controlled and organized in such a way that processes occur at the correct time and in the right place. For many processes, random diffusion is insufficient to achieve coordination especially in the crowded and viscous cytoplasm (Fulton 1982; I. Yu et al. 2016). As

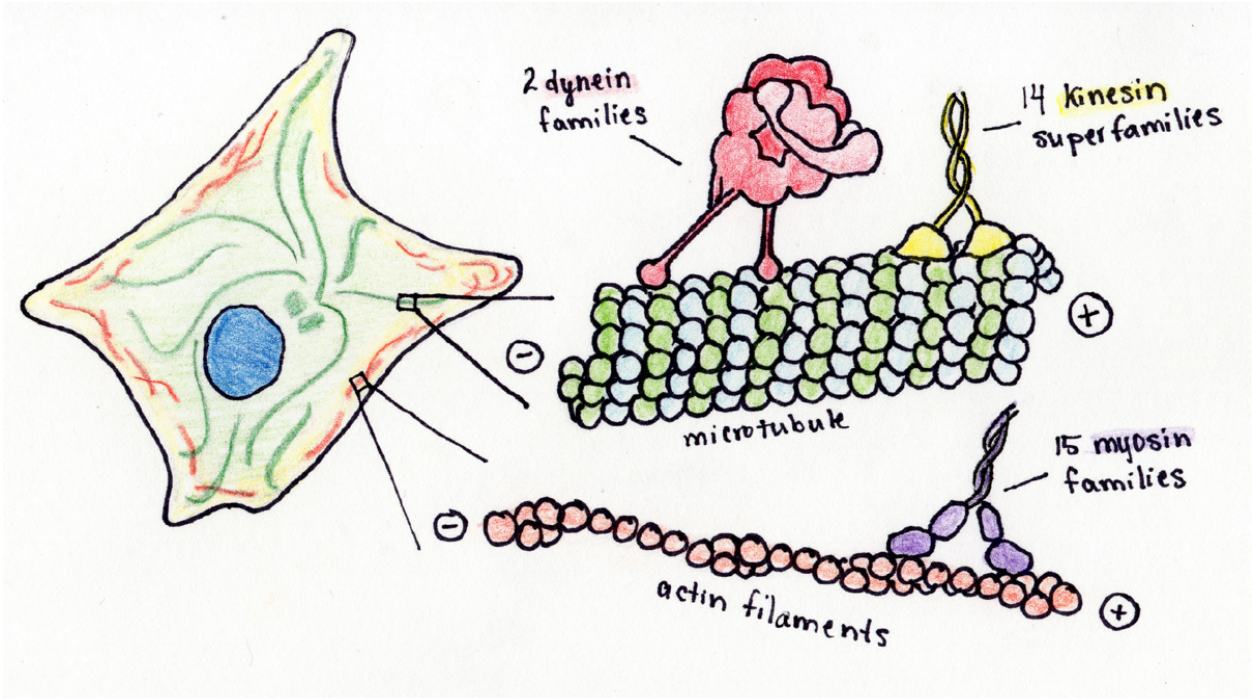

Fig. 1.1 Two main cytoskeletal networks in cells, microtubules and actin filaments. Cartoon schematic showing left) a cell with a blue nucleus, dark green microtubules, and orange actin filaments, right top) microtubule made of green α-tubulin and blue β-tubulin heterodimers, with red dynein and yellow kinesin motors, right bottom) actin with purple myosin motor.

such, a complex dynamic network of protein polymers called the cytoskeleton facilitates this spatio-temporality. Cytoskeletal polymers exist within the cytoplasm of cells and extend from the cell nucleus to the cell membrane giving the cell its shape, thus "cyto-skeleton." These polymer networks are critical for a myriad of cellular functions, including cell migration, cell signaling, cell division, and intracellular transport of vesicles and organelles. Additionally, they form critical structures within the cell like the mitotic spindle, flagella, and cilia. Even though cytoskeletal elements are more common in eukaryotic cells, bacteria and archaea have homologous proteins that also form polymers for cell structure and division.

To facilitate a complex set of cellular behaviors, eukaryotic cells evolved two main networks, actin fibers and microtubules, that build the foundational framework of the cell. The first indication of these networks likely came from early microscopy studies by Walter Flemming in the mid 1800s. One of his illustrations shows what we now iconically understand to be the mitotic spindle, though the relationship between the "thick fibers" (chromosomes) and the "thin fibers" (microtubules) was not known at the time, and both were thought to be manifestations of nuclear structure as the cell was dividing (Flemming 1878). In the late 1800s, live cell imaging in diatoms led to the concept that the cytoplasm in living cells contained "spindle fibers" that had sporadic organization that could interact with the extracellular matrix (Lauterborn 1896). Though characterization of the cytoskeleton was underway, it wasn't until about 50 years later that actin was identified during WWII in a Hungarian lab studying muscle contraction (Szent-Györgyi 1942), and almost 70 years later that microtubules were imaged and given a name in a study of plant cells (Ledbetter and Porter 1963).

Actin fibers and microtubules are both polarized cytoskeletal filaments built from smaller subunits, actin and tubulin, respectively. Both actin and tubulin are globular proteins. Actin monomer contains two domains, outer and inner, which both contain two subdomains resulting in flat rectangular-like shape (Dominguez and Holmes 2011). Tubulin is a heterodimer of α- and β-tubulin which both contain a nucleotide binding pocket but only β-tubulin has catalytic hydrolyzing activity (Downing and Nogales 1998). The C-terminal end of all tubulins have a flexible tail that aligns along the outside of the microtubule in polymer form. Actin and tubulin disassembly and assembly into polymers depends on ATP- or GTPase activity of individual subunits, with the process of dynamic instability of polymer growing and shrinking important for many cellular processes as well (H. P. Erickson and O'Brien 1992; R. Li and Gundersen 2008).

For example, rapid depolymerization of the microtubules in a mitotic spindle is critical for chromosome segregation, and depolymerization of actin filaments is important for cell migration (Carlier et al. 1997; Petry 2016). Moreover, both of these networks have a polarity, where the slow-growing ends of microtubules and pointed ends of actin (minus ends) are directed towards the center of the cell, and the quick-growing ends of microtubules and barbed ends of actin (plus ends) are directed outwards towards the cell periphery (Fletcher and Mullins 2010). Cytoskeletal polarity helps orient cellular structures in addition to directing intracellular transport.

Cytoskeletal functions depend on their inherent dynamics in addition to molecular motors that use the protein polymer networks as roads. There are three major types of motors: microtubule-based kinesin and dynein, and actin-based myosin. Each of these motor proteins convert chemical energy from adenosine triphosphate (ATP) hydrolysis into mechanical energy to transport themselves and their cargos along their respective polymers (Knight and Molloy 1999; Vale and Milligan 2000). This ATP-ase activity is localized in a catalytic motor domain which is typically dimerized through a coil-coiled element which is flanked by a tail domain (Schliwa 1999; Veigel et al. 1999; Hancock and Howard 1998). As such, ATP hydrolysis and the subsequent mechanical output results in a "stepping" on cytoskeletal filaments and allows for intracellular transport. The motors themselves leverage the inherent polarity of the filaments, with kinesin and myosin motors walking towards the plus-ends of microtubules and actin fibers, respectively (Verhey and Hammond 2009; N. Hirokawa et al. 2009; Amanda Hartman and Spudich 2012), and dynein motors, along with some myosin motors, that walk towards the minus-ends of microtubules (Vallee, Shpetner, and Paschal 1989). Kinesin motors in eukaryotes are encoded by at least 45 KIF genes that are categorized into 15 superfamilies, called kinesin-1 to kinesin-14 (Nobutaka Hirokawa et al. 2009). Before the mid-2000s, kinesins were being named by diverse and inconsistent criteria, resulting in a revised nomenclature that keeps the individual names, but alters the classification scheme "to minimize confusion" resulting in non-intuitive schemas like KIF1A classified as a kinesin-3 motor, and KIF5A as a kinesin-1 motor (Lawrence et al. 2004). Most kinesins are involved in trafficking, but some of them have particular functions for example tethering mitotic spindles and chromosome segregation by KIF18A or anchoring by KIF7 (Mayr et al. 2007; Yue et al. 2018). Myosin motors for actin filament-based transport also have a complex phylogeny, with ~30 genes encoding myosin classified into 15 families (Sellers 2000). Dynein motors are much more straightforward as they only fall into two major subgroups, axonemal and

cytoplasmic, further broken down into seven classes (Höök and Vallee 2006). Cytoplasmic dynein-1 is the motor responsible for most cellular trafficking and retrograde transport.

1.2 Chemical codes direct cellular processes

How motor proteins are accurately trafficked in cells is, in part, due to chemical modifications to tubulin and actin. Beyond the cytoskeleton, most proteins in the cell can have post translational modifications (PTM) which impacts cell signaling, degradation, and other cellular functions in general. These PTMs are covalent additions to proteins and increase the functional diversity of cytoskeletal elements. Sets of enzymes called writers, erasers, and readers add, remove, and recognize chemical modifications, respectively. The complex landscape of readers, writers, and erasers of chemical modifications depends on existing, yet dynamic, chemical modifications.

1.2.1 Tubulin code

Tubulin code comprises chemical modifications to tubulin proteins, but also a number of different isotypes. The concept of isotypes and modifications controlling microtubule function was proposed as early as the 1970s when genotyping identified α- and β-tubulin isotypes in different species and covalent modifications were first identified (Cavalier-Smith 1978; Ludueña 1998). However, due to the complexity of the system, the tubulin code resisted functional characterization for many years, until finally being named in the 2000s (Verhey and Gaertig 2007).

Tubulin isotypes come from expression of alternative tubulin genes. The complexity and mysterious genetic evolution of tubulin genes is reflected in the confusing nomenclature, which makes them really fun to talk about at conferences (Khodiyar et al. 2007). Sequence alignments show that eukaryotic tubulin is highly conserved, but are extremely divergent from their prokaryotic relatives FtsZ, the most similarity within the GTP-ase domains rather than the protofilament interface (Harold P. Erickson 2007). Nevertheless, during tubulin evolution the number of isotypes varied across species and phyla, for example yeast have two a-tubulins and one b-tubuln (Schatz et al. 1986; Neff et al. 1983), whereas humans have eight genes for each. Surveying isotypes across organisms, it was observed that different tissues and cell types had different expression levels of particular isotypes. For example, α-tubulin isotypes in root, leaf, and

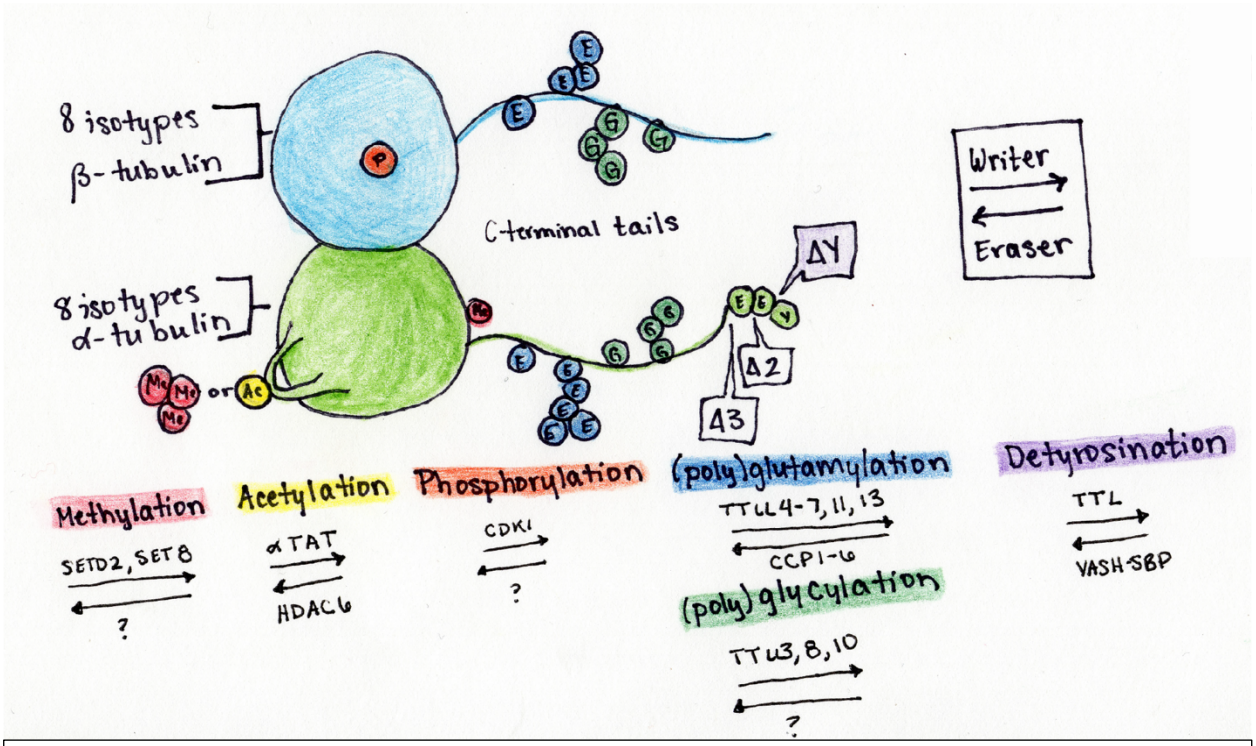

Fig. 1.2 Tubulin code. Cartoon showing top) tubulin dimer with a-tubulin in green and b-tubulin in blue. Each tubulin monomer has eight isotypes and a long C-terminal tail which is highly modified, and bottom) the most common chemical modifications to tubulin, color-coded as they are above, with known writer and eraser enzymes listed.

flower cells in plants have different expression levels, *Drosophila* α-tubulin isotypes can be male- or female-specific in sex cells, and in mice and chickens a-tubulin isotypes have varied expression in all cell types (Carpenter et al. 1992; Theurkauf et al. 1986; Panda et al. 1994). Despite the fact that expression is somewhat tissue-specific, not all isotypes are functionally distinct (Schatz, Georges, and Solomon 1987; Hoffman and Cleveland 1988; Bond et al. 1986). That said, some can have profound impact on cell function, in particular the β-tubulin isoforms. For example, expressing βTub3 in place of βTub2 in *Drosophila* testes resulted in the inability to form an axoneme or meiotic spindle (Hoyle and Raff 1990). Additionally, the loss of αTub1A is perinatal lethal and leads to forebrain dysmorphology (Bitterman et al. 2018) and the overexpression of βTub3 in non-brain cells correlates with cancer (Person et al. 2017).

In addition to having different isotypes, tubulin can be subjected to a number of PTMs. Common tubulin-specific PTMs include phosphorylation, acetylation, methylation, and ribosome-independent tyrosination, (poly)glutamylation, and (poly)glycylation. Moreover, removal of single

amino acids such as tyrosine and glutamate residues on the α-tubulin C-terminal tail (CTT) result in detyrosinated tubulin (dY), or del2- and del3-tubulin (Verhey and Gaertig 2007; Ian Yu, Garnham, and Roll-Mecak 2015; Gadadhar et al. 2017; Janke and Magiera 2020). Most PTMs label distinct microtubule populations in cells and as such are expected to encode for particular cellular functions. For example, acetylation marks are found on long-lasting microtubules in addition to decorating microtubule-based structures like the mitotic spindle and primary cilia. Additionally, neuronal microtubules typically have detyrosination and polyglutamylation marks which are thought to be important for neuronal differentiation (Mansfield and Gordon-Weeks 1991; Eddé et al. 1990; Rüdiger et al. 1992; Audebert et al. 1994).

How PTMs are thought to alter microtubule function is due to interactions with other microtubule associated proteins (MAPs) and motor proteins. For example, tyrosinated tubulin is critical for initiation of dynein-dynactin transport, resulting in an increase in landing rates (McKenney et al. 2016). Polyglycylation and/or polyglutamylation of the β-tubulin CTT influences kinesin-1 binding. In addition, α-tubulin acetylation drastically changes the binding and motility of kinesin-1 (Hammond et al. 2009; Reed et al. 2006), and polyglutamylation increases kinesin-3 pausing and run length (Lessard et al. 2019). Kinesin-2 motors have a 2.5x and 2x increase in velocity and processivity, respectively, on detyrosinated microtubules over tyrosinated microtubules (Sirajuddin, Rice, and Vale 2014). Some of these phenomena are especially highlighted in neurons where complex roads of modified microtubules stretch out into the complex network of dendrites and axons. In neuronal cultured neurons, kinesin-1 motors preferentially bind to and walk on acetylated microtubules, where kinesin-3 will tread on tyrosinated microtubules. With acetylation and tyrosination occurring on distinct populations of microtubules in neurons, chemical modifications seem to create separate tracks for particular kinesin motor families (Tas et al. 2017). These previous studies suggest microtubule PTMs form different tracks in cells that kinesin motors somehow recognize and "choose." Other MAPs can also bind along the surface of the microtubule lattice and read PTMs. For example, plus-end binding proteins like EB1 and CLIP-170 recognize tyrosinated form of tubulin through their CAP-Gly domain (Komarova et al. 2005; Roberts, Goodman, and Reck-Peterson 2014; Peris et al. 2006). Taken together, microtubule PTMs are important for many cellular functions and help direct protein-protein interactions throughout the cell.

1.2.2 Actin code

Like tubulin, actin also has a wide range of isotypes and chemical modifications. There are three α-isoforms of skeletal, cardiac, and smooth muscle actin, in addition to β- and γ-isoforms found in non-muscle cells. These isoforms only differ by a few amino acids with most of the variation occurring towards the N-terminus of the protein (Hanson and Lowy 1963). Despite their sequence and structural similarities, actin isoforms have distinct roles in cells. For example, knockout of cardiac α-actin results in disorganization of cardiac myofibrils and mice without skeletal a-actin have weak muscles and die within a week whereas mice lacking smooth α-actin have defects in blood pressure regulation (Kumar et al. 1997; Crawford et al. 2002; Schildmeyer et al. 2000). However, in some cases isoforms have overlapping functions. Expressing cardiac α-actin rescued muscle performance in skeletal α-actin knock-out models (Nowak et al. 2009). The cytoplasmic isoforms β- and γ-actin are also nearly identical, with differences on the N-terminal residues. Knockout of β-actin, mice will die during early development, but otherwise knockout of γ-actin or knock-down of β-actin has little impact on survival despite impacts on the formation of sensory hair cells and wound healing (Shawlot et al. 1998; Belyantseva et al. 2009). These studies indicate that particular action isotypes are critical for some functions but not necessarily for survival.

In addition to isotypes, actin can also be modified. Actin PTMs are found on 94 different side chains, meaning that about 45% of actin residues can be modified (Varland, Vandekerckhove, and Drazic 2019). That said, not all actin PTMs are present on the same molecule and instead are found in particular organisms, tissue types, or within particular regions of a cell. Most actin, both muscle and non-muscle isoforms, have acetylation on their N-terminus as part of their synthesis (Redman and Rubenstein 1984). Other common modifications are phosphorylation, oxidation, sumoylation, and methylation (Varland, Vandekerckhove, and Drazic 2019; Vedula and Kashina 2018; Terman and Kashina 2013). Oxidation and reduction (redox) reactions on actin substrates impact actin dynamics, for example without actin oxidation cells will have abnormal actin polymerization and decreased neuron growth and development (Wilson and González-Billault 2015). Impaired dynamics impacts cellular processes like cell division, where without oxidized actin filaments a cell cannot complete cytokinesis, and cell motility (Frémont et al. 2017; Fiaschi et al. 2006; Munnamalai and Suter 2009). Actin methylation occurs on multiple residues, but best characterized is methylation at position H73. Methylation of H73 regulates how flexible actin is

and is associated with actin polymerization and ATP hydrolysis (Nyman et al. 2002), and prevents primary dystocia (Wilkinson et al. 2018). While there are many other modifications to actin, suffice to say that the combination of isotypes and covalent modifications impact actin-based functions in cells and improper regulation of modifying enzymes leads to impairments in cellular and organismal functions.

1.2.3 Histone code

The most common or well-known system of PTMs is probably the histone code. Histones are the proteins around which DNA winds, and different modifications to histone isotypes lead to exposed or unexposed DNA. As such, histone modifications impact transcription, thus impacting protein expression of the whole cell.

Much like the aforementioned proteins, histones have a number of isotypes. The combination of isotypes H2A, H2B, H3 and H4 come together to form an octamer. In addition, linker histone H1 has a different sequence and structure than the core histones (Kasinsky, Lewis, and Dacks 2001). The core histones, not including H1, are highly conserved across eukaryotes in both protein sequence and structure. Histone proteins have an essential role in gene regulation and protein expression, with some, like, H2A and H3 families, having specific roles for example in DNA repair, gene silencing, and gene expression (Talbert and Henikoff 2010a). Variations of some of these isotypes, CenH3, H3.3, H2A.Z, and H2A.X diverged in modern eukaryotes to perform specialized functions. CenH3, or centromere-specific histone variant H3, also known as CENP-A in humans, has 60% identity with canonical H3 yet replaces it during cell division because it interacts with microtubules (Santaguida and Musacchio 2009; Earnshaw and Rothfield 1985). Because chromosomes need to be divided evenly into daughter cells during mitosis, it's important that DNA makes centromeric-mediated interactions with the microtubules that constitute the mitotic spindle. Similarly, variant H3.3 replaces H3 during S-phase when DNA is being replicated (Tagami et al. 2004). Even though only four amino acids differ between H3 and H3.3, deletions of H3.3 genes result in sterility and can be lethal (Hödl and Basler 2009; Cui, Liu, and Gorovsky 2006). Like H3, H2 family has variations, H2A.Z, H2A.X, and macroH2A, where the former are found at transcription start sites to promote RNA Polymerase recruitment, and the latter are recruited for double-strand break repair in DNA (Zlatanova and Thakar 2008; Altaf et al. 2009; Buschbeck et al. 2009). Other less common histone variants exist and are discussed in (Talbert and

Henikoff 2010b). Even though most histones are highly conserved, most sequence differences are found in their flexible N-terminal tails which are accessible even when incorporated into nucleosomes.

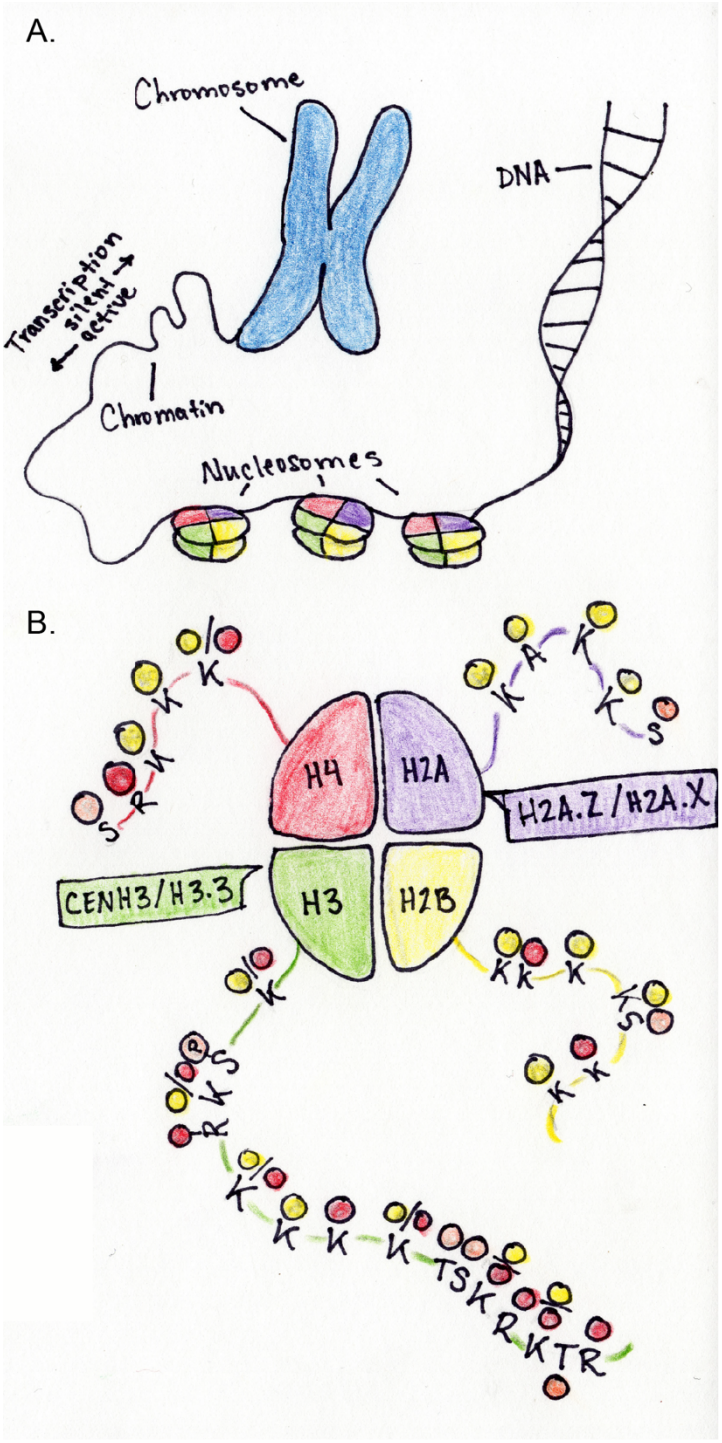

Fig. 1.3 Histone Code. A) Cartoon showing how DNA (right) wraps around histones to form nucleosomes (center), which are further condensed into chromatin, and finally blue chromosomes (left). Chromatin can either be in a transcriptionally active or silent state depending on how loose or tightly it's condensed. B) Cartoon showing the four histones incorporated into a nucleosome, H2A (purple), H2B (yellow), H3 (green), and H4 (red). Each histone has a long N-terminal tail which is highly modified with methylation (red), acetylation (yellow), and phosphorylation (orange) shown on amino acids depicted by their single-letter abbreviation. H2A and H3 variants are also listed in the colored

Histone proteins can be highly modified, with most of the chemical moieties found on the N-terminal tails of histones. Histone PTMs contribute to epigenetic regulation, because the modifications change and alter gene expression (Weinhold 2006). In addition to genetic sequence, epigenetic modifications alter gene activity without changing the DNA sequence and can be traced back to hereditary and

environmental factors. Histone tails are highly modified and the combination of PTMs dictate conformational changes in chromatin, thus leading to transcriptionally active or silent regions of the genome. Moreover, because of the slight sequence differences in histone isotypes and variants, histone PTMs are found on specific residues within the flexible N-terminal tails of particular isotypes, thus adding another layer of complexity to the system. For example, trimethylation of lysine 9 on H3 (H3K9me3) is associated with condensed chromatin (silent) while trimethylation of lysine 4 on histone 3 is enriched at promoter regions (active) (Fischle et al. 2005; Ekwall 2007; H. Santos-Rosa et al. 2002). The enzymes that modify histone tails are extremely specific to the residue, and sometimes require other modifications to be present. Indeed, some writer enzymes contain "reading" domains, for example many histone acetyltransferases (HATs) contain a bromodomain that recognizes acetylated lysine residues, meaning that the domain helps positively or negatively regulate activity (Jacobson et al. 2000). As such, a combinatorial code likely regulates whether a gene is transcriptionally active or silent, where multiple PTMs cooperatively restructure chromatin. For example, Ser10 phosphorylation on H3 inhibits Lys9 methylation but promotes Lys9 acetylation in such a way that marks for transcriptional activation (Rea et al. 2000; Cheung et al. 2000). This robustness or redundancy in function helps ensure the epigenetic code isn't thrown off kilter without the presence of one particular modification, such that the loss of a single modification doesn't disrupt proper transcriptional activities. Additionally, reversible reactions are critical because chromatin must fluctuate between condensed and exposed across the cell cycle. If the histone code does become dysregulated, gene expression and the cell cycle are directly affected. As such, mutations in histone readers, writers, and erasers often have diseases, especially cancers, associated with them (Helena Santos-Rosa and Caldas 2005; Cohen, Poręba, and Kamieniarz 2011).

1.3 Research goals

Typically, each of the aforementioned codes are researched and discussed in the confines of their own system: the tubulin code impacts microtubule dynamics and kinesin and dynein transport, the actin code changes cell motility and myosin processivity, and the histone code alters transcription. While these phrases are true, there is an increasing focus on how the codes communicate and impact one another in a cell and organism.

Most directly, cytoskeletal networks actin and microtubules are connected by protein cross-linkers. Actin filaments can guide and stabilize microtubules near the cell periphery, and microtubules cannot grow neuronal growth cones if actin networks are disorganized (Waterman-Storer and Salmon 1997; Zhou, Waterman-Storer, and Cohan 2002). Recently it was also found that actin filaments can be found inside the microtubule lumen using cryogenic electron tomography (Paul et al. 2020). Though the impact of actin inside the microtubule is not known yet, it's hypothesized that it could alter microtubule dynamics or other protein interactions. Some microtubule associated proteins (MAPs) bridge actin and microtubules together. The spectraplakin family of proteins are spatiotemporally regulated and as such leverage the polarity of both actin filaments and microtubules (Zhang, Yue, and Wu 2017). MAP1 and MAP2 family proteins also cross-link polymers in axons particularly in developing neurons to allow for synaptic plasticity, and to help stabilize the actin ring during cleavage furrow of cell division (Tortosa et al. 2011; Morales and Fifkova 1989; Cueille et al. 2007). Additionally, tau protein, which binds to microtubules in neuron cells to establish neuronal polarity and stabilize microtubules, also organizes actin filaments. Disruption of actin within the growth cone perturbs tau localization, and conversely tau-deficient neurons show actin-dependent alterations in growth cone development (DiTella et al. 1994; Kempf et al. 1996).

Histones can also make protein-protein interactions with cytoskeletal elements. Unlike tubulin, actin can exist in both the cytoplasm and the nucleus. Initial observational studies showed that actin filaments existed in the nucleus (Ishikawa, Bischoff, and Holtzer 1969) and has since been found to be important in regulating transcription, chromatin remodeling, and DNA repair (Fomproix and Percipalle 2004; Shen et al. 2000; Andrin et al. 2012). More specifically, increased actin filaments in the nucleus increases histone deacetylase activity, thus decreasing histone acetylation suggesting that actin can regulate histone modifying enzymes (Serebryannyy, Cruz, and de Lanerolle 2016). In addition, histones alter actin structure, with H1 able to help polymerize actin and H2A and H2B able to facilitate actin bundling (Magri, Zaccarini, and Grazi 1978; Sol et al. 2016). For microtubules that are not found in the nucleus, histones only have a chance to make protein-protein interactions during cell division when the nuclear envelope disappears. As previously discussed, histone variant CenH3 contacts kinetochore microtubules to ensure proper chromosome segregation.

Beyond direct or mediated protein-protein contacts, histones and the cytoskeleton share some PTM readers, writers, and erasers. Histone deacetylase 6 (HDAC6) acts on a-tubulin and is the only member of the histone deacetylase family that's found in the cytoplasm (Boyault et al. 2007). N-lysine methyltransferase 5A (KMT5A or SET8) methylates both lysine 4 of H4 in addition to tubulin at lysine 311 (Chin et al. 2020). SET8-dependent methylation has been associated with cell cycle progression and without SET8 cells have delayed mitotic progression and premature chromosome condensation (Wu and Rice 2011). These associated mitotic defects were thought to be histone dependent. However, because microtubules are critical in forming the mitotic spindle and can be methylated by the same enzyme performing histone methylation, there is a strong possibility that tubulin methylation is required for proper cell division. SMYD2, responsible for modifying histone 3 lysine 4 (H3K4me3) and p53 at lysine 370, can also methylate a-tubulin. SMYD2 methylation is mediated by cyclin-dependent kinases CDK4/6 which regulates methyltransferase activity, thus impacting both tubulin and histone PTMs (L. X. Li et al. 2020). Similarly, SETD2, a methyltransferase that canonically trimethylates histone 3 at position lysine 36 has been implicated in tubulin methylation (Park et al. 2016). Imaging experiments show that methylation appears on minus-ends of microtubules in the mitotic spindle, and all but disappears when SETD2 is knocked-out. Moreover, mutations in SETD2 implicated in kidney cancers seem to tune histone and tubulin methylation. In addition, recent studies also show that SETD2 can also methylate actin and impact cell migration (Seervai et al. 2020).

The following studies here aim to understand the biochemical underpinnings of how SETD2 distinguishes amongst its different substrates. By utilizing *in vitro* biochemical reconstitution with recombinant proteins, we want to understand how SETD2 recognizes and methylates tubulin in addition to actin. In addition, we want to determine if SETD2 has a preference for soluble dimers or monomers, or for microtubules and actin filaments respectively. To try and understand how SETD2 is regulated, we want to focus on the domains that contain mutations found in cancers, because *in vivo* data suggests that particular mutations seem to tune substrate activity. This system of cytoskeletal methylation by SETD2 needs to be studied *in vitro* so we can understand the necessary components and understand what is sufficient for methylation. These studies hope to identify particular domains or protein-protein interactions that regulate SETD2, with the goal of understanding how histone, tubulin, and actin chemical codes crosstalk in cells.

1.4 References

Altaf, Mohammed, Andreanne Auger, Marcela Covic, and Jacques Côté. 2009. "Connection between Histone H2A Variants and Chromatin Remodeling Complexes." *Biochemistry and Cell Biology = Biochimie et Biologie Cellulaire* 87 (1): 35–50.

Amanda Hartman, M., and James A. Spudich. 2012. "The Myosin Superfamily at a Glance." *Journal of Cell Science* 125 (7): 1627–32.

Andrin, Christi, Darin McDonald, Kathleen M. Attwood, Amélie Rodrigue, Sunita Ghosh, Razmik Mirzayans, Jean-Yves Masson, Graham Dellaire, and Michael J. Hendzel. 2012. "A Requirement for Polymerized Actin in DNA Double-Strand Break Repair." *Nucleus* 3 (4): 384–95.

Audebert, S., A. Koulakoff, Y. Berwald-Netter, F. Gros, P. Denoulet, and B. Eddé. 1994. "Developmental Regulation of Polyglutamylated Alpha- and Beta-Tubulin in Mouse Brain Neurons." *Journal of Cell Science* 107 (Pt 8) (August): 2313–22.

Belyantseva, I. A., B. J. Perrin, K. J. Sonnemann, M. Zhu, R. Stepanyan, J. McGee, G. I. Frolenkov, et al. 2009. "-Actin Is Required for Cytoskeletal Maintenance but Not Development." *Proceedings of the National Academy of Sciences*. https://doi.org/10.1073/pnas.0900221106.

Bitterman, Elizabeth, Ryan Liegel, Chelsea Menke, Andrew Timms, David Beier, Beth Kline-Fath, Howard M. Saal, Howard M. Saal, and Rolf Slottman. 2018. "Differential Requirements of Tubulin Genes in Mammalian Forebrain Development."

Bond, J. F., J. L. Fridovich-Keil, L. Pillus, R. C. Mulligan, and F. Solomon. 1986. "A Chicken-Yeast Chimeric Beta-Tubulin Protein Is Incorporated into Mouse Microtubules in Vivo." *Cell* 44 (3): 461–68.

Boyault, C., K. Sadoul, M. Pabion, and S. Khochbin. 2007. "HDAC6, at the Crossroads between Cytoskeleton and Cell Signaling by Acetylation and Ubiquitination." *Oncogene* 26 (37): 5468–76.

Carlier, M. F., V. Laurent, J. Santolini, R. Melki, D. Didry, G. X. Xia, Y. Hong, N. H. Chua, and D. Pantaloni. 1997. "Actin Depolymerizing Factor (ADF/cofilin) Enhances the Rate of Filament Turnover: Implication in Actin-Based Motility." *The Journal of Cell Biology* 136 (6): 1307–22.

Carpenter, J. L., S. E. Ploense, D. P. Snustad, and C. D. Silflow. 1992. "Preferential Expression of an Alpha-Tubulin Gene of Arabidopsis in Pollen." *The Plant Cell* 4 (5): 557–71.

Cavalier-Smith, T. 1978. "The Evolutionary Origin and Phylogeny of Microtubules, Mitotic Spindles and Eukaryote Flagella." *Bio Systems* 10 (1-2): 93–114.

Cheung, Peter, Kirk G. Tanner, Wang L. Cheung, Paolo Sassone-Corsi, John M. Denu, and C. David Allis. 2000. “Synergistic Coupling of Histone H3 Phosphorylation and Acetylation in Response to Epidermal Growth Factor Stimulation.” *Molecular Cell* 5 (6): 905–15.

Chin, Hang Gyeong, Pierre-Olivier Esteve, Cristian Ruse, Jiyoung Lee, Scott E. Schaus, Sriharsa Pradhan, and Ulla Hansen. 2020. “The Microtubule-Associated Histone Methyltransferase SET8, Facilitated by Transcription Factor LSF, Methylates α-Tubulin.” *The Journal of Biological Chemistry*. https://doi.org/10.1074/jbc.RA119.010951.

Cohen, I., E. Poręba, and K. Kamieniarz. 2011. “Histone Modifiers in Cancer: Friends or Foes?” *& Cancer*. https://journals.sagepub.com/doi/abs/10.1177/1947601911417176.

Crawford, K., R. Flick, L. Close, D. Shelly, R. Paul, K. Bove, A. Kumar, and J. Lessard. 2002. “Mice Lacking Skeletal Muscle Actin Show Reduced Muscle Strength and Growth Deficits and Die during the Neonatal Period.” *Molecular and Cellular Biology* 22 (16): 5887–96.

Cueille, N., C. Tallichet Blanc, S. Popa-Nita, S. Kasas, S. Catsicas, G. Dietler, and B. M. Riederer. 2007. “Characterization of MAP1B Heavy Chain Interaction with Actin.” *Brain Research Bulletin* 71 (6): 610–18.

Cui, Bowen, Yifan Liu, and Martin A. Gorovsky. 2006. “Deposition and Function of Histone H3 Variants in Tetrahymena Thermophila.” *Molecular and Cellular Biology* 26 (20): 7719–30.

DiTella, M., F. Feiguin, G. Morfini, and A. Caceres. 1994. “Microfilament-Associated Growth Cone Component Depends upon Tau for Its Intracellular Localization.” *Cell Motility and the Cytoskeleton* 29 (2): 117–30.

Dominguez, Roberto, and Kenneth C. Holmes. 2011. “Actin Structure and Function.” *Annual Review of Biophysics* 40: 169–86.

Downing, K. H., and E. Nogales. 1998. “Tubulin Structure: Insights into Microtubule Properties and Functions.” *Current Opinion in Structural Biology* 8 (6): 785–91.

Earnshaw, William C., and Naomi Rothfield. 1985. “Identification of a Family of Human Centromere Proteins Using Autoimmune Sera from Patients with Scleroderma.” *Chromosoma* 91 (3-4): 313–21.

Eddé, B., J. Rossier, J. P. Le Caer, E. Desbruyères, F. Gros, and P. Denoulet. 1990. “Posttranslational Glutamylation of Alpha-Tubulin.” *Science* 247 (4938): 83–85.

Ekwall, Karl. 2007. “Epigenetic Control of Centromere Behavior,” December. https://doi.org/10.1146/annurev.genet.41.110306.130127.

Erickson, Harold P. 2007. “Evolution of the Cytoskeleton.” *BioEssays: News and Reviews in Molecular, Cellular and Developmental Biology* 29 (7): 668–77.

Erickson, H. P., and E. T. O’Brien. 1992. “Microtubule Dynamic Instability and GTP Hydrolysis.” *Annual Review of Biophysics and Biomolecular Structure* 21: 145–66.

Fiaschi, Tania, Giacomo Cozzi, Giovanni Raugei, Lucia Formigli, Giampietro Ramponi, and Paola Chiarugi. 2006. “Redox Regulation of β-Actin during Integrin-Mediated Cell Adhesion.” *The Journal of Biological Chemistry* 281 (32): 22983–91.

Fischle, Wolfgang, Boo Shan Tseng, Holger L. Dormann, Beatrix M. Ueberheide, Benjamin A. Garcia, Jeffrey Shabanowitz, Donald F. Hunt, Hironori Funabiki, and C. David Allis. 2005. “Regulation of HP1–chromatin Binding by Histone H3 Methylation and Phosphorylation.” *Nature* 438 (7071): 1116–22.

Flemming, Walther. 1878. “Zur Kenntnis Der Zelle Und Ihrer Theilungserscheinungen.” *Schr Nat Wiss Ver Schlesw-Holst* 3: 23–27.

Fletcher, Daniel A., and R. Dyche Mullins. 2010. “Cell Mechanics and the Cytoskeleton.” *Nature* 463 (7280): 485–92.

Fomproix, Nathalie, and Piergiorgio Percipalle. 2004. “An Actin–myosin Complex on Actively Transcribing Genes.” *Experimental Cell Research* 294 (1): 140–48.

Frémont, Stéphane, Hussein Hammich, Jian Bai, Hugo Wioland, Kerstin Klinkert, Murielle Rocancourt, Carlos Kikuti, et al. 2017. “Oxidation of F-Actin Controls the Terminal Steps of Cytokinesis.” *Nature Communications* 8 (February): 14528.

Fulton, A. B. 1982. “How Crowded Is the Cytoplasm?” *Cell*. https://www.cell.com/cell/pdf/0092-8674(82)90231-8.pdf.

Gadadhar, Sudarshan, Satish Bodakuntla, Kathiresan Natarajan, and Carsten Janke. 2017. “The Tubulin Code at a Glance.” *Journal of Cell Science* 130 (8): 1347–53.

Hammond, Jennetta W., Dawen Cai, T. Lynne Blasius, Zhe Li, Yuyang Jiang, Gloria T. Jih, Edgar Meyhofer, and Kristen J. Verhey. 2009. “Mammalian Kinesin-3 Motors Are Dimeric in Vivo and Move by Processive Motility upon Release of Autoinhibition.” *PLoS Biology* 7 (3): 0650–63.

Hancock, William O., and Jonathon Howard. 1998. “Processivity of the Motor Protein Kinesin Requires Two Heads.” *The Journal of Cell Biology* 140 (6): 1395–1405.

Hanson, Jean, and J. Lowy. 1963. “The Structure of F-Actin and of Actin Filaments Isolated from Muscle.” *Journal of Molecular Biology* 6 (1): 46–IN5.

Hirokawa, N., Y. Noda, Y. Tanaka, and S. Niwa. 2009. “Kinesin Superfamily Motor Proteins and Intracellular Transport.” *Nature Reviews. Molecular Cell Biology*. https://idp.nature.com/authorize/casa?redirect_uri=https://www.nature.com/articles/nrm2774&casa_token=97IAS4bN1wYAAAAA:nuPFimg5zIPb8R_4Vtx_trsFy6XY5kWKNadh2tus11LgWKB_cJ65IclwzZqAJCicR2c2qtdZmqqFji4.

Hirokawa, Nobutaka, Yasuko Noda, Yosuke Tanaka, and Shinsuke Niwa. 2009. “Kinesin Superfamily Motor Proteins and Intracellular Transport.” *Nature Reviews. Molecular Cell Biology* 10 (10): 682–96.

Hödl, Martina, and Konrad Basler. 2009. “Transcription in the Absence of Histone H3. 3.” *Current Biology: CB* 19 (14): 1221–26.

Hoffman, P. N., and D. W. Cleveland. 1988. “Neurofilament and Tubulin Expression Recapitulates the Developmental Program during Axonal Regeneration: Induction of a Specific Beta-Tubulin Isotype.” *Proceedings of the National Academy of Sciences of the United States of America* 85 (12): 4530–33.

Höök, Peter, and Richard B. Vallee. 2006. “The Dynein Family at a Glance.” *Journal of Cell Science* 119 (Pt 21): 4369–71.

Hoyle, H. D., and E. C. Raff. 1990. “Two Drosophila Beta Tubulin Isoforms Are Not Functionally Equivalent.” *The Journal of Cell Biology* 111 (3): 1009–26.

Ishikawa, H., R. Bischoff, and H. Holtzer. 1969. “Formation of Arrowhead Complexes with Heavy Meromyosin in a Variety of Cell Types.” *The Journal of Cell Biology* 43 (2): 312–28.

Jacobson, Raymond H., Andreas G. Ladurner, David S. King, and Robert Tjian. 2000. “Structure and Function of a Human TAFII250 Double Bromodomain Module.” *Science* 288 (5470): 1422–25.

Janke, Carsten, and Maria M. Magiera. 2020. “The Tubulin Code and Its Role in Controlling Microtubule Properties and Functions.” *Nature Reviews. Molecular Cell Biology* 21 (6): 307–26.

Kasinsky, H. E., J. D. Lewis, and J. B. Dacks. 2001. “Origin of H1 Linker Histones.” *The FASEB*. https://faseb.onlinelibrary.wiley.com/doi/abs/10.1096/fj.00-0237rev.

Kempf, Martina, Albrecht Clement, Andreas Faissner, Gloria Lee, and Roland Brandt. 1996. “Tau Binds to the Distal Axon Early in Development of Polarity in a Microtubule- and Microfilament-Dependent Manner.” *The Journal of Neuroscience*. https://doi.org/10.1523/jneurosci.16-18-05583.1996.

Khodiyar, Varsha K., Lois J. Maltais, Barbara J. Ruef, Katherine M. B. Sneddon, Jennifer R. Smith, Mary Shimoyama, Fernando Cabral, et al. 2007. "A Revised Nomenclature for the Human and Rodent Alpha-Tubulin Gene Family." *Genomics* 90 (2): 285–89.

Knight, A. E., and J. E. Molloy. 1999. "Coupling ATP Hydrolysis to Mechanical Work." *Nature Cell Biology*. https://idp.nature.com/authorize/casa?redirect_uri=https://www.nature.com/articles/ncb0899_E87&casa_token=cN0YFZysA8AAAAAA:U07l1IGfqwiB0bydUScXC6re5T2M-r0x3QUwRlo2Mk8KXvZ-93IYATdHn4Oa80xNSNZRYlxgUY6t2N8.

Komarova, Yulia, Gideon Lansbergen, Niels Galjart, Frank Grosveld, Gary G. Borisy, and Anna Akhmanova. 2005. "EB1 and EB3 Control CLIP Dissociation from the Ends of Growing Microtubules." *Molecular Biology of the Cell* 16 (11): 5334–45.

Kumar, A., K. Crawford, L. Close, M. Madison, J. Lorenz, T. Doetschman, S. Pawlowski, et al. 1997. "Rescue of Cardiac -Actin-Deficient Mice by Enteric Smooth Muscle -Actin." *Proceedings of the National Academy of Sciences*. https://doi.org/10.1073/pnas.94.9.4406.

Lauterborn, Robert. 1896. *Untersuchungen über bau: kernteilung und bewegung der diatomeen*. W. Engelmann.

Lawrence, Carolyn J., R. Kelly Dawe, Karen R. Christie, Don W. Cleveland, Scott C. Dawson, Sharyn A. Endow, Lawrence S. B. Goldstein, et al. 2004. "A Standardized Kinesin Nomenclature." *The Journal of Cell Biology* 167 (1): 19–22.

Ledbetter, M. C., and K. R. Porter. 1963. "A' Microtubule' in Plant Cell Fine Structure." *The Journal of Cell Biology* 19 (1): 239–50.

Lessard, Dominique V., Oraya J. Zinder, Takashi Hotta, Kristen J. Verhey, Ryoma Ohi, and Christopher L. Berger. 2019. "Polyglutamylation of Tubulin's C-Terminal Tail Controls Pausing and Motility of Kinesin-3 Family Member KIF1A." *The Journal of Biological Chemistry* 294 (16): 6353–63.

Li, Linda Xiaoyan, Julie Xia Zhou, Xiaodong Wang, Hongbing Zhang, Peter C. Harris, James P. Calvet, and Xiaogang Li. 2020. "Cross-Talk between CDK4/6 and SMYD2 Regulates Gene Transcription, Tubulin Methylation, and Ciliogenesis." *Science Advances* 6 (44). https://doi.org/10.1126/sciadv.abb3154.

Li, Rong, and Gregg G. Gundersen. 2008. "Beyond Polymer Polarity: How the Cytoskeleton Builds a Polarized Cell." *Nature Reviews. Molecular Cell Biology* 9 (11): 860–73.

Ludueña, R. F. 1998. “Multiple Forms of Tubulin: Different Gene Products and Covalent Modifications.” *International Review of Cytology* 178: 207–75.

Magri, E., M. Zaccarini, and E. Grazi. 1978. “The Interaction of Histone and Protamine with Actin. Possible Involvement in the Formation of the Mitotic Spindle.” *Biochemical and Biophysical Research Communications* 82 (4): 1207–10.

Mansfield, S. G., and P. R. Gordon-Weeks. 1991. “Dynamic Post-Translational Modification of Tubulin in Rat Cerebral Cortical Neurons Extending Neurites in Culture: Effects of Taxol.” *Journal of Neurocytology* 20 (8): 654–66.

Mayr, Monika I., Stefan Hümmer, Jenny Bormann, Tamara Grüner, Sarah Adio, Guenther Woehlke, and Thomas U. Mayer. 2007. “The Human Kinesin Kif18A Is a Motile Microtubule Depolymerase Essential for Chromosome Congression.” *Current Biology: CB* 17 (6): 488–98.

McKenney, Richard J., Walter Huynh, Ronald D. Vale, and Minhajuddin Sirajuddin. 2016. “Tyrosination of α-tubulin Controls the Initiation of Processive Dynein–dynactin Motility.” *The EMBO Journal* 35 (11): 1175–85.

Morales, Marisela, and Eva Fifkova. 1989. “Distribution of MAP 2 in Dendritic Spines and Its Colocalization with Actin.” *Cell and Tissue Research* 256 (3): 447–56.

Munnamalai, Vidhya, and Daniel M. Suter. 2009. “Reactive Oxygen Species Regulate F-Actin Dynamics in Neuronal Growth Cones and Neurite Outgrowth.” *Journal of Neurochemistry* 108 (3): 644–61.

Neff, N. F., J. H. Thomas, P. Grisafi, and D. Botstein. 1983. “Isolation of the Beta-Tubulin Gene from Yeast and Demonstration of Its Essential Function in Vivo.” *Cell* 33 (1): 211–19.

Nowak, Kristen J., Gianina Ravenscroft, Connie Jackaman, Aleksandra Filipovska, Stefan M. Davies, Esther M. Lim, Sarah E. Squire, et al. 2009. “Rescue of Skeletal Muscle α-Actin–null Mice by Cardiac (fetal) α-Actin.” *The Journal of Cell Biology* 185 (5): 903–15.

Nyman, Tomas, Herwig Schüler, Elena Korenbaum, Clarence E. Schutt, Roger Karlsson, and Uno Lindberg. 2002. “The Role of MeH73 in Actin Polymerization and ATP Hydrolysis.” *Journal of Molecular Biology* 317 (4): 577–89.

Panda, D., H. P. Miller, A. Banerjee, R. F. Ludueña, and L. Wilson. 1994. “Microtubule Dynamics in Vitro Are Regulated by the Tubulin Isotype Composition.” *Proceedings of the National Academy of Sciences of the United States of America* 91 (24): 11358–62.

Park, In Young, Reid T. Powell, Durga Nand Tripathi, Ruhee Dere, Thai H. Ho, T. Lynne Blasius, Yun Chen Chiang, et al. 2016. “Dual Chromatin and Cytoskeletal Remodeling by SETD2.” *Cell* 166 (4): 950–62.

Paul, Danielle M., Judith Mantell, Ufuk Borucu, Jennifer Coombs, Katherine J. Surridge, John M. Squire, Paul Verkade, and Mark P. Dodding. 2020. “In Situ Cryo-Electron Tomography Reveals Filamentous Actin within the Microtubule Lumen.” *The Journal of Cell Biology* 219 (9). https://doi.org/10.1083/jcb.201911154.

Peris, Leticia, Manuel Thery, Julien Fauré, Yasmina Saoudi, Laurence Lafanechère, John K. Chilton, Phillip Gordon-Weeks, et al. 2006. “Tubulin Tyrosination Is a Major Factor Affecting the Recruitment of CAP-Gly Proteins at Microtubule plus Ends.” *The Journal of Cell Biology* 174 (6): 839–49.

Person, Fermín, Waldemar Wilczak, Claudia Hube-Magg, Christoph Burdelski, Christina Möller-Koop, Ronald Simon, Mercedes Noriega, et al. 2017. “Prevalence of βIII-Tubulin (TUBB3) Expression in Human Normal Tissues and Cancers.” *Tumor Biology*. https://doi.org/10.1177/1010428317712166.

Petry, Sabine. 2016. “Mechanisms of Mitotic Spindle Assembly.” *Annual Review of Biochemistry* 85 (June): 659–83.

Rea, S., F. Eisenhaber, D. O’Carroll, B. D. Strahl, and Z. W. Sun. 2000. “Regulation of Chromatin Structure by Site-Specific Histone H3 Methyltransferases.” *Nature*. https://idp.nature.com/authorize/casa?redirect_uri=https://www.nature.com/articles/35020506&casa_token=g9f9MHYk5XcAAAAA:jDI0QPDi_ZO4eFFV15aX0AdIh1t65lKF05n8wMyW1aWvnAkkWTVwMhhCQ6ZDUr3T4EigwkOq9Sq8JS4.

Redman, Kent L., and Peter A. Rubenstein. 1984. “[16] Actin Amino-Terminal Acetylation and Processing in a Rabbit Reticulocyte Lysate.” *Methods in Enzymology*. https://doi.org/10.1016/0076-6879(84)06018-3.

Reed, Nathan A., Dawen Cai, T. Lynne Blasius, Gloria T. Jih, Edgar Meyhofer, Jacek Gaertig, and Kristen J. Verhey. 2006. “Microtubule Acetylation Promotes Kinesin-1 Binding and Transport.” *Current Biology: CB* 16 (21): 2166–72.

Roberts, Anthony J., Brian S. Goodman, and Samara L. Reck-Peterson. 2014. “Reconstitution of Dynein Transport to the Microtubule plus End by Kinesin.” *eLife* 3: 1–16.

Rüdiger, M., U. Plessman, K. D. Klöppel, J. Wehland, and K. Weber. 1992. “Class II Tubulin, the Major Brain Beta Tubulin Isotype Is Polyglutamylated on Glutamic Acid Residue 435.” *FEBS Letters* 308 (1): 101–5.

Santaguida, Stefano, and Andrea Musacchio. 2009. “The Life and Miracles of Kinetochores.” *The EMBO Journal* 28 (17): 2511–31.

Santos-Rosa, Helena, and Carlos Caldas. 2005. “Chromatin Modifier Enzymes, the Histone Code and Cancer.” *European Journal of Cancer* 41 (16): 2381–2402.

Santos-Rosa, H., R. Schneider, A. J. Bannister, and J. Sherriff. 2002. “Active Genes Are Tri-Methylated at K4 of Histone H3.” *Nature*. https://idp.nature.com/authorize/casa?redirect_uri=https://www.nature.com/articles/nature01080&casa_token=HcUY6lWchVoAAAAA:H6wEnF8XmVJuv26ubWa9TpItCi---170ekypAR_ZJHbsHxzZ6jJ0cEfefy_REYBzWtIIGPrG0pKsMV4.

Schatz, P. J., G. E. Georges, and F. Solomon. 1987. “Insertions of up to 17 Amino Acids into a Region of Alpha-Tubulin Do Not Disrupt Function in Vivo.” *Molecular and Cellular*. https://mcb.asm.org/content/7/10/3799.short.

Schatz, P. J., L. Pillus, P. Grisafi, F. Solomon, and D. Botstein. 1986. “Two Functional Alpha-Tubulin Genes of the Yeast Saccharomyces Cerevisiae Encode Divergent Proteins.” *Molecular and Cellular Biology* 6 (11): 3711–21.

Schildmeyer, Lisa A., Renee Braun, George Taffet, Mariella Debiasi, Alan E. Burns, Allan Bradley, and Robert J. Schwartz. 2000. “Impaired Vascular Contractility and Blood Pressure Homeostasis in the Smooth Muscle α-actin Null Mouse.” *FASEB Journal: Official Publication of the Federation of American Societies for Experimental Biology* 14 (14): 2213–20.

Schliwa, Manfred. 1999. “Structural and Functional Features of the Kinesin Molecule.” *Biology of the Cell*. https://doi.org/10.1016/s0248-4900(99)90099-0.

Seervai, Riyad N. H., Rahul K. Jangid, Menuka Karki, Durga Nand Tripathi, Sung Yun Jung, Sarah E. Kearns, Kristen J. Verhey, et al. 2020. “The Huntingtin-Interacting Protein SETD2/HYPB Is an Actin Lysine Methyltransferase.” *Science Advances*. https://doi.org/10.1126/sciadv.abb7854.

Sellers, J. R. 2000. “Myosins: A Diverse Superfamily.” *Biochimica et Biophysica Acta* 1496 (1): 3–22.

Serebryannyy, Leonid A., Christina M. Cruz, and Primal de Lanerolle. 2016. “A Role for Nuclear Actin in HDAC 1 and 2 Regulation.” *Scientific Reports*. https://doi.org/10.1038/srep28460.

Shawlot, William, Jian Min Deng, Laurel E. Fohn, and Richard R. Behringer. 1998. “Restricted [beta]-Galactosidase Expression of a Hygromycin-lacZ Gene Targeted to the [beta]-Actin Locus and Embryonic Lethality of [beta]-Actin Mutant Mice.” *Transgenic Research* 7 (2): 95.

Shen, X., G. Mizuguchi, A. Hamiche, and C. Wu. 2000. “A Chromatin Remodelling Complex Involved in Transcription and DNA Processing.” *Nature* 406 (6795): 541–44.

Sirajuddin, Minhajuddin, Luke M. Rice, and Ronald D. Vale. 2014. “Regulation of Microtubule Motors by Tubulin Isotypes and Post-Translational Modifications.” *Nature Cell Biology*. https://doi.org/10.1038/ncb2920.

Sol, Asaf, Yaniv Skvirsky, Edna Blotnick, Gilad Bachrach, and Andras Muhlrad. 2016. “Actin and DNA Protect Histones from Degradation by Bacterial Proteases but Inhibit Their Antimicrobial Activity.” *Frontiers in Microbiology* 7 (August): 1248.

Szent-Györgyi, Albert. 1942. *Studies from the Institute of Medical Chemistry, University Szeged: Vol. 2*. S. Karger.

Tagami, Hideaki, Dominique Ray-Gallet, Geneviève Almouzni, and Yoshihiro Nakatani. 2004. “Histone H3.1 and H3.3 Complexes Mediate Nucleosome Assembly Pathways Dependent or Independent of DNA Synthesis.” *Cell*. https://doi.org/10.1016/s0092-8674(03)01064-x.

Talbert, Paul B., and Steven Henikoff. 2010a. “Histone Variants—ancient Wrap Artists of the Epigenome.” *Nature Reviews. Molecular Cell Biology* 11 (4): 264–75.

———. 2010b. “Histone Variants — Ancient Wrap Artists of the Epigenome.” *Nature Reviews Molecular Cell Biology*. https://doi.org/10.1038/nrm2861.

Tas, Roderick P., Anaël Chazeau, Bas M. C. Cloin, Maaike L. A. Lambers, Casper C. Hoogenraad, and Lukas C. Kapitein. 2017. “Differentiation between Oppositely Oriented Microtubules Controls Polarized Neuronal Transport.” *Neuron* 96 (6): 1264–71.e5.

Terman, Jonathan R., and Anna Kashina. 2013. “Post-Translational Modification and Regulation of Actin.” *Current Opinion in Cell Biology* 25 (1): 30–38.

Theurkauf, W. E., H. Baum, J. Bo, and P. C. Wensink. 1986. “Tissue-Specific and Constitutive Alpha-Tubulin Genes of Drosophila Melanogaster Code for Structurally Distinct Proteins.” *Proceedings of the National Academy of Sciences of the United States of America* 83 (22): 8477–81.

Tortosa, Elena, Carolina Montenegro-Venegas, Marion Benoist, Steffen Härtel, Christian González-Billault, Jose A. Esteban, and Jesús Avila. 2011. “Microtubule-Associated Protein 1B (MAP1B)

Is Required for Dendritic Spine Development and Synaptic Maturation." *The Journal of Biological Chemistry* 286 (47): 40638–48.

Vale, R. D., and R. A. Milligan. 2000. "The Way Things Move: Looking under the Hood of Molecular Motor Proteins." *Science*. https://science.sciencemag.org/content/288/5463/88.abstract?casa_token=JO_CiarT_tcAAAAA:rhvyFrBJskaWBjCNYWSt2Fw-4FZYwPmO8aQgY2Uv--T3znyF9zQmbpao_jIiR0OU1PfEYQjwMeEG.

Vallee, R. B., H. S. Shpetner, and B. M. Paschal. 1989. "The Role of Dynein in Retrograde Axonal Transport." *Trends in Neurosciences*. https://doi.org/10.1016/0166-2236(89)90138-0.

Varland, Sylvia, Joël Vandekerckhove, and Adrian Drazic. 2019. "Actin Post-Translational Modifications: The Cinderella of Cytoskeletal Control." *Trends in Biochemical Sciences* 44 (6): 502–16.

Vedula, Pavan, and Anna Kashina. 2018. "The Makings of the 'Actin Code': Regulation of Actin's Biological Function at the Amino Acid and Nucleotide Level." *Journal of Cell Science* 131 (9). https://doi.org/10.1242/jcs.215509.

Veigel, Claudia, Lynne M. Coluccio, James D. Jontes, John C. Sparrow, Ronald A. Milligan, and Justin E. Molloy. 1999. "The Motor Protein Myosin-I Produces Its Working Stroke in Two Steps." *Nature* 398 (6727): 530–33.

Verhey, Kristen J., and Jacek Gaertig. 2007. "The Tubulin Code." *Cell Cycle* 6 (17): 2152–60.

Verhey, Kristen J., and Jennetta W. Hammond. 2009. "Traffic Control: Regulation of Kinesin Motors." *Nature Reviews. Molecular Cell Biology* 10 (11): 765–77.

Waterman-Storer, Clare M., and E. D. Salmon. 1997. "Actomyosin-Based Retrograde Flow of Microtubules in the Lamella of Migrating Epithelial Cells Influences Microtubule Dynamic Instability and Turnover and Is Associated with Microtubule Breakage and Treadmilling." *Journal of Cell Biology*. https://doi.org/10.1083/jcb.139.2.417.

Weinhold, Bob. 2006. "Epigenetics: The Science of Change." National Institute of Environmental Health Sciences. https://ehp.niehs.nih.gov/doi/abs/10.1289/ehp.114-a160.

Wilkinson, Alex W., Jonathan Diep, Shaobo Dai, Shuo Liu, Yaw Shin Ooi, Dan Song, Tie-Mei Li, et al. 2018. "SETD3 Is an Actin Histidine Methyltransferase That Prevents Primary Dystocia." *Nature*, December, 1.

Wilson, Carlos, and Christian González-Billault. 2015. “Regulation of Cytoskeletal Dynamics by Redox Signaling and Oxidative Stress: Implications for Neuronal Development and Trafficking.” *Frontiers in Cellular Neuroscience* 9 (September): 381.

Wu, Shumin, and Judd C. Rice. 2011. “A New Regulator of the Cell Cycle: The PR-Set7 Histone Methyltransferase.” *Cell Cycle* 10 (1): 68–72.

Yue, Yang, Lynne Blasius, Stephanie Zhang, Shashank Jariwala, Benjamin Walker, Barry J. Grant, Jared C. Cochran, and Kristen J. Verhey. 2018. “Altered Chemomechanical Coupling Causes Impaired Motility of the Kinesin-4 Motors KIF27 and KIF7.” *The Journal of Cell Biology* 217 (4): 1319–34.

Yu, Ian, Christopher P. Garnham, and Antonina Roll-Mecak. 2015. “Writing and Reading the Tubulin Code.” *The Journal of Biological Chemistry* 290 (28): 17163–72.

Yu, I., T. Mori, T. Ando, R. Harada, J. Jung, and Y. Sugita. 2016. “Biomolecular Interactions Modulate Macromolecular Structure and Dynamics in Atomistic Model of a Bacterial Cytoplasm.” *eLife*. https://elifesciences.org/articles/19274.

Zhang, Jamie, Jiping Yue, and Xiaoyang Wu. 2017. “Spectraplakin Family Proteins – Cytoskeletal Crosslinkers with Versatile Roles.” *Journal of Cell Science*. https://doi.org/10.1242/jcs.196154.

Zhou, Feng-Quan, Clare M. Waterman-Storer, and Christopher S. Cohan. 2002. “Focal Loss of Actin Bundles Causes Microtubule Redistribution and Growth Cone Turning.” *The Journal of Cell Biology* 157 (5): 839–49.

Zlatanova, Jordanka, and Amit Thakar. 2008. “H2A.Z: View from the Top.” *Structure* 16 (2): 166–79.

Chapter 2 - Cytoskeletal Methylation by SETD2

2.1 Forward

This chapter will introduce cellular post-translational modifications, focusing on the Histone and Tubulin Codes. Working closely with our collaborators, the Walker Lab at the Baylor College of Medicine and Rathmell lab at Vanderbuilt, we explore tubulin methylation by SETD2 biochemically. Part of this work is published in Kearns 2020 on *bioRxiv* and submitted (at time of thesis publication) to *JBC*. In addition, we find that SETD2 also methylates another cytoskeletal element, actin, published in Riyad 2020 *Sci. Advances*, in collaboration with the Walker lab of the Baylor College of Medicine.

2.2 Introduction

Microtubules are dynamic cytoskeletal polymers that maintain cell shape, serve as tracks for intracellular trafficking, provide a structural framework for cell division, and form the structural elements of cilia. How microtubules achieve their many varied cellular functions comes, in part, from a tubulin code of multiple isoforms of α- and β-tubulin dimers and varied post-translational modifications (PTMs) (Verhey and Gaertig 2007; Gadadhar et al. 2017; Roll-Mecak 2019). For example, differentiated cells express varying amounts of α- and β-tubulin isotypes to perform specialized roles (Leandro-García et al. 2010). Additionally, within each cell there are

subpopulations of microtubules with PTMs that further regulate microtubule-based functions. Analogous to how the histone code directs chromatin function, the combination of tubulin isotypes and PTMs comprise a tubulin code that specializes microtubule function in cells.

One key chromatin modifier that contributes to both the histone and tubulin codes is SET domain containing 2 (SETD2). Our previous work demonstrated that SETD2 can methylate tubulin and that methylation occurs at Lysine 40 of α-tubulin (αTubK40me3) (Park et al. 2016). In a mitotic spindle context, which is where tubulin methylation has been found in cells, the correct bipolar geometry structure is critical for proper cell division. The microtubules comprising the mitotic spindle form interpolar microtubules to establish spindle bipolarity, aid in chromosome congression (Zhai, Kronebusch, and Borisy 1995; O'Toole, Morphew, and McIntosh 2019), and connect kinetochores with spindle poles to segregate chromatids (Maiato et al. 2017; Musacchio 2015). As such, microtubules are highly dynamic and regulated during spindle formation and mitosis (T. Mitchison et al. 1986; T. J. Mitchison 1989; Lu and Johnston 2013; Petry 2016). Defects in the mitotic spindle, be they microtubule-, kinetochore-, or motor protein-driven, cause abnormal spindle structure resulting in chromosome mis-segregation and aneuploidy (Silkworth and Cimini 2012). Checkpoints during cell division exist to prevent improper cell division, but in disease or cancer states, aberrant cell growth and division override the elaborate checkpoint pathways (Vermeulen, Van Bockstaele, and Berneman 2003). In dividing cells, αTubK40me3 localizes to the minus ends of microtubules that form the mitotic spindle, and is enzymatically added by SETD2. This methyltransferase also tri-methylates histones at the histone 3 lysine 36 (H3K36me3) (Edmunds, Mahadevan, and Clayton 2008). Many aspects of SETD2 function are still unexplained, such as how SETD2 recognizes and differentiates substrates.

Here, I took a biochemical reconstitution approach to define the minimal components required to methylate tubulin *in vitro*. Using a purified N-terminal truncated construct of SETD2 which contains everything from the SET domain, beyond the SRI-domain, to the C-terminus of the enzyme (tSETD2) and recombinant human tubulin (Yu et al. 2016; Ti, Alushin, and Kapoor 2018; Ti, Wieczorek, and Kapoor 2020), I had precise control of tubulin isotype and PTM-state *in vitro* and could generate mutant versions of tubulin to probe site selectivity of SETD2 methylation. I demonstrate that tSETD2 is sufficient to methylate tubulin *in vitro* and has a higher activity towards tubulin dimers over microtubules. I verify that the methylation site is on α-tubulin lysine 40 (αTubK40), the same site that can be acetylated (L'Hernault and Rosenbaum 1985; LeDizet

and Piperno 1987; Davenport et al. 2014), and find that tSETD2 sequesters tubulin in solution, thus altering microtubule dynamics. I found that SETD2 recognizes the negatively-charged C-terminal tail of α-tubulin. Additionally, work with collaborators found that SETD2 also methylates actin as well, and I found that globular and filamentous actin are both substrates because the methylation site, K68, is accessible in both populations. This work begins to understand how cytoskeletal substrates are recognized for SETD2-mediated methylation.

2.3 Results

2.3.1 SETD2 can methylate tubulin in vitro

To investigate the underlying biochemistry of tubulin methylation by SETD2, we generated a truncated construct containing everything from the catalytic SET domain to the C-terminus in

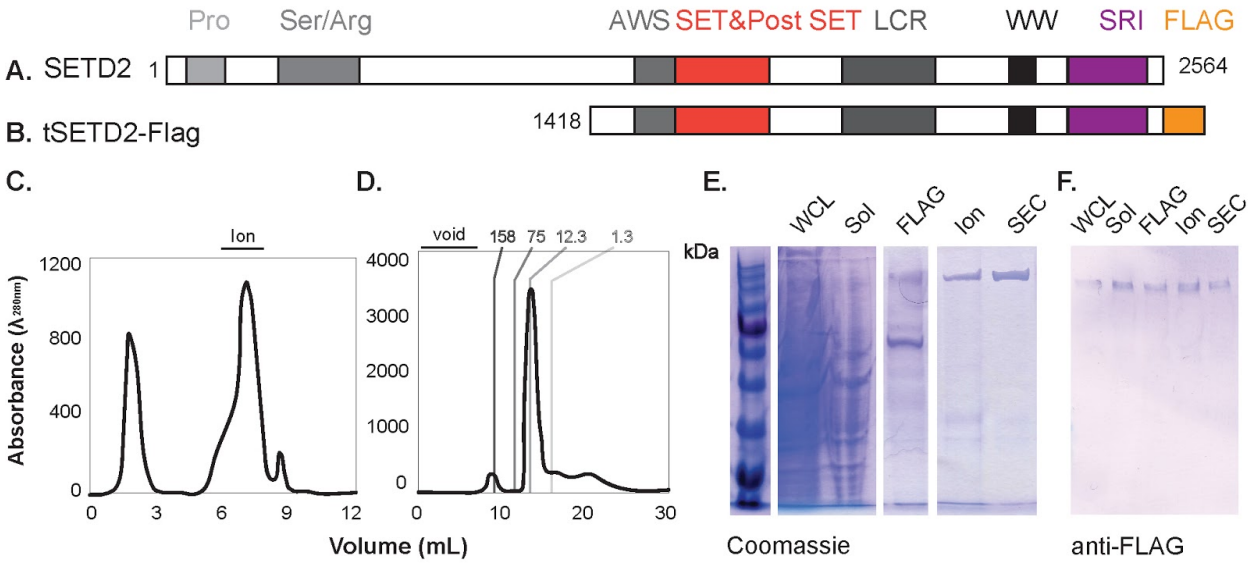

Fig. 2.1 Purification of tSETD2-Flag. A-B) Cartoon diagram depicting domains of A) Full length SETD2 and B) tSETD2-FLAG, the latter being the construct we utilize in experiments, henceforth. While there are many domain architectures in this protein (depicted in various grey colors), we will be focusing on the catalytic SET domain (red), and SRI domain (purple). Note that the C-terminal FLAG tag (yellow) will be used for purification, immunofluorescence, and western blots in later experiments. C-D) 280 nm absorbance spectra of C) Ion exchange and D) size exclusion chromatography. E) Coomassie gel and F) anti-FLAG western blot of fractions of whole cell lysate (WCL), soluble fraction after ultracentrifugation (Sol), FLAG-bead elution (FLAG), post-ion exchange (Ion), and size exclusion chromatography fractions (SEC).

We first tested to see how this construct expressed in cells. We transfected tSETD2-FLAG into COS-7 cells and cultured them before fixing and immunostaining them with antibodies anti-FLAG and -tubulin, and DNA (DAPI) followed by fluorescent secondary antibodies for imaging. Using fluorescence microscopy, we observed cells mostly in interphase (Fig. 2.2A) and were lucky enough to catch a handful of cells undergoing mitosis. During interphase, tSETD2-Flag predominantly localized in the nucleus whereas during mitosis tSETD2-FLAG dispersed throughout the cell's cytoplasm (Fig. 2.2B). This is comparable to full length SETD2-FLAG localization in cells (Fig. 2.2A-B). These data suggest that tSETD2-FLAG construct localizes normally *in vivo* and, as such, likely folds properly and behaves as expected in cells.

I purified this truncated construct with a series of purification steps (Fig. 2.1C-F). First, HEK293 cells overexpressing tSETD2-FLAG were harvested (Whole cell lysate, WCL) and

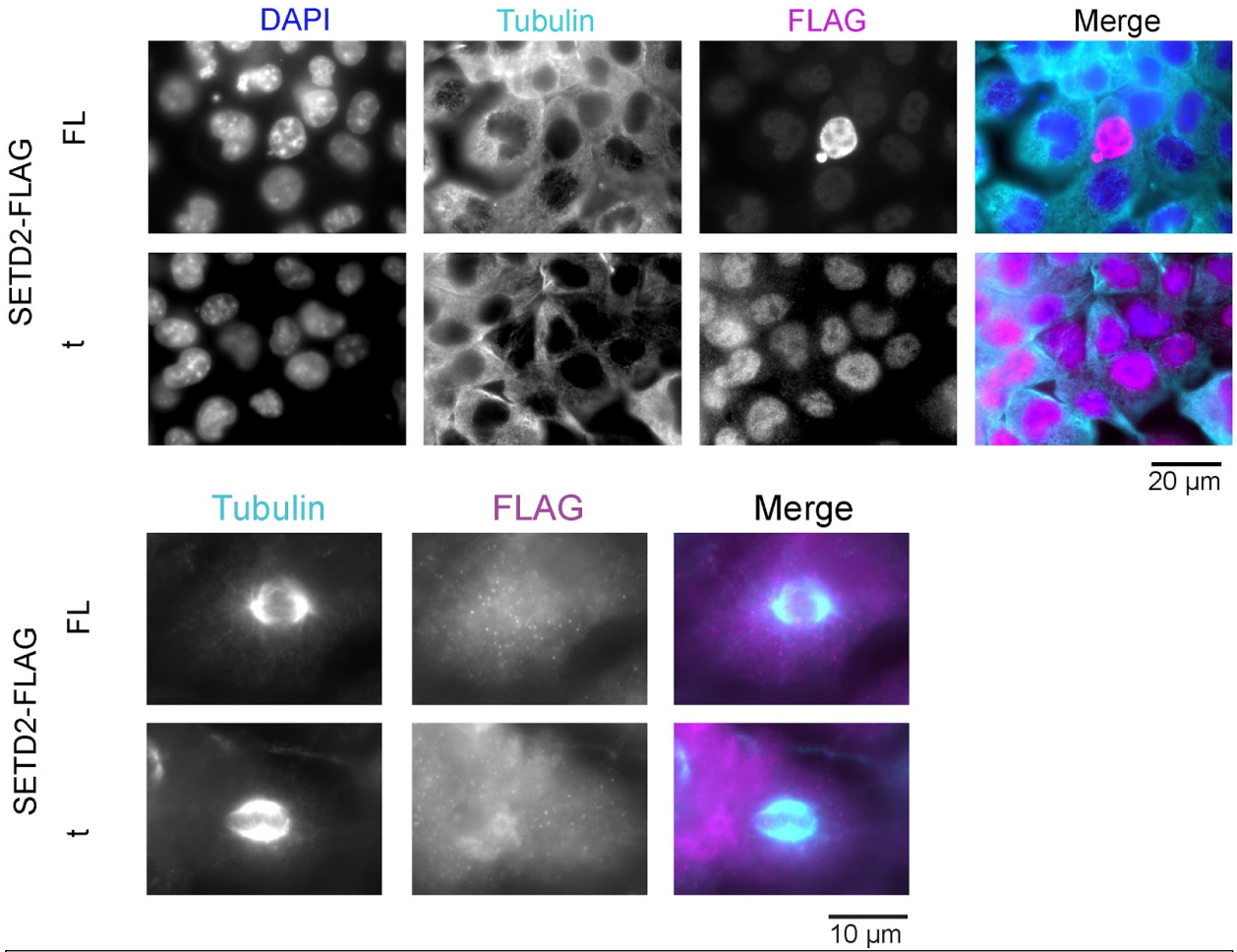

Fig. 2.2 SETD2 overexpression in COS-7 cells. Top) Interphase cells and Bottom) Mitotic cells stained for DNA (DAPI, dark blue), tubulin (cyan), and FLAG (pink).

clarified (Sol.) before being added to FLAG resin. FLAG elution was run through an ion exchange column (Fig. 2.1C) before size exclusion chromatography (Fig. 2.2D). Fractions were analyzed by Coomassie gel (Fig. 2.1E) and western blot with anti-FLAG antibodies (Fig. 2.1F).

I then turned towards biochemical experiments to monitor methyltransferase activity. To do this. I utilized an assay that monitors the production of S-adenosyl-homocysteine (SAH), a byproduct of SAM-dependent methyl transfer, via enzyme-coupling resulting in fluorescence (Dorgan et al. 2006). In this coupled assay, SAH is converted into resorufin. With a standard curve of resorufin concentrations and fluorescence, fluorescence over time is converted to methyltransferase activity. When tSETD2-FLAG is given its methyl donor SAM in addition to either histone H3 peptide (aa 21-44) or porcine brain tubulin substrate, the observed fluorescence over time suggests methyl transfer activity towards both substrates (Fig. 2.3A). To control for any potential auto-methylation of tSETD2-FLAG, enzyme without substrate with SAM was monitored as well and the background signal was subtracted (Fig. 2.3C). When the concentration of substrate is varied, the measured initial velocities generate a Michaelis-Menten plot of reaction velocity as a function of substrate concentration (Fig. 2.3B). From this type of kinetic plot, kinetic constants can be derived like the Michaelis-Menten constant, K_M, a kinetic constant describing the concentration of substrate that results in half the enzyme's maximal activity, and the v_{max}, the maximal activity rate (Fig. 2.3D). K_M values for tubulin and H3 peptide substrates (0.75±0.06 mM and 0.45±0.32 mM, respectively) suggest that tSETD2-FLAG has slightly different affinities depending on substrate. However, the v_{max} with tubulin protein (3.98±0.12 nmol/min) as a substrate was lower compared to H3 peptide (5.41±0.48 nmol/min), suggesting that tSETD2 has a higher activity toward the H3 peptide. Taken together, these data indicated that, while the reconstituted protein has activity towards tubulin substrates, it has better activity with histone peptide substrate.

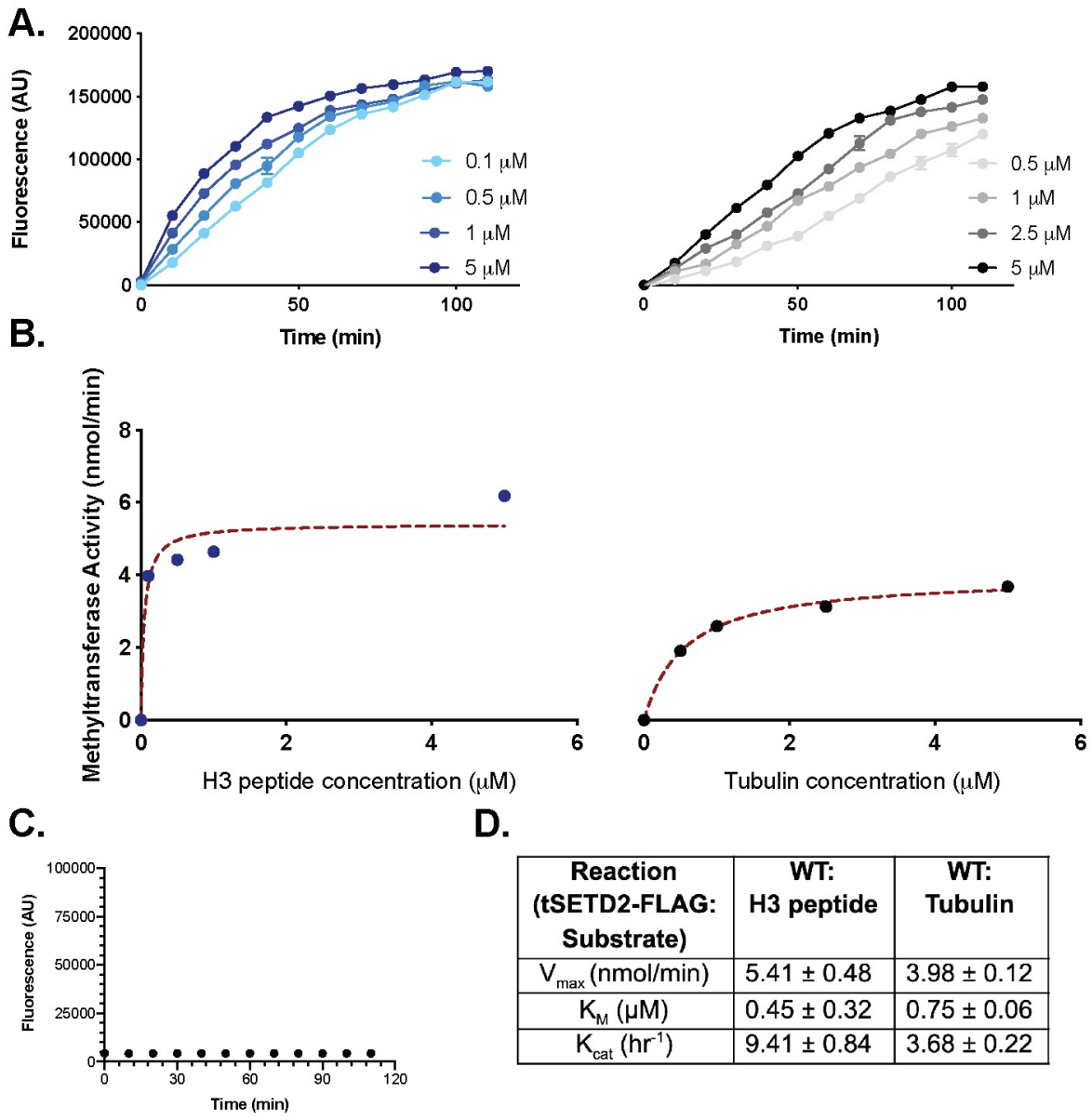

Reaction (tSETD2-FLAG: Substrate)	WT: H3 peptide	WT: Tubulin
V_{max} (nmol/min)	5.41 ± 0.48	3.98 ± 0.12
K_M (μM)	0.45 ± 0.32	0.75 ± 0.06
K_{cat} (hr^{-1})	9.41 ± 0.84	3.68 ± 0.22

Fig. 2.3 Methylation activity of tSETD2-FLAG. A-B. tSETD2-FLAG with various concentrations of histone H3 peptide (blue) or tubulin (black) substrates. A) Fluorescence traces and B) Michaelis-Menten curves. C. tSETD2-FLAG without substrate to background subtract automethylation. D. Kinetic values calculated from B.

At physiological temperatures, tubulin will self-assemble into microtubule polymers and grow and shrink in a process called dynamic instability (Walker et al. 1988; Desai and Mitchison 1997; Manka and Moores 2018). As such, we next wanted to determine if tSETD2-FLAG was

modifying tubulin dimers or microtubule polymers (Fig. 2.4A). To test this, we used small molecules: taxol to stabilize polymerized microtubules and podophyllotoxin to inhibit polymerization thus ensuring a tubulin dimer state (Jordan, Thrower, and Wilson 1992; Ojima et al. 1999), which we confirmed visually with cryoEM (Fig. 2.4B), We performed a similar methyltransferase assay as before, monitoring fluorescence over time (Fig. 2.4C). From this, we found that the activity of tSETD2-FLAG is almost three-fold higher for dimers than microtubule polymers when the substrate concentration is 5 μM (Fig. 2.4D). That said, when we varied the substrate concentration to calculate Michaelis-Menten constant and vmax, we found that the binding kinetics are similar. For tubulin dimers and microtubules, K_M values are 0.057±0.038 μM and 0.048±0.013 μM, respectively (Fig. 2.4E). This suggested that tSETD2-FLAG has a slightly higher affinity for microtubules but higher activity towards tubulin dimers.

To verify that tSETD2-FLAG can bind microtubules, a microtubule sedimentation assay was performed. This assay assesses protein-microtubule interactions by measuring the amount of protein that co-pellets with microtubules by centrifugation followed by SDS-PAGE analysis of the supernatant and pellet fractions. If tSETD2-FLAG can bind to microtubules, signal at 125 kDa would be in the pellet fraction, whereas if it does not associate to the polymer, it would be in the soluble fraction. A strong signal appeared in the soluble fraction at 125 kDa, the size of tSETD2-FLAG, nevertheless, there was a small signal in the pellet fraction as well (Fig. 2.4F) suggesting that tSETD2-FLAG can bind to microtubules However, without a negative control of tSETD2-FLAG alone, the protein found in the pellet fraction could just be aggregation, but we believe this to be unlikely. Taken together, tSETD2-FLAG can bind and methylate both tubulin dimers and microtubule polymers but has a higher activity toward tubulin dimers.

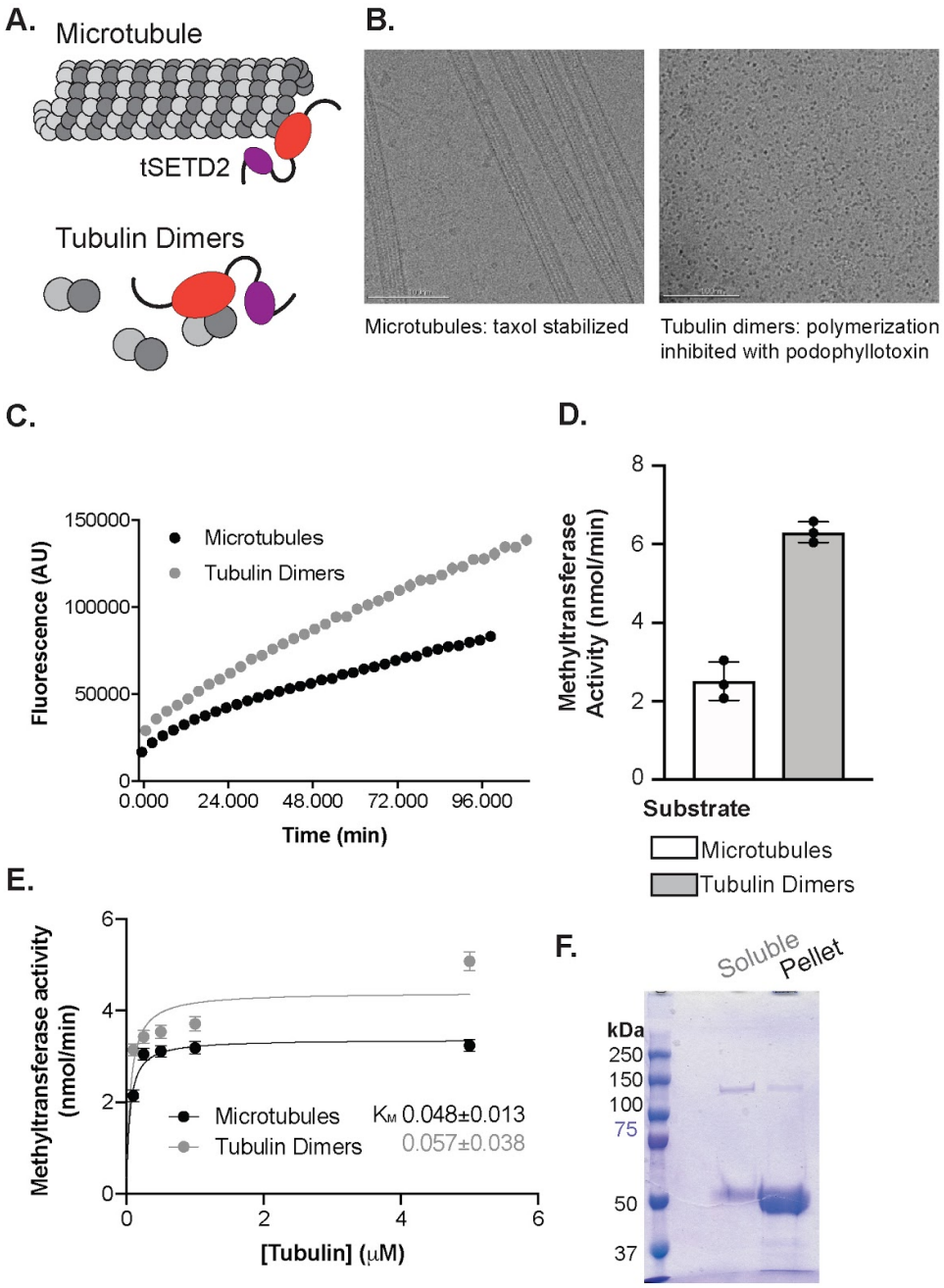

Fig. 2.4 tSETD2-FLAG has higher activity with tubulin dimers. A) Cartoon schematic of microtubules and tubulin dimers. B) CryoEM micrographs of left) taxol stabilized microtubules and right) tubulin dimers. C) Fluorescence traces of methyltransferase activity of tSETD2-FLAG with microtubules (black) and tubulin dimers (grey). D) Quantification of methyltransferase activity of tSETD2-FLAG. E) Michaelis-Menten kinetic plots varying substrate concentration of microtubules (black) or tubulin dimers (grey). F) Co-pelleting assay showing tSETD2-FLAG binding to microtubules (pellet).

2.3.2 SETD2 methylates tubulin at alpha-K40

To determine the tubulin methylation site by tSETD2-FLAG, we used recombinant single-isotype tubulin rather than porcine brain tubulin. The tubulin that we have been using so far, again, is sourced from pig brains and as such it has many different isotypes and PTMs. In trying to study a particular component of the complex tubulin code, we did not want all of these

compounding factors of existing modifications. In addition, having many isotypes and other modifications will make identification of a single, and sparse, modification difficult to detect biochemically. As such, I reduced the complexity of the system by using a recombinant tubulin. Historically, it has been difficult to express and purify recombinant tubulin because of the complex folding pathway tubulin requires (Lewis, Tian, and Cowan 1997; Beghin, Galmarini, and Dumontet 2007; Matthews 2009). As such, tubulin cannot be expressed and purified in bacteria, and instead higher-order organisms and expression systems are required, like yeast, insect, or mammalian cells (Johnson et al. 2011; Minoura et al. 2013; Yu et al. 2016).

For our studies, we expressed and purified single isotype αTub1B/βTub3 using an insect expression plasmid generously gifted from the Kapoor Lab. We used this isotype combination because it is the one most expressed in the brain and as such would serve as a good comparison to our experiments so far (Leandro-García et al. 2010; Bitterman et al. 2018). In this dual expression system, each tubulin monomer has an affinity tag separated by a TEV cleavage site in order to utilize affinity chromatography during purification yet still be able to have tag-less tubulin at the end of the day (Fig. 2.5A). After using affinity columns in tandem, HisTrap (Fig. 2.5B) and StrepTrap (Fig. 2.5C), size exclusion is performed post-TEV cleavage to get purified tubulin dimers (Fig. 2.5D). Each fraction was analyzed by SDS-PAGE gel (Fig. 2.5E) In order to use this purified tubulin for experiments, it was necessary to concentrate the protein down to at least 3 mg/mL before flash freezing and storing at -80C.

Once we had purified tubulin, we verified that it would form functional microtubule polymers. We did this by using a non-hydrolyzable GTP analogue, GMPCPP, to make stabilized microtubules. To image microtubules via total internal reflection fluorescence microscopy (TIRFM), we additionally spiked the polymerization mixture with biotinylated and fluorescently

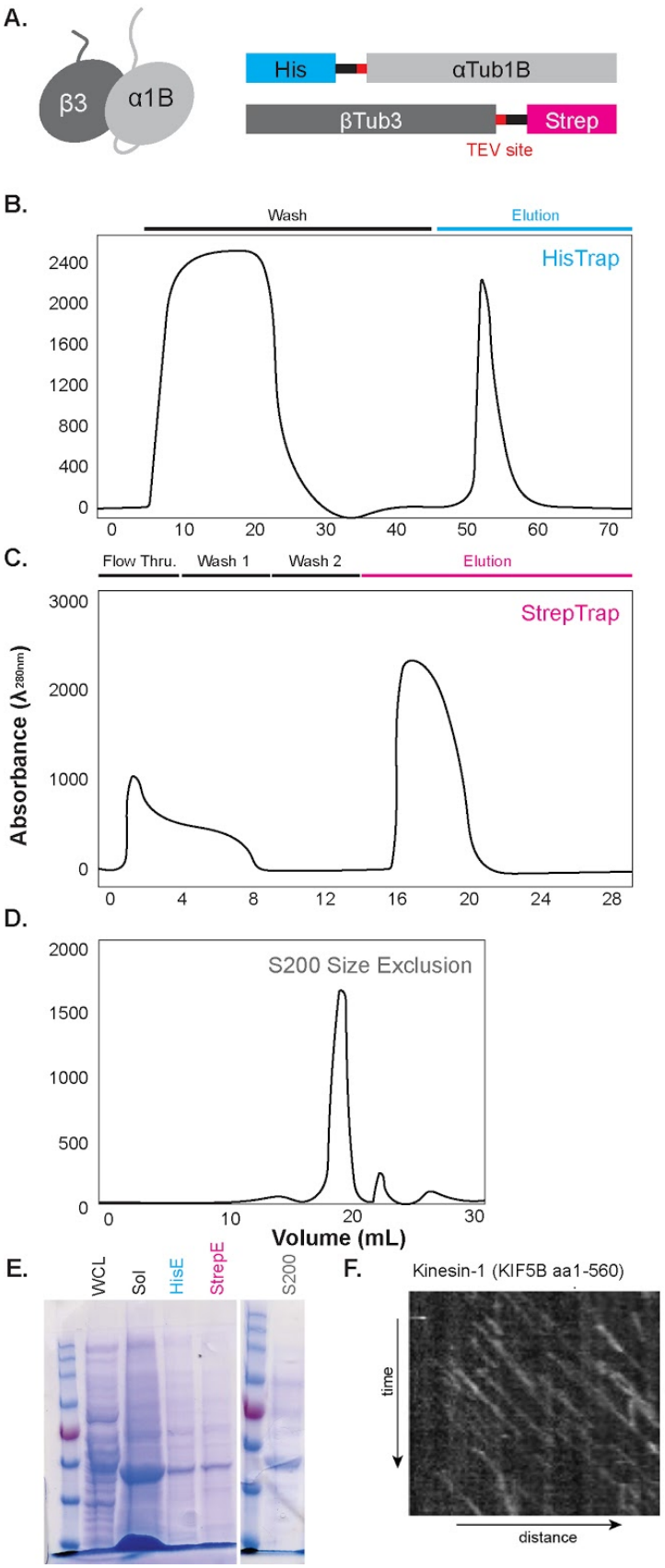

tagged porcine brain tubulin. We next determined if these microtubules are functional as molecular roads for kinesin motility. We overexpressed kinesin-1 (*Rattus norvegicus (Rn)* KIF5C 1-560) with an m-Citrine tag (KIF5C560-mCit) in COS-7 cells and generated a cell lysate containing these fluorescently labeled proteins. Adding

Fig. 2.5 Purifying functional single-isotype tubulin from insect cells. A) Cartoon schematic of left) alpha and beta tubulin and right) single isotype construct of αTub1B/βTub3. B-E) Purification of single isotype tubulin using B) HisTrap affinity, C) StrepTrap affinity, and D) size exclusion chromatography. E) Coomassie gel electrophoresis of each step along the purification. F) Single isotype tubulin was polymerized in the presence of biotin- and 674-labeled porcine brain tubulin for TIRF microscopy. Fluorescently labeled kinesin-1 motor (KIF5B-560-3xmCit) lysate was added and motility was observed over time. Kymograph analysis on microtubules shows single-molecule progression indicating functional microtubules.

these kinesins from cell lysate to a flow chamber in the presence of ATP, we were able to monitor single-molecule motility showing that our microtubules are functional (Fig. 2.5F).

Previous studies indicated that methylation occurred on αTubK40, a site that is found on a flexible loop of α-tubulin (Fig. 2.6A). We wanted to verify these previous findings and seek to identify any other methylation sites to tubulin by SETD2. As such we performed site-directed mutagenesis to generate αTubK40A (Fig. 2.6B-C), I verified that the αTubK40A-containing tubulin can form microtubules imaged via TIRFM (Fig. 2.6D). I then carried out methyltransferase activity assays with both the WT and αK40A single-isotype recombinant tubulin. I found that tSETD2-FLAG had reduced activity against αTubK40A when compared to the WT control (Fig. 2.6E-F).

The decrease in methyltransferase activity with αK40A suggested that either there are additional methylation sites on tubulin, or that the K40 loop of α-tubulin is important for substrate recognition by tSETD2-FLAG. To identify other methylation sites, mass spectrometry experiment was performed mixing tSETD2-FLAG in the presence and absence of SAM in the presence and absence of recombinant tubulin substrate, either WT or aTubK40A. Reaction mixtures were digested with chymotrypsin, followed by LC-MS/MS, and analyzed with PEAKS X. Interestingly, we were only able to detect methylation in the reaction with SAM with WT recombinant tubulin, suggesting that there are no other detectable methylation sites on tubulin (Fig. 2.6 G). The residual activity we see in the methyltransferase activity, as such, could be background methylation of tSETD2 of another protein that was pulled down during purification. Additionally, our mass spectrometry shows only a single methylation on αK40, whereas previous studies using tubulin from cells identified trimethylation. These discrepancies suggest that there may be other methyltransferases in cells that perform mono- or di-methylation to prime tubulin for methylation by SETD2, or that any additional methylation site not being picked up by our protein digestion and mass spectrometry parameters. That said, our data shows that tSETD2-FLAG methylates tubulin at the αTubK40 position *in vitro*.

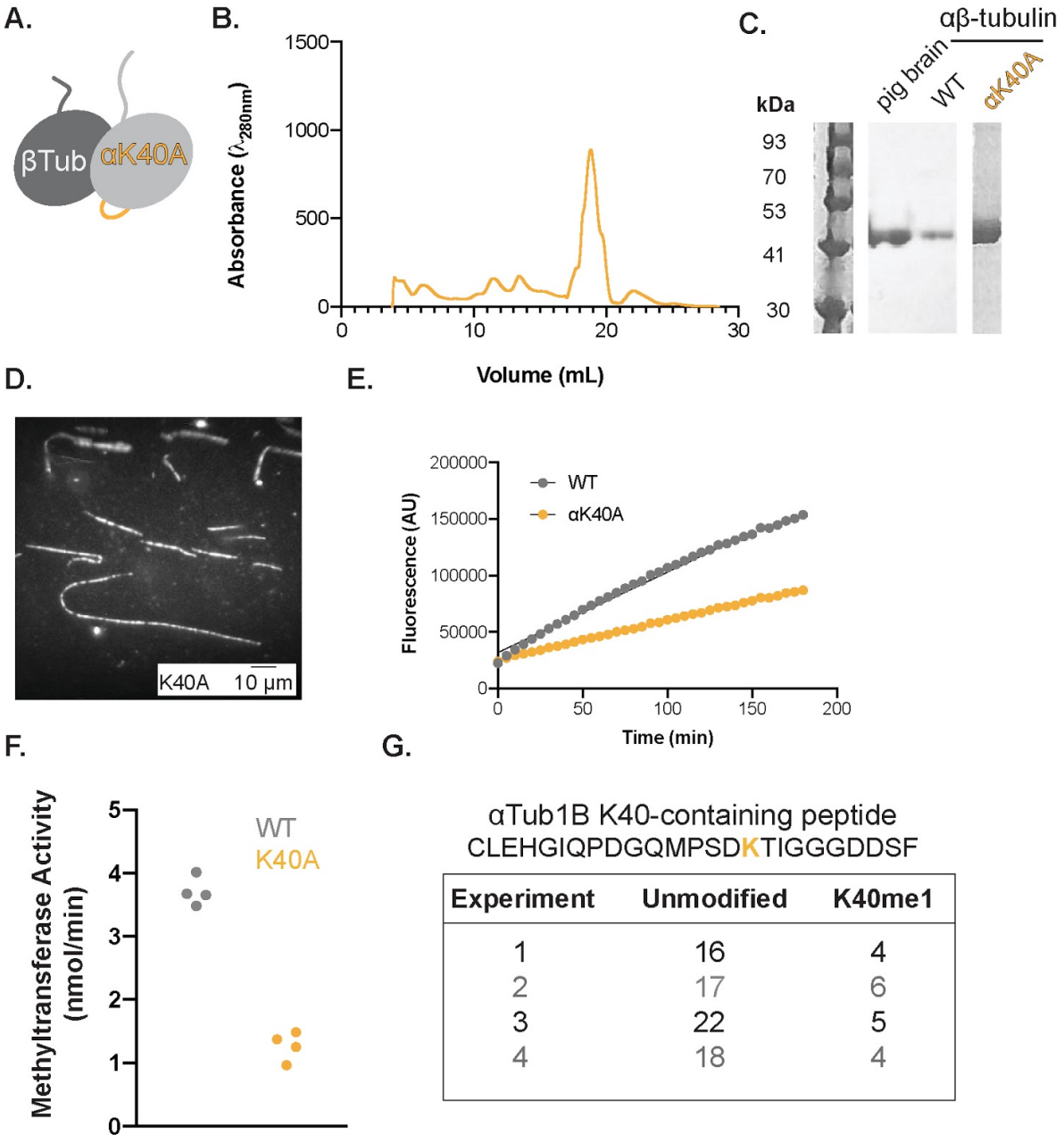

Experiment	Unmodified	K40me1
1	16	4
2	17	6
3	22	5
4	18	4

Fig. 2.6 tSETD2-FLAG methylates αK40A. A) Cartoon schematic showing the K40 loop in yellow. B-C) αTub1B/βTub3 αK40A was expressed and purified from insect cells and analyzed by B) size exclusion chromatography and C) Coomassie gel. D) Purified αK40A was co-polymerized with biotin- and 488-labeled porcine tubulin for TIRF and formed microtubules. E) Representative fluorescence traces of tSETD2-FLAG against WT and αK40A single isotype tubulins. F) Calculated methyltransferase activity of tSETD2-FLAG with WT or αK40A tubulin. Each dot indicates the average result from a single experiment across n=4 experiments. G) Mass spectrometry analysis of tubulin peptides. Table shows the only peptide modified in the presence of both tSETD2-FLAG and SAM, followed by the number of peptides either unmodified or with K40 mono-methylated per experiment.

2.3.3 Tubulin methylation alters microtubule dynamics

Some components of the tubulin code are known to alter microtubule dynamics. For example, αTub1B/βTub3, has a much higher catastrophe rate and slower growth rate compared to αTub1B/βTub2B, due to slightly different lateral contacts made by the different isotypes within the microtubule lattice (Ti et al. 2018). *In vivo*, aTubK40 acetylated microtubules are more resistant to cold and nocodazole or colchicine treatment, however the *in vitro* data remains inconsistent. In a similar vein, tyrosinated or detyrosinated microtubules seem to have little impact on tubulin polymerization *in vitro*. That said, tyrosination can impact microtubule dynamics by regulating the interactions between severing proteins like kinesin-13 and MCAK (Ems-McClung et al. 2010, McHugh et al. 2019). Similarly, microtubule glutamylation can regulate microtubule fragmentation by spastin (Valenstein et al. 2016). Some modifications have a polymerization inhibition effect, like the acetylation of βTubK252 or phosphorylation of βS172 (Janke et al. 2020). Given the possibility that tubulin modifications can impact microtubule dynamics, we sought to determine if tubulin methylation altered polymerization and depolymerization rates.

To determine if methylation altered dynamics, recombinant single isotype tubulin polymerization dynamics were observed by TIRF microscopy. First, we generated single isotype GMPCPP seeds spiked with streptavidin- and rhodamine-labeled porcine tubulin. From there, we added single isotype tubulin in the presence of tSETD2-FLAG with and without methyl donor SAM, along with 5% 488-labeled porcine tubulin for imaging. As a control, we performed microtubule dynamics assays with just recombinant tubulin. Microtubule dynamics were imaged using total internal reflection microscopy (TIRF-M) for 30 minutes.

Generated kymographs from time-lapse images were analyzed to measure the growth and shrinkage rates of both the minus- and plus- ends, along with the rate of catastrophe and maximum microtubule length. In the presence of tSETD2-FLAG both with and without SAM, we noticed that plus-ends grew and shrunk slower with methylated tubulin than with un-modified tubulin. Minus-end growth was also slower with methylated tubulin, but minus-end shrinkage was slightly quicker. Also, we saw a lower catastrophe frequency when microtubules were formed in the presence of tSETD2-FLAG despite forming shorter microtubules overall. Taken together, it's tempting to say that methylated tubulin largely suppresses microtubule dynamics at both the minus- and plus- ends. However, because these results are seen with and without the methyl donor

SAM, more likely the presence of tSETD2-FLAG protein is indirectly influencing microtubule. dynamics, perhaps by altering the amount of free tubulin to be incorporated into microtubules, rather than methylated tubulin drastically altering polymerization and depolymerization rates.

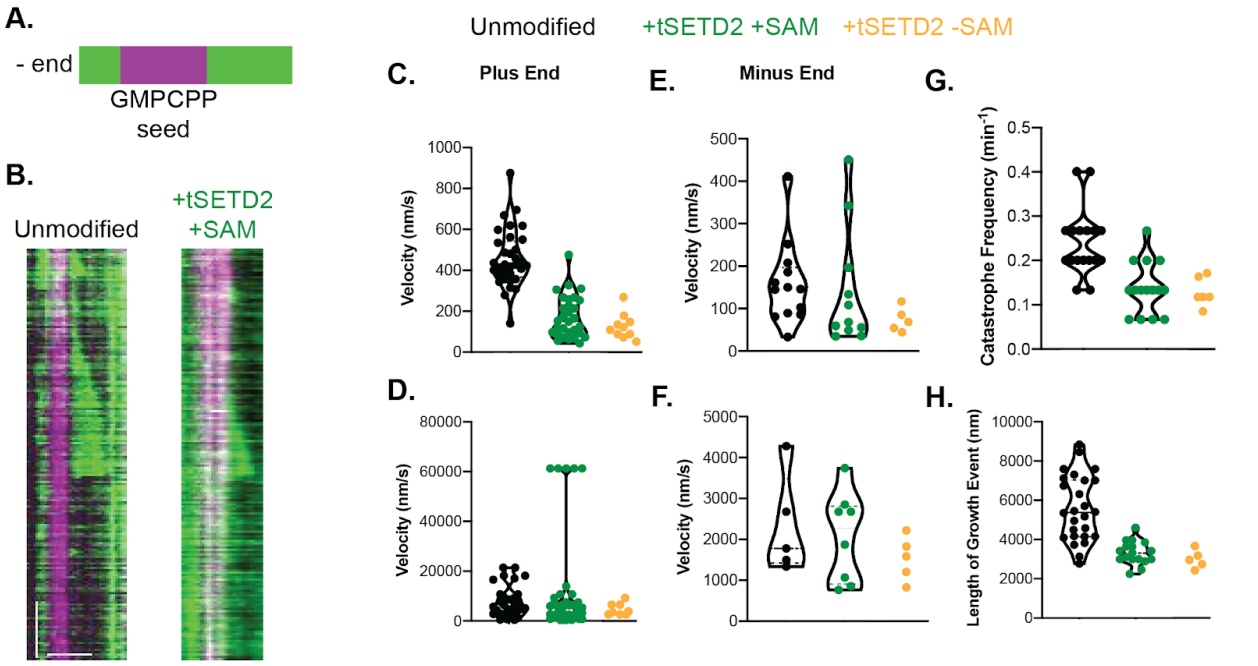

Fig 2.7 Presence of SETD2 alters microtubule dynamics. A) Cartoon schematic of dynamic assay with pink GMPCPP seeds and green dynamic microtubules. B) Kymographs of microtubules dynamics (left) without tSETD2-FLAG or (right) with tSETD2-FLAG and SAM. C-H) Microtubule dynamic properties measured of the C-D) plus-ends, E-F) minus ends with C&E) growth rates and D&F) shrinkage rates displayed. G) Catastrophe frequency of the plus-ends. H) Length of microtubule growth during the experiment.

2.3.4 SETD2 recognizes α-tubulin C-terminal tail

Previous work has demonstrated that the interaction between SETD2 and RNA Pol II involves electrostatic interactions between positively-charged residues in the SETD2 SRI domain and negatively-charged phosphorylated C-terminal repeat domains of RNA Pol II. This led us to hypothesize that SETD2 recognition of tubulin involves similar charge-charge interactions, particularly between positively-charged residues in the SETD2 SRI domain and the negatively-charged C-terminal tails (CTTs) of α- and/or β-tubulin. Even though there is no sequence

conservation between C-terminal of RNA Pol II or tubulin tails, both phosphorylated RNA Pol II and tubulin tails have a similar pattern of negative charge.

Truncations of the CTTs of either α-tubulin (αTub1BΔCTT/βTub3 = ΔαTubCTT) or β-tubulin (αTub1B/βTub3ΔCTT = ΔβTubCTT) were generated (Fig. 2.8A-C). Both of these generated constructs were transformed into baculovirus. Tailless tubulin dimers were expressed and purified from insect cells using a combination of affinity and size-exclusion chromatography (Fig. 2.8B-C). Thus far, when IP experiments were performed, an antibody with an epitope that recognizes the β-tubulin CTT was used. This antibody clearly would not work for recognizing ΔβTubCTT, and as such an antibody that recognizes the N-terminus of α-tubulin, TU-01, was used for western blot analysis (Fig. 2.8D).

tSETD2-FLAG binding to tailless tubulins was assessed by using a co-immunoprecipitation assay. Immobilized tSETD2-FLAG was incubated with either ΔαTubCTT or ΔβTubCTT tubulin proteins and then we analyzed the bead-bound fraction. Whereas tSETD2-Flag pulled down porcine brain and ΔβTubCTT tubulins, it was less able to co-precipitate ΔαTubCTT tubulin (Fig. 2.8E-F). This shows that the CTT of a-tuublin is required for tSETD2-FLAG binding. From these experiments, we conclude that tSETD2-Flag binds to tubulin via the negatively charged CTT of α-tubulin.

Next, I checked to see if the CTT influenced the ability of tSETD2-FLAG to microtubules. The ability of the ΔαTubCTT or ΔβTubCTT tubulin proteins to form microtubules was assessed by using the purified tubulin to first generated GMPCPP seeds spiked with biotin- and fluorescently- labeled porcine tubulin, and then polymerizing off the seeds to form microtubules, as seen by TIRF microscopy (Fig. 2.9A). Next, a copelleting assay was performed to assess if tSETD2-FLAG could bind to ΔαTubCTT or ΔβTubCTT microtubules, where binding to the lattice would mean a 125 kDa signal in the pellet (P) fraction (Fig. 2.9B). tSETD2-FLAG can bind to WT, detyrosinated, and ΔβCTT microtubules but less well to ΔαCTT microtubules. This suggests that, even when incorporated into the microtubule lattice, the α-tubulin CTT is critical for tSETD2-FLAG binding.

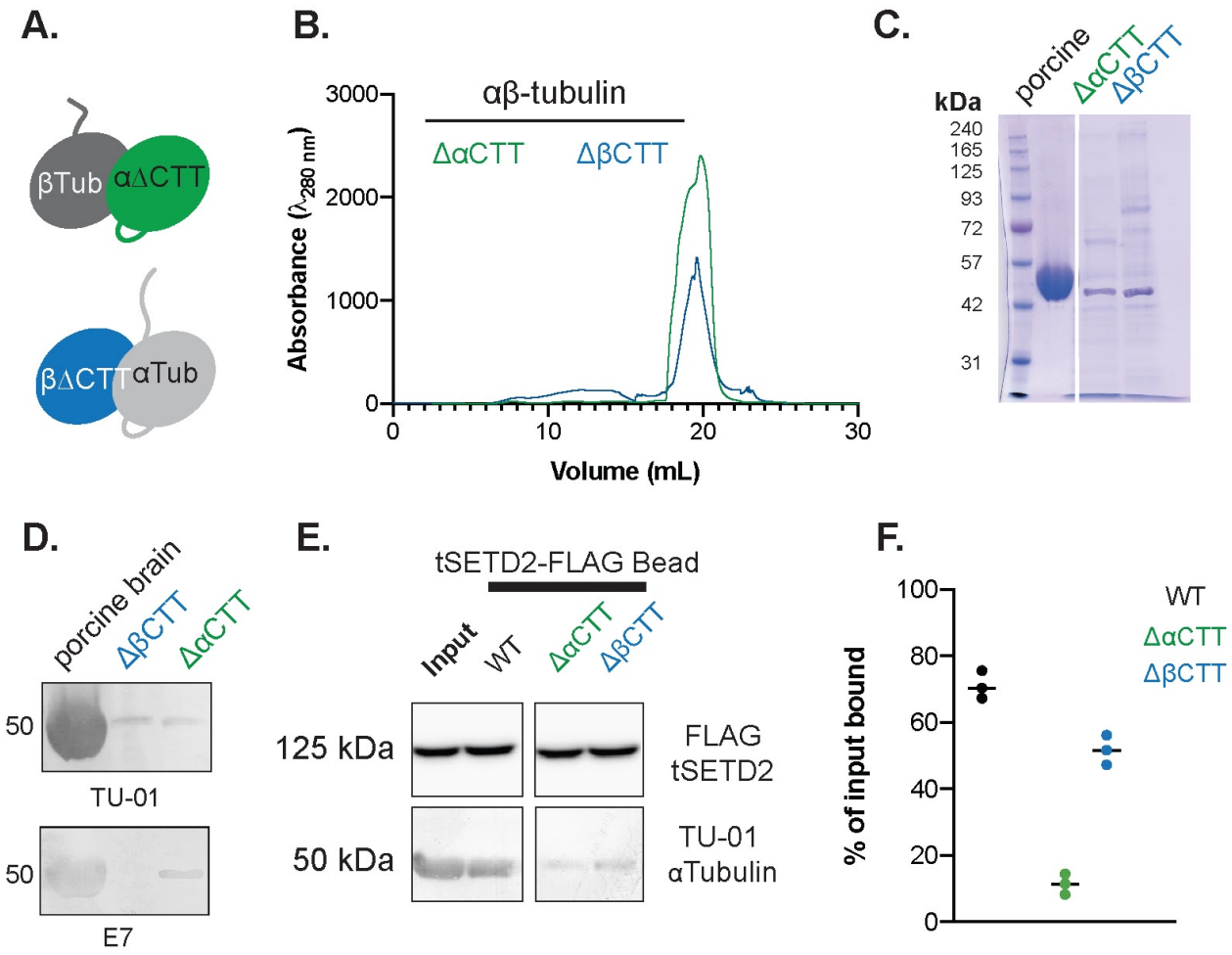

Fig. 2.8 tSETD2-FLAG recognizes α-tubulin C-terminal tail. A) Cartoon of tailless tubulin, either ΔαCTT (top) or ΔβCTT (bottom). These tubulin mutations were introduced into the single-isotype αTub1B/βTub3 tubulin and expressed and B-C) purified from insect cells. Purified tubulin was analyzed by B) size exclusion chromatography and C) Coomassie gel electrophoresis, in addition to D) western blot with two different tubulin antibodies, TU-01 which recognizes the N-terminus of a-tubulin or E7 which recognizes the C-terminus of b-tubulin. E) Coimmunoprecipitation of tSETD2-FLAG with porcine brain, ΔαCTT, or ΔβCTT tubulins. Shown are western blots of the bead pellets with antibodies to tSETD2-FLAG (FLAG, top) and the N-terminus of α-tubulin (TU-01, bottom). The far-left column shows the input for the reaction with porcine tubulin. F) Quantification of amount of tubulin copelleting with tSETD2-FLAG compared to input. Each dot represents the percent bound from one experiment and the line represents the average across three independent experiments.

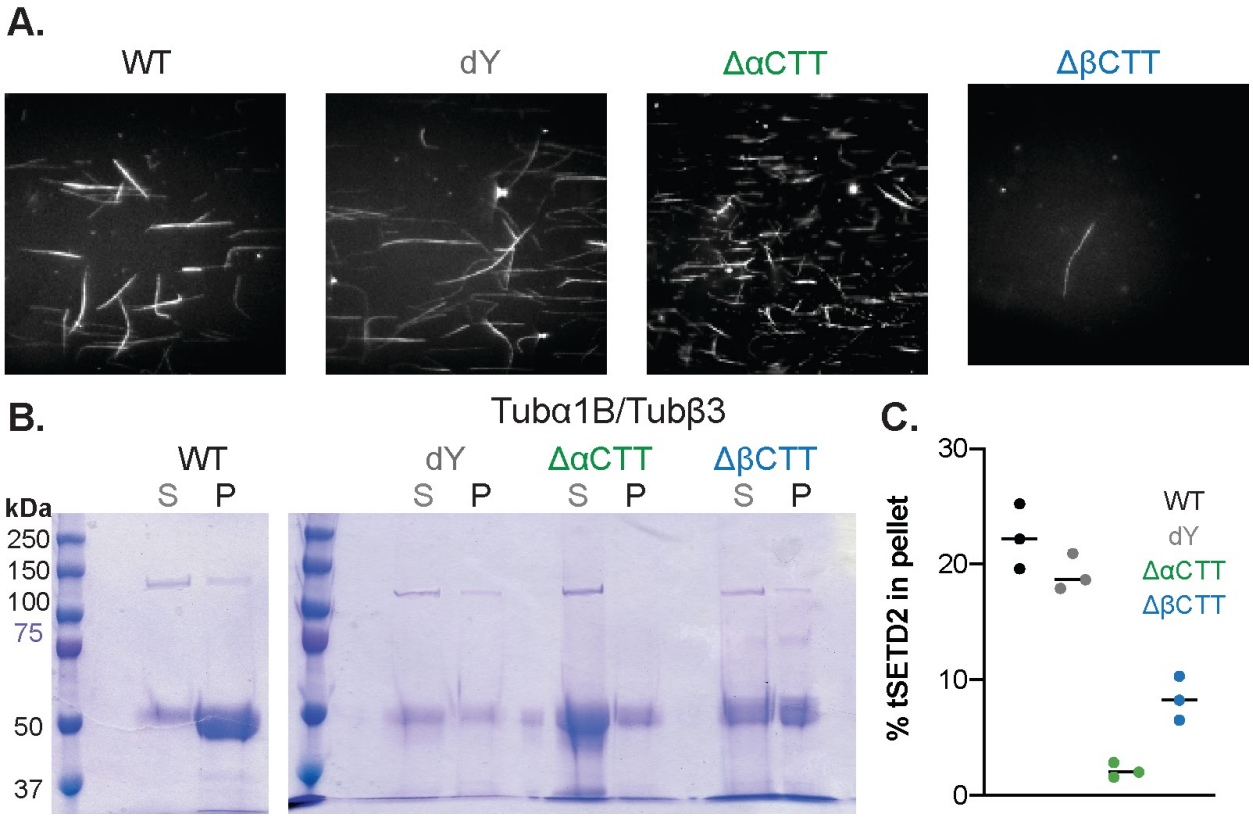

Fig. 2.9 tSETD2-FLAG cannot bind ΔαCTT microtubules. A) TIRF micrographs of GMPCPP-stabilized single-isotype αTub1B/βTub3 microtubules WT (black), dY (grey), ΔαCTT (green), and ΔβCTT (blue) spiked with biotin- and 488-labeled porcine tubulin. B) Co-pelleting of tSETD2-FLAG with single isotype microtubules, analyzing soluble (S) and pellet (P) fractions. C) Quantification of amount of tSETD2-FLAG in the pellet fraction. Each dot represents the percent in the pellet from one experiment.

2.3.5 SETD2 methylates actin

Similar to microtubules, actin filaments are a critical component of the cell's cytoskeletal network. Actin fibers contribute to muscle contraction, cell motility, cell division and signaling, cytokinesis and cell morphology, and cargo transport with myosin motors (Cooper 2000; Blanchoin et al. 2014). Based on ours and others' findings that SETD2 modifies microtubules, we were curious to identify any other cytoplasmic or cytoskeletal substrates. Performing a co-IP with SETD2 and whole cell lysate, we found that it could bind endogenous actin in addition to actin purified from

rabbit muscle (Seervai et al. 2020). Surprisingly, we were able to detect SETD2 both in nuclear and cytoplasmic compartments of interphase cells, suggesting that SETD2 does not entirely return to the nucleus after cell division. Fluorescence microscopy staining against actin, SETD2, and a pan-trimethyl mark also shows co-localization of these components in the cytoplasm, especially along the periphery of cells (Seervai et al. 2020). In SETD2 knockout cells, the tri-methyl mark does not appear on actin filaments, suggesting a SETD2-dependence to actin methylation (Seervai et al. 2020). Together, this suggests that SETD2 is able to methylate actin filaments in cells.

Because there are different isoforms of actin in cells, we wanted to identify the type of actin SETD2 could methylate by using actin purified from cardiac muscle, smooth muscle, and skeletal muscle in addition to human actin purified from mammalian (HEK293) and bacterial (*E. coli*) cells (Fig. 2.10A-B). tSETD2-FLAG was able to methylate

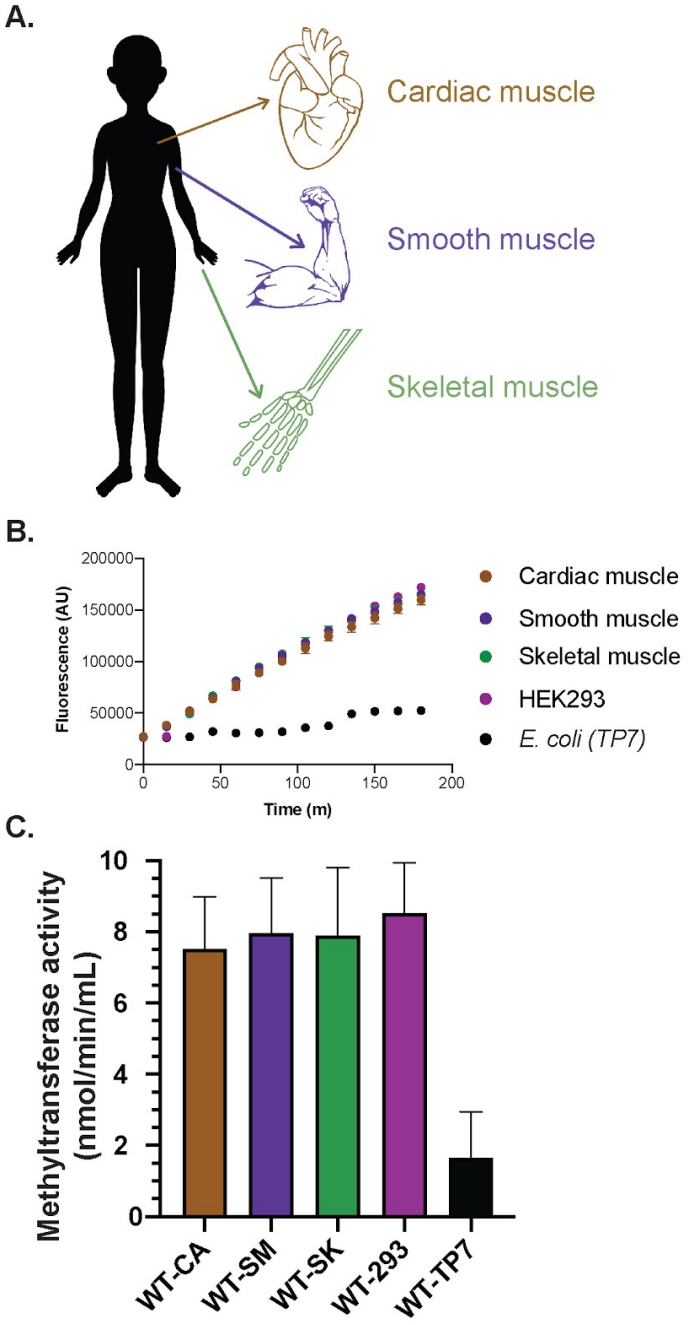

Fig. 2.10 tSETD2-FLAG methylates actin. A) Cartoon schematic of different actin sources used in the B-C) Methyltransferase activity assay. B) Representative fluorescent traces of tSETD2-FLAG with actin substrate natively purified from cardiac, smooth, or skeletal muscle, or recombinantly overexpressed from HEK293 or *E. coli* TP7 cells. C) Calculated methyltransferase activity of tSETD2-FLAG against actin substrates. The bars show the average +/- SD across n=3 experiments.

actin from all of these sources, except actin purified from bacterial cells, indicating that proper folding of actin or modifications may be required for methylation by SETD2. This is seen both in the fluorescent traces in addition to the calculated activity at 5 µM actin substrate concentration (Fig. 2.10B-C).

Next, we were curious to find out if tSETD2-FLAG methylated monomer or polymer actin, because Fig. 2.10B-C did not take polymerization state into account. To ensure a monomeric state, we treated actin purified from rabbit skeletal muscle with Latrunculin A, an actin polymerization inhibitor (Coué et al. 1987; Ayscough et al. 1997; Spector et al. 1983; Fujiwara et al. 2018). The actin state with and without LatA was verified using negative stain electron microscopy (Fig. 2.11A). From the collected micrographs, we see that actin filaments can be observed in the absence of LatA but that actin cannot form filaments in the presence of LatA. Next, we performed the fluorescence-based methyltransferase assay using these two populations of actin, either monomer or polymer, and calculated the activity by measuring the initial velocity of the reactions. tSETD2-FLAG activity was similar in the presence or absence of LatA suggesting that the activity toward monomer and polymer is about the

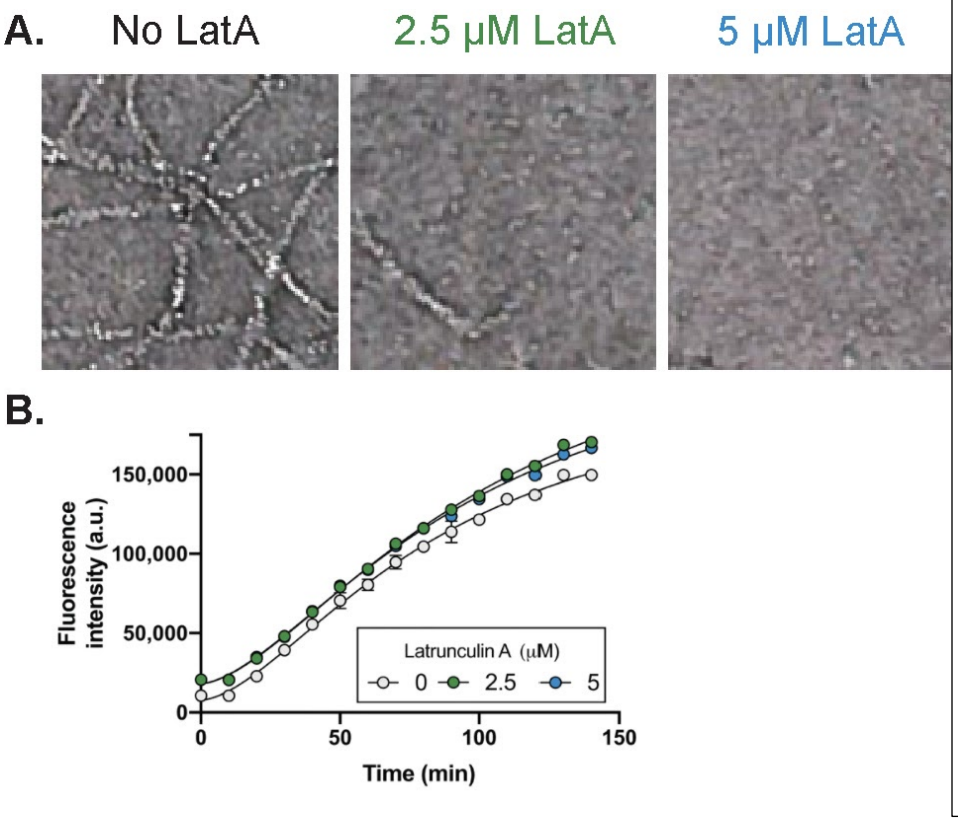

Fig. 2.11 tSETD2-FLAG methylates both actin monomers and filaments. A) Negative-stained micrographs of actin with or without polymerization inhibitor Latrunculin A (LatA) at different concentrations. B) Representative fluorescent traces of tSETD2-FLAG methyltransferase reactions against actin with various concentrations of LatA.

same (Fig. 2.11B). This suggests that the site of methylation is in an accessible site when actin is in filament form.

Next, we wanted to identify the site of actin methylation by tSETD2-FLAG. We hypothesized that the site could either be K18 or K68 (Fig. 2.12A-B) based on sequence similarity with histone and tubulin. To test these two sites, we generated peptides either containing amino acids 14-36 or 63-84, with the target lysine mono-, di-, or tri-methylated, or lacking - methyl groups. Additionally, we used the tSETD2-Flag catalytically dead R1625C mutant as a negative control. As expected, the R1625C mutant has low or no activity for any substrate. In contrast, tSETD2-FLAG was able to methylate both peptides with ~2-fold higher activity for the peptide containing K68 (Fig. 2.12B). Furthermore, tSETD2-FLAG had the higher activity toward the di-methylated peptide, yet still could methylate non- and mono-methylated peptides.

To test whether ActK68 is methylated in cells, mass spectrometry was performed on lysates from wild-type and SETD2-deficient cells by the Walker lab. Amongst the actin peptides identified, Act68me was found in SETD2-proficient but not in SETD2-deficient cells (Seervai et al. 2020). Moreover, performing mass spectrometry on purified tSETD2-FLAG, ActK68me was detected in trace amounts, suggesting that tiny amounts of actin are co-purifying with tSETD2-FLAG but more importantly that SETD2 can methylate ActK68 *in vivo* when overexpressed (Fig. 2.12C). Given that K68 is in a relatively accessible site along actin filaments (Fig. 2.12A), this explains our previous findings that tSETD2-FLAG has comparable activity with monomer and filamentous actin substrates.

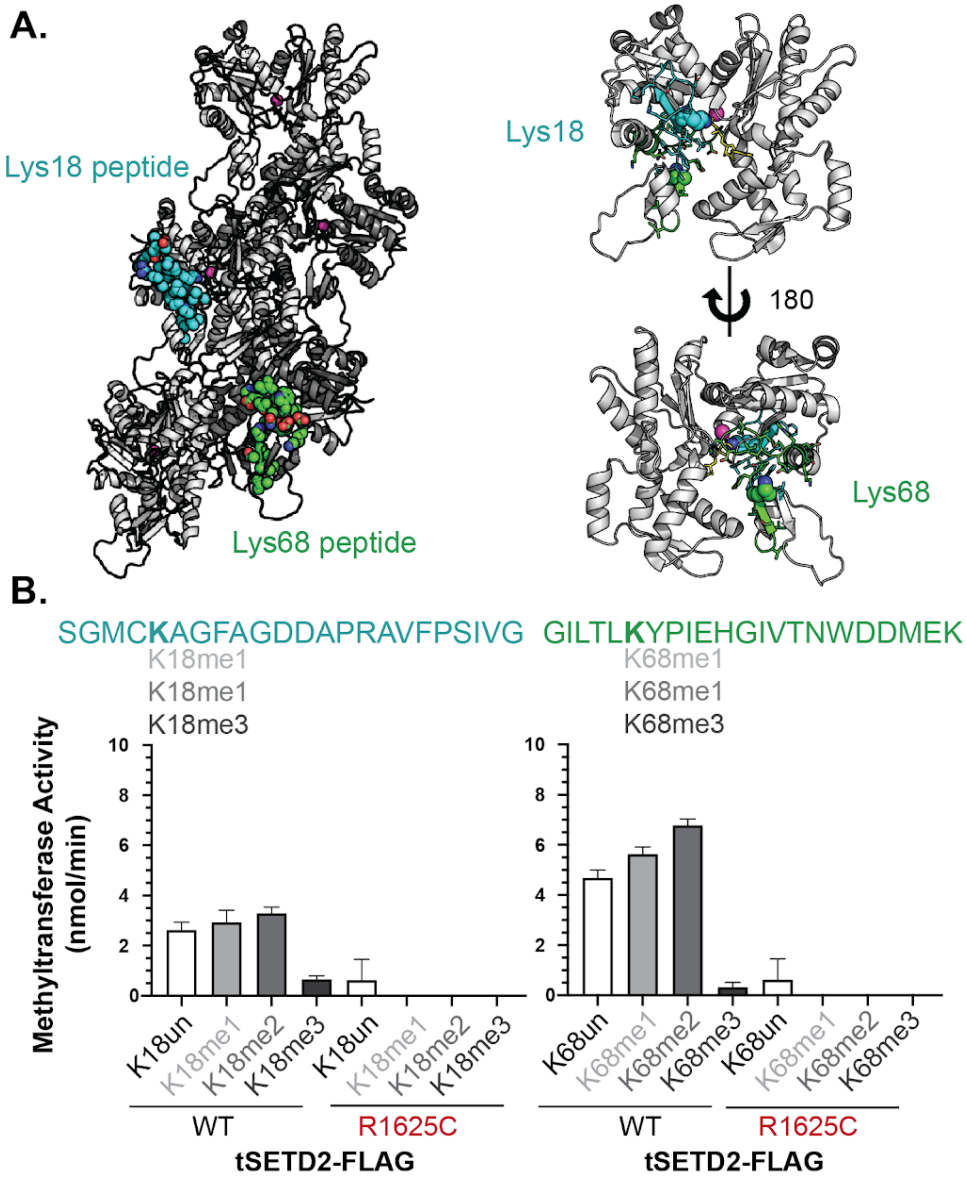

C.

TLKYPIEHGIVTNWDDMEKIW

	Modified peptides	Total peptides
Kme1	3.75±1.71	
Kme2	1.75±0.96	16.00±5.29
Kme3	1.25±0.95	

Fig.2.12 tSETD2-FLAG methylates actin at K68. A) Ribbon diagram of left) actin filament and right) globular actin with two potential sites of methylation colored blue (K18) or green (K68). B) Peptides of two potential sites of methylation were synthesized with no, mono, di, or tri methylation at the prospective lysine, either K18 (left, blue) or K68 (right, green). These peptides were mixed with tSETD2-FLAG, either WT or R1625C, and SAM and activity was measured and calculated. Bars show average +/- SD of n=3 experiments. C) Actin peptides containing K68 identified in mass spectrometry analysis of tSETD2-FLAG purified from HEK293 cells, suggesting trace amounts of actin are co-purifying and being modified by tSETD2-FLAG *in vivo* shown as the average number of peptides across three experiments.

2.4 Discussion

2.4.1 Accessing the methylation site of tubulin

Since the first study identified tubulin methylation in cells by SETD2 (Park et al. 2016), our work provides some biochemical underpinnings of tubulin methylation. Beyond SETD2, recent studies have found other tublin methyltransferases. The histone H4 lysine 20 methylating enzyme SET8, along with transcription factor LSF, has been identified as a modifier of α-tubulin at K311 (Chin et al. 2020), which would be on the surface of tubulin if incorporated into the microtubule lattice. Although the cellular implication of loss of K311 methylation in cells remains to be determined, these data suggest that transcription factors, LSF in the case of SET8, can recruit writer enzymes to target tubulin and other dual chromo-cytoskeletal modifiers could link histone and tubulin codes. Other proteins, similarly, have been linked to both codes like tubulin tyrosine ligase like 12 (TTLL12). TTLL12 has both SET-like and TTL-like domains, despite being unable to catalyze either histone methylation or tubulin detyrosination (Brants et al. 2012). However, altered TTLL12 expression results in changes to histone 4 lysine 20 trimethylation (H4K20me3) suggesting that it could act as a reader for histone and tubulin modifications. Our work here, in addition to a growing body of literature, identifies and characterizes tubulin methylating and dual chromo-cytoskeletal regulating enzymes.

By exploiting known tubulin-targeting agents, we found that SETD2 preferentially methylates the dimeric form of tubulin vs. microtubule polymers, though is able to methylate both tubulin states. Our mass spectrometry experiments only identified a single site, αTubK40, that is methylated. Because the K40 residue resides on a flexible loop of α-tubulin that is located within the lumen of a polymerized microtubule (Soppina et al. 2012; Eshun-Wilson et al. 2019), it could be accessible to modifying enzymes when tubulin is in either the soluble dimer or microtubule form. However, given the large size of the full length endogenous SETD2 protein (~290 kDa) and the restricted size of the microtubule lumen (~17 nm diameter), it has been puzzling how SETD2 could access the K40 residue within the microtubule lumen.

One possibility for how SETD2 can access K40 is the lumen is that it enters from the end as αTAT does. Acetylation on microtubules is randomly distributed and activity is diffusion-limited (Akella et al. 2010; Szyk et al. 2014). A second possibility is that SETD2 enters along the lattice. Microtubules sometimes have defects in their lattice, due to high mechanical stress (Dye,

Flicker, and Lien 1992; Schaedel et al. 2015) or microtubule severing enzymes (Vemu et al. 2018; Triclin et al. 2018). Total microtubule catastrophe and depolymerization, despite lattice defects and removed tubulin dimers, can be rescued with the addition of GTP or GTP-like analog tubulin (Dimitrov et al. 2008; de Forges et al. 2016; Aumeier et al. 2016). Moreover, the nucleotide state of tubulin impacts the microtubule lattice structure with either the GTP or hydrolyzed GDP form corresponding to an elongated straight or compact and bent form of tubulin when incorporated into the lattice (Weisenberg, Deery, and Dickinson 1976; Buey, Díaz, and Andreu 2006; Alushin et al. 2014; Piedra et al. 2016; Ayukawa et al. 2020). Together, the dynamics present in the microtubule lattice suggest a sort of microtubule breathing, during which enzymes could access the microtubule lumen.

2.4.2 Kinetics

Methyltransferase activity was monitored using a fluorescence-based time dependent assay that coupled the consumption of the methyl donor, S-adenosyl-methionine (SAM) to a colorimetric readout. These types of experiments helped us determine the differential activity of tSETD2-FLAG amongst histones, tubulin, and actin (Fig. 2.3 & Fig. 2.10), between tubulin dimers and microtubules (Fig. 2.4), and with wild-type and K40A recombinant tubulin (Fig. 2.6). However, we had some interesting observations looking at the fluorescence traces themselves during our analysis.

We noticed that in the methyltransferase reaction with histone peptide, increasing concentrations of substrate resulted in comparable fluorescence end-point values, despite having differing initial slopes of fluorescence over time (Fig. 2.3A, left). We would expect that different concentrations would have different end-point values increasing with substrate concentration. Despite this, our Michaelis-Menton analysis of the concentration-dependent activity (Fig. 2.3B, left) showed comparable kinetic rates of tSETD2-FLAG with H3 peptide as previous studies with histone peptides and nucleosome substrates (Eram et al. 2015) (Fig. 2.3D). Additionally, for tubulin substrates, we noticed that there were two slopes across time, suggesting kinetic complexity. We would anticipate that the two slopes are due to the mixed substrate population of tubulin dimers and microtubules, but more careful kinetic analysis would be required to know for certain. Given this, the Michaelis-Menton analysis (Fig 2.3B, right) and the subsequent kinetic

constants derived (Fig. 2.3D) has limitations in their interpretation given the mixed substrate population. When we look at methyltransferase reactions with known populations of tubulin dimers and microtubules, see two distinct slopes depending on the population (Fig. 2.4C). However, we also noticed that there is a small burst-like shape early on in the microtubule fluorescence trace. This burst is not seen in reactions with the recombinant tubulin (Fig. 2.6E). As such, we would expect that there could be a small amount of tubulin dimers in the microtubule population that are consumed more quickly by tSETD2-FLAG. Again, however, more careful experimental set-up and kinetic analysis would be required to determine the underlying mechanism.

While these interesting kinetics are tempting to derive implications from, without different types of experiments we cannot interpret the existing data. To better understand what's going on, future experiments will have to tease apart the competition between tubulin dimers and microtubules. Moreover, other types of analyses, beyond Michaelis-Menton and steady state kinetics, could be done to tease apart the complexity of the reaction. For example, transient state enzyme kinetic reactions could help characterize steps along the pathway of an enzyme-catalyzed reaction such as substrate binding, catalytic reactions, and product release.

2.4.3 Multiple modifications at αK40

Our mass spectrometry analysis identified α-tubulin K40 as the only detectable site of methylation by tSETD2 on the recombinant single-isotype αTub1B/βTub3. This confirms and extends the previous work where tri-methylation was detected at this site in mammalian cells (Park et al. 2016). In our mass spectrometry experiments, we were only able to detect a mono-methylation mark on αK40 whereas in cells, trimethylated tubulin was detected (Park et al. 2016). The canonical SETD2 activity is with di-methylated histone substrates. While this suggests that mono- or di-methylated tubulin could be a preferred substrate for SETD2, it is known that SETD2 can mono-methylate substrates (Chen et al. 2017), but typically will di- or tri-methylate substrates. As such, tubulin methylation may require priming by other methyltransferases before SETD2 makes its mark in cells.

Although mutation of K40A did not completely abolish methyltransferase activity measured in the fluorescence-based assay, we were unable to detect any other methylated peptides for α- or β-tubulin by mass spectrometry. It is possible that SETD2 is able to methylate another

tubulin residue that we have been unable to detect in our mass spectrometry analysis, perhaps because the methylated peptide does not ionize well or the amount is below the limit of detection. It is also possible that tSETD2-FLAG or a co-purifying methyltransferase enzyme from HEK293 cells is able to methylate a contaminating protein that co-purifies with tubulin from the insect cells and/or with tSETD2-FLAG from the HEK293 cells. Further work will be required to discern between these possibilities.

The K40 residue of α-tubulin is also known to be acetylated by alpha tubulin acetyltransferase (αTAT) (Akella et al. 2010; Shida et al. 2010). Whether SETD2 and αTAT compete for access to the K40 residue has been unclear. Given our results demonstrating a higher activity of SETD2 towards soluble tubulin and recent work demonstrating that αTAT1 preferentially acetylates polymerized microtubules and enters the microtubule lumen (Shida et al. 2010; Kormendi et al. 2012; Szyk et al. 2014; Coombes et al. 2016; Ly et al. 2016), the two enzymes appear to work on tubulin in different contexts. Specifically, SETD2 preferentially methylates soluble tubulin whereas αTAT preferentially acetylates polymerized tubulin. The interplay between these enzymes is likely to play a role in specific cellular events. For example, elevated levels of α-tubulin acetylation correlate positively with metastatic potential (Boggs et al. 2015) and αTAT inhibits cancer cell motility (Lee et al. 2018), whereas SETD2-mediated tubulin methylation corresponds with genomic stability and correct mitotic spindle formation (Park et al. 2016; Chiang et al. 2018).

Interestingly, both SETD2 (Eram et al. 2015; Kearns et al., 2020) and αTAT (Shida et al. 2010) display slow enzymatic rates toward the tubulin substrate *in vitro.* SETD2 also shows similar low k_{cat} values towards purified nucleosome substrates (Eram et al. 2015). In a histone methylating context, SETD2 is typically recruited by other protein complexes (e.g. IWS1, SPT6, and RNA Pol II) (Yoh et al. 2007; Cermakova et al. 2019) suggesting that substrate binding and enzyme kinetics could be higher in cells. Future work will be required to understand recruitment and activity *in vivo*.

2.4.4 Dynamics

Performing microtubule dynamics assay with single isotype tubulin in the presence of tSETD2-FLAG with and without the methyl donor SAM, we found that dynamic properties changed when the enzyme was present, but not necessarily due to enzymatic activity. Because

dynamics were the same with and without SAM, the added tSETD2-Flag is likely acting in an indirect manner, perhaps by sequestering free tubulin dimers. As such, the alteration in the tubulin economy, and not methylated tubulin, would impact microtubule dynamics. Our mass spectrometry results indicate that tubulin methylation does not efficiently label many tubulin dimers: less than 20% of single-isotype αTub1B. We'd suspect that microtubules with modifications that sparse will likely not have drastic differences in dynamics compared to un-modified. My dynamic assay indicates that tSETD2-FLAG may alter the amount of free tubulin dimers. In cells, microtubules are assembled from a finite pool of tubulin dimers (a so-called "tubulin economy"). Tubulins are a valuable resource that can be used to create polymers, organize the cytoskeleton, and regulate other microtubule-associated proteins like motors (Ohi, Strothman, and Zanic 2021). With soluble tubulin highly enriched at the centrosome (Baumgart et al. 2019), it is possible that SETD2 sequestration of free tubulin wouldn't be impacting tubulin polymerization and instead is creating a pool of methylated tubulin for the spindle to utilize at the centrosome to create the mitotic spindle.

Other post-translational modifications have been studied in terms of stabilizing or destabilizing, rather than altering the tubulin economy. For example, acetylation of aTubK40 is known to mark cold- and stress-stabilize microtubules and as such the acetylated microtubules have lower catastrophe and depolymerization rates (Piperno, LeDizet, and Chang 1987; Xu et al. 2017). Conversely, however, overexpression of HDAC6, a microtubule deacetylase, in cells has no impact on microtubule growth or dynamics (Zilberman et al. 2009) and tubulin acetylation reduces the microtubule nucleation rate while increasing the depolymerization rate (Portran et al. 2017). Together, these findings suggest that acetylation at αTubK40, while increasing the stabilization and resistance of microtubules, can also inhibit polymerization or increase rates of depolymerization depending on microtubule state. Acetylation at βTubK252 and phosphorylation of βS172 both inhibit tubulin polymerization (Chu et al. 2011; Ori-McKenney et al. 2016). Levels of tyrosination/detyrosination seem to have no effect on tubulin polymerization, but some depolymerizing enzymes like kinesin-13 (MCAK, or KIF2C) preferentially act on tyrosinated microtubules (Raybin and Flavin 1977; Ferreira et al. 2020). This last finding of tubulin modifications read by other enzymes, thus having a larger impact on dynamics gets at the interplay of the tubulin code with the microtubule associated protein (MAP) code. MAPs that bind to and sometimes decorate the microtubule lattice can have a larger impact on microtubule dynamics in

addition to motor protein motility (Monroy et al. 2020). As such, the tubulin code could be underlying the MAP code, both indirectly having an impact on cytoskeletal dynamics in cells.

Tubulin methylation in particular is only detected at the minus ends of mitotic spindle microtubules. Compared to the enzymatic rates of tubulin methylation (slow), cell division occurs very quickly and, more specifically, microtubules that connect to the kinetochore are very dynamic (T. Mitchison et al. 1986; T. J. Mitchison 1989). As such, I would anticipate that other proteins, structural or enzymatic, would have to be present near the centrosomes in order to promote microtubule nucleation and dynamics. Future work will distinguish the mechanism of how methylated tubulin is incorporated into microtubules in cells and identify other protein-protein interactions key to the proper formation of the mitotic spindle.

2.4.5 A tail of tubulin recognition

Our results also demonstrate that tSETD2 requires the CTT of α-tubulin, a negatively-charged region of the protein, for binding. This is interesting given previous work demonstrating that the SRI domain of SETD2 interacts with the phosphorylated, and thus negatively-charged, C-terminal repeat domains of Pol II (Rebehmed et al. 2014; Kizer et al. 2005; Kanu et al. 2015). It is thus tempting to speculate that charge-charge interactions are key for recognition of substrates by the SRI domain of SETD2. However, actin has recently been shown to be methylated by SETD2 (Seervai et al. 2020) and unlike tubulin and RNA Pol II, actin does not have a long flexible negatively-charged tail or loop within its structure. However, in these studies, actin methylation by SETD2 required other binding partners, namely the Huntingtin protein, HTT, and the actin binding adaptor protein HIP1R. Future work will be required to delineate the mechanism by which SETD2 recognizes actin and other substrates.

While our results suggest that SETD2 does not compete with α TAT for modification of the K40 residue, it likely competes with other tubulin-interacting proteins and/or modifying enzymes that target the CTT. The flexible CTTs of tubulin subunits extend from the surface of the microtubule and form a negatively-charged surface that appears to serve as a recognition site for a large number of microtubule associated proteins. For example, tubulin tyrosine ligase (TTL) makes critical electrostatic interactions with α-tubulin residues E445, E446, and E447 in order to align the CTT within the active site (Prota et al. 2013). The VASH-SVBP complex that removes the terminal tyrosine from α-tubulin (Liu et al. 2019; F. Li et al. 2020) makes electrostatic

interactions with a compound that mimics the tubulin CTT residues (F. Li et al. 2019). Similarly, the tubulin CTTs are essential for microtubule recognition by tubulin tyrosine ligase-like 7 (TTLL), an enzyme that adds glutamate chains to the CTTs of both α- and β-tubulin (Garnham et al. 2015; Szyk et al. 2011). As such, our work adds SETD2 to the growing list of tubulin modifying enzymes that recognizes tubulin CTTs. Given that the SRI domain of SETD2 makes electrostatic interactions with the negatively charged CTT of α-tubulin, additional negative charge from polyglutamates added by TTLL enzymes could change the binding and activity of SETD2 to tubulin. Future work will need to look at the crosstalk between tubulin PTMs.

2.4.6 SETD2 activity is actin' up

In addition to methylating tubulin, SETD2 can modify actin as well. In coordination with binding partners HTT and HIP1R, actin is methylated by SETD2 thus regulating actin polymerization dynamics and cell migration (Seervai et al. 2020). Moreover, actin is methylated at K68 near the DNaseI binding loop (D-loop, amino acids 39 to 43). This loop contains several modifiable residues (Varland, Vandekerckhove, and Drazic 2019), and is structurally proximal to another methylated lysine residue K84 (M.-M. Li et al. 2013). In addition to methylation, K68 itself is susceptible to acetylation, SUMOylation, and ubiquitination (Terman and Kashina 2013), suggesting a regulation of modifications at this position.

While SETD2 methylates both polymerized and monomeric actin in vitro (Fig. 2.11B), the K68me3 mark is more abundant on actin filaments in cells (Seervai et al. 2020). In cells, LatA treatment leads to a loss of methylated actin, yet had little effect on actin polymerization. This could mean the lack of actin methylation leads to less dynamic actin that is resistant to LatA-induced polymerisation. Because SETD2-deficient cells have a loss of dynamic actin, the susceptibility to depolymerization/repolymerization cycles of methylated actin could also contribute to actin dynamics in SETD2-proficient cells during migration (Svitkina 2018). Moreover, cells from *Setd2*-null mice had disorganized stress fibers and lamellipodia (Hu et al. 2010), suggesting that the disruption of the actin cytoskeleton, in addition to loss of histone H3K26me3 and tubulin spindle methylation, is detrimental.

Actin is a target for modifications on 94 of its amino acids, comprising over 90% of total modifiable residues (Varland, Vandekerckhove, and Drazic 2019; Terman and Kashina 2013), yet the structural and functional implications of many PTMs remain unknown. One actin modification

that has been structurally characterized, however, is methylation at histidine 73 (H73) by SETD3 (Wilkinson et al. 2018). H73 methylation has been known for over fifty years, but was only recently identified to be modified by SETD3, a histone methyltransferase that also methylates histone 3 at lysine 4 and 36 (Eom et al. 2011). Structural analysis of SETD3 with actin peptides suggest that both proteins must undergo significant conformational changes upon binding to each other, with loops in SETD3 shifting more than 4Å (Guo et al. 2019; Wilkinson et al. 2018; Zheng, Zhang, and Li 2020). However, the actin and histone peptides bind in opposite N-to-C orientations and the actin H73 and histone H3K36 are recognized by distinct residues of the SET domain (Zheng, Zhang, and Li 2020). With SETD3 and SETD2 sharing a homologous catalytic SET domain, this has implications in how histone methyltransferases bind and recognize their substrates. Beyond just actin methylation, our findings with SETD2 expand the paradigm that some epigenetic machinery has chromato-cytoskeletal activity important for modifying both nuclear and cytoskeletal proteins. As such, we find that SETD2 methylates key components: histones during transcription, microtubules during cell division, and actin for cell migration, though future work will need to identify how SETD2 is localized to different parts of the cell to perform its myriad methylation functions.

2.5 Materials and Methods

Plasmids.

An active truncated SETD2 construct (1418-2564) with a FLAG affinity tag (tSETD2-Flag) for mammalian pInducer expression was gifted by the Walker Lab. Single isoform αTub1B/βTub3 plasmid encoding *Homo sapiens* α-tubulin 1B and β-tubulin 3 in pFastBac Dual vector (ThermoFisher 10712024) was obtained from the Kapoor lab for insect cell expression (Ti, Wieczorek, and Kapoor 2020). Point mutations and domain deletions were generated using QuickChange site-directed mutagenesis with Q5 Polymerase (NEB). All plasmids were verified by DNA sequencing. A truncated, constitutively active kinesin-1 [rat KIF5C(1-560)] (Cai et al., 2007) was used for single molecule TIRF assays.

Purification.

SETD2. tSETD2-Flag was transfected into HEK 293 Freestyle cells with FectoPRO transfection reagent (116-010) and cells were harvested 48 hours later at 5K rpm for 15 mins (Beckman JLA 8.1 (363563)). Pellet was suspended in lysis buffer (50 mM HEPES pH 7.5, 50 mM MgCl2, 150 mM NaCl, cOmplete protease inhibitor tablet (Sigma Aldrich, 4693159001) and cells were lysed with 20 strokes of a dounce homogenizer. This was ultracentrifuged (Beckman Ti70 337922) at 40K rpm for 40 mins and the supernatant was filtered with 1.0 um glass fiber filter (Pall Laboratory) and incubated with FLAG M2 affinity beads (Sigma Aldrich) equilibrated in lysis buffer for 3 hours. Beads were rinsed with 3 column volumes (CV) of wash buffer (50 mM NaPi pH 7.2, 150 mM NaCl, 5 mM BME), 3 CV salt buffer (wash buffer at 500 mM NaCl), and again with wash buffer before elution buffer (wash buffer with 300 ng 3x-FLAG peptide (Sigma Aldrich)) was added and incubated with beads overnight. Eluent was then run over ion exchange column (DEAE Sepharose, GE Life Sciences) on a 0-75% salt buffer gradient, and size exclusion chromatography (Superose 6 Increase 10/300, Fisher Scientific) with gel filtration buffer (50 mM NaPi pH 7.2, 150 mM NaCl, 5 mM BME, 5% glycerol). Fractions were pooled and concentrated down with an Amicon Ultra 100K MWCO centrifugal filter unit and snap frozen in liquid nitrogen and stored at -80C.

αTub1B/βTub3 tubulin. As previously described in (Ti et al. 2018; Ti et al. 2020). Briefly, the Bac-to-Bac system (Life Technologies) was used to generate recombinant baculovirus in sf9 cells. High Five cells (Thermo Fisher, B85502), grown to 3 million cells/ml in Lonza Insect XPRESS (Fisher Scientific, BW12-730Q), were infected with P3 viral stocks at ~10 mL/L. Cells were cultured in suspension at 27°C and harvested at 60 hours after infection. The following steps were done on ice or at 4°C. Cells were lysed in an equal volume of lysis buffer (50 mM HEPES, 20 mM imidazole, 100 mM KCl, 1 mM MgCl2, 0.5 mM β-mercaptoethanol, 0.1 mM GTP, 3 U/ml benzonase, 1X Roche Complete EDTA-free protease inhibitor, pH 7.2) by dounce homogenization (20 strokes) and the homogenate was centrifuged at 55,000 rpm in a Type 70 Ti rotor (Beckman Coulter) for 1 hr. The supernatant was then filtered through a 0.22 μm membrane (Fisher Scientific, 09740113) and loaded onto a 5 ml HisTrap HP column (GE life science 17-5247-01) pre-equilibrated with lysis buffer. The column was washed with 35 ml lysis buffer until the UV absorption reached baseline, then eluted with nickel elution buffer (1X BRB80 (80 mM PIPES, 1mM MgCl2, 1mM EGTA), 500 mM imidazole, 0.2 mM GTP, 2 mM β-mercaptoethanol, pH 7.2).

The fractions containing proteins were pooled, diluted 3-fold with lysis buffer and loaded one 5 ml StrepTrap HP column (GE life science 29-0486-53). The column was washed with 25 ml 66% lysis buffer + 33% nickel elution buffer, 25 ml of wash buffer 1 (1X BRB80, 1 mM β-mercaptoethanol, 0.1 mM GTP, 0.1 % Tween-20, 10% glycerol, pH 7.2), and 25 ml of wash buffer 2 (1X BRB80 1 mM β-mercaptoethanol, 0.1 mM GTP, 10 mM MgCl2, 5 mM ATP, pH 7.2). The bound protein was then eluted with ~5 ml StrepTrap elution buffer (1XBRB80, 20 mM Imidazole, 2 mM β-mercaptoethanol, 0.2 mM GTP, 3 mM desthiobiotin, pH 7.2). The StrepTrap eluate was mixed with 4 mg of previously purified TEV protease (~8 mg/ml stored in 40 mM HEPES, 150 mM KCl, 30%(w/v) glycerol, 1 mM MgCl2, 3 mM β-mercaptoethanol, pH 7.5) and incubated for 2 hr on ice. The TEV-digested protein solution was concentrated with an Amicon Ultra 50K MWCO centrifugal filter unit (Millipore UFC901024) to 2 mL, and loaded onto a Superdex 200 Increase 10/300 GL column equilibrated in size-exclusion buffer (1XBRB80, 5%(w/v) glycerol, 0.2 mM GTP, 2 mM β-mercaptoethanol, pH 6.8). Tubulin eluted at ~15 ml and was concentrated to >3 mg/ml with an Amicon Ultra 50K MWCO centrifugal filter unit. The purified tubulin was snap frozen in liquid nitrogen and stored at -80°C. Tail-less tubulin eluted at ~18 mL and concentrated with an Amicon Ultra 30K MWCO centrifugal filter unit, but otherwise was purified the same way.

Methyltransferase assay.

Activity of tSETD2-Flag constructs was surveyed using a Methyltransferase Fluorescence Assay Kit (Cayman Chemical, 700150). This continuous enzyme-coupled assay continuously monitors SAM-dependent methyltransferases by generating a fluorescent compound, resorufin, from the reaction product, AdoHcy. Fluorescence is analyzed with an excitation wavelength of 530-540 nm and an emission wavelength of 585-595 nm using a PHERAstar Plate Reader (BMG Labs). A standard curve of resorufin concentration and fluorescence was used to determine concentration-dependent fluorescence. The initial velocities of the reaction curves were obtained by linear-regression, and then were plotted in a concentration-dependent manner to obtain Michaelis-Menten plots, and as such values for Km and vmax (Prism Version 8.1.1).

Dimer or microtubule stabilization. Microtubule polymerization was inhibited by the addition of 50 μM of podophyllotoxin (Millipore Sigma, P4405). Microtubule stabilization occurred with 100

μM taxol (Cytoskeleton Inc, TXD01). Stocks were made at 2 mg/mL and then diluted to perform methyltransferase assay in BRB80.

Mass Spectrometry.

Purified single isoform tubulin and tSETD2-Flag were incubated at molar ratio of 5:1 with excess S-adenosylmethionine (Sigma Aldrich, 86867-01-8) for 2 hours at room temperature. Enzyme mixture was digested with fresh Chymotrypsin (Sigma Aldrich, 11418467001) and put onto a Thermo Scientific mass spectrometer with an Orbitrap Fusion Tribrid with ETD and a Q Exactive HF equipped with a nano-LC system (Dionex RSLC-nano). Analysis of PTMs conducted with PEAKS X.

Pull-down assay.

FLAG M2 beads were blocked with 3% BSA in PBS for 1 hour and equilibrated in the reaction buffer (tSETD2-Flag size-exclusion buffer, described previously). tSETD2-Flag protein (WT or variants) was added at 20 μM with a putative binding partner for 2 hours in the presence of SAM. For tubulin, 0.25 mg/mL of porcine tubulin (Cytoskeleton, Inc.) was used, for actin, 0.25 mg/mL of rabbit actin (Cytoskeleton, Inc. AKL99) was used, and for RNA Polymerase II, 10 μL of HEK293 Freestyle clarified lysate was used. Beads were spun down and the supernatant was collected as the fraction of unbound substrate. The beads were then resuspended in the reaction buffer to the total reaction volume, and the same amount of supernatant and beads were added to SDS-PAGE gel. Analysis of binding was conducted by western blot with the following antibodies: anti-FLAG (Sigma Aldrich, A9469, 1:1000), anti-tubulin antibodies E7 (DSHB, AB_528499, 1:1000) and/or TU-01 (Abcam, ab7750, 1:1000), anti-RNA Polymerase II (Abcam, ab193468, 1:1000), and anti-actin (Fisher Scientific, MS1295P0), with secondary antibody anti-mouse (Enzo Life Science, ADI-SAB-100-J, 1:1000) or anti-rabbit (Enzo Life Science, ADI-SAB-300-J, 1:1000), respectively. Binding was quantified by measuring the background-subtracted intensity of each band with Fiji ImageJ (Schindelin et al. 2012) as a fraction of the input intensity. Each experiment was performed three times, independently.

Immunohistochemistry.

COS7 (CRL-1651) cells transiently expressing tSETD2-Flag constructs (Lipofectamine 2000 and OptiMEM) were fixed with 4% formaldehyde in PBS, treated with 50 mM NH4Cl in PBS to quench unreacted formaldehyde and permeabilized with 0.2% Triton X-100 in PBS. Subsequently, cells were blocked in blocking solution (0.2% fish skin gelatin in PBS). Primary antibodies tubulin (DSHB, AB_528499, 1:2000) and Flag (Abcam, ab205606, 1:2000), and secondary antibodies were applied in blocking solution at room temperature for 1 h each, washing in between with blocking solution. Nuclei were stained with 10.9 µM 4′,6-diamidino-2-phenylindole (DAPI) and cover glasses were mounted in ProlongGold (Life Technologies). Cells were incubated 3x for 5 min in blocking solution to remove unbound antibodies. Images were collected on an inverted epifluorescence microscope (Nikon TE2000E) equipped with a 60x, 1.40 numerical aperture oil-immersion objective and a 1.5x tube lens on a Photometrics CoolSnapHQ camera driven by NIS-Elements (Nikon) software.

Microtubule polymerization.

GMPCPP-stabilized. We first prepared αTub1B/βTub3 microtubule seeds. Tubulin was thawed, mixed with GMPCPP (final 1.5 mM), diluted to ~ 1.5 mg/ml with 1XBRB80+5% glycerol, centrifuged at 90,000 rpm for 10 min at 4°C (TLA120.1 Beckman Coulter), and then polymerized by incubation at 37°C for 30 mins. The microtubules were pelleted at 90,000 rpm for 10 min at 37°C (TLA120.1 Beckman Coulter) and re-suspended in warm (37°C) 1XBRB80 supplemented with 1 mM TCEP. Next, we used these microtubule seeds to polymerize GTP-bound αTub1B/βTub3. Another aliquot of recombinant tubulin was thawed, diluted to a final concentration ~3 mg/ml (1XBRB80, 33% glycerol, 1 mM GTP), and spun at 90,000 rpm for 10 min at 4°C (TLA120.1 Beckman Coulter). After incubation at 37°C for 2 mins, the supernatant was mixed with GMPCPP-seeds from the prior step and then incubated at 37°C for 30 mins followed by centrifugation at 90,000 rpm for 10 min at 37°C (TLA120.1 Beckman Coulter). The microtubule pellets were rinsed twice with 100 µl warm (37°C) EM buffer (1X BRB80, 1 mM DTT, 0.1 mM ATP, 0.05% Nonidet P-40) before suspending in 30 µl cold EM buffer and then incubated on ice for 1 hr. After a centrifugation at 90,000 rpm for 10 min at 4°C, the supernatant containing depolymerized GDP-tubulin (~2 mg/ml, measured by Bradford assay) was mixed with GMPCPP (final 2 mM) and then incubated on ice for 10 mins. After an incubation at 37°C for 2 mins, the protein solution was mixed with 30 µl warm (37°C) EM buffer followed by 37°C

incubation for another 1 hr. The polymerized GMPCPP-microtubules were pelleted by 90,000 rpm for 10 min at 37°C (TLA120.1 Beckman Coulter) and suspended in warm (37°C) EM buffer.

Taxol-stabilized. αTub1B/βTub3 tubulin were thawed, mixed with GTP (final concentration 2 mM), diluted to ~ 1 mg/ml with 1XBRB80 with 5% glycerol, and centrifuged at 90,000 rpm for 10 min at 4°C (TLA120.1 Beckman Coulter) to remove any aggregates from the freeze-thaw cycle. After incubation at 37°C for 2 mins, the supernatant was mixed with 1 μM taxol (final 0.1 μM, 37°C 10 mins), followed by mixing with 10 μM taxol (final 1 μM, 37°C 10 mins), and then mixed with 100 μM taxol (final 10 μM, 37°C 15 mins). The microtubules were pelleted at 90,000 rpm for 10 min at 37°C (TLA120.1 Beckman Coulter) and re-suspended in warm (37°C) EM buffer containing 15 μM taxol.

Single Molecule TIRF Assay

Flow cell and experimental set up. Single isoform microtubules were polymerized with taxol stabilization as described above, but spiked with 2% labeled porcine brain tubulin (HiLyte). Microtubules were stored in the dark at room temperature for up to 2 weeks. Flow cells were prepared by attaching a #1.5 mm2 coverslip (Thermo Fisher Scientific) to a glass slide (Thermo Fisher Scientific) using double-sided tape. Microtubules were diluted in a freshly made BRB80 buffer supplemented with 10 μM taxol, infused into flow cells, and incubated for four minutes to allow for nonspecific absorption to the glass. Flow cells were then incubated with blocking buffer [30 mg/mL casein in P12 buffer (12 mM Pipes/KOH pH 6.8, 1 mM MgCl2, 1 mM EGTA) supplemented with 10 μM taxol] for four minutes. Flow cells were then infused with motility mixture (0.5–1.0 μL of COS7 cell lysate [see below for preparation], 25 μL P12 buffer, 15 μL blocking buffer, 1 mM ATP, 0.5 μL 100 mM DTT, 0.5 μL, 0.5 μL 20 mg/mL glucose oxidase, 0.5 μL 8 mg/mL catalase, and 0.5 μL 1 M glucose), sealed with molten paraffin wax.

Imaging conditions. Microtubules were imaged on an inverted Nikon Ti-E/B total internal reflection fluorescence (TIRF) microscope with a perfect focus system, a 100 × 1.49 NA oil immersion TIRF objective, three 20 mW diode lasers (488 nm, 561 nm, and 640 nm) and EMCCD camera (iXon+ DU879; Andor). Image acquisition was controlled using Nikon Elements software and all assays were performed at room temperature. Motility data were analyzed by first generating maximum intensity projections to identify microtubule tracks (width = 3 pixels) and then generating kymographs in ImageJ (National Institutes of Health). Only motility events that lasted

for at least three frames were analyzed. Furthermore, events that ended as a result of a motor reaching the end of a microtubule were included; therefore, the reported run lengths for highly processive motors are likely to be an underestimation.

Kinesin cell lysate preparation. COS-7 (African green monkey kidney fibroblasts, American Type Culture Collection, RRID:CVCL_0224) were grown at 37°C with 5% (vol/vol) CO2 in Dulbecco's Modified Eagle Medium (Gibco) supplemented with 10% (vol/vol) Fetal Clone III (HyClone) and 2 mM GlutaMAX (L-alanyl-L-glutamine dipeptide in 0.85% NaCl, Gibco). Cells are checked annually for mycoplasma contamination and were authenticated through mass spectrometry (the protein sequences exactly match those in the African green monkey genome). 24 hr after seeding, the cells were transfected with plasmids encoding for the expression of KIF5B (1-560) motor tagged with three tandem monomeric citrines (3x-mCit) transfection reagent (Mirus), and Opti-MEM Reduced Serum Medium (Gibco). Cells were trypsinized and harvested 24 hr after transfection by low-speed centrifugation at 3000 x g at 4°C for 3 min. The pellet was resuspended in cold 1X PBS, centrifuged at 3000 x g at 4°C for 3 min, and the pellet was resuspended in 50 µL of cold lysis buffer [25 mM HEPES/KOH, 115 mM potassium acetate, 5 mM sodium acetate, 5 mM MgCl2, 0.5 mM EGTA, and 1% (vol/vol) Triton X-100, pH 7.4] with 1 mM ATP, 1 mM phenylmethylsulfonyl fluoride, and 1% (vol/vol) protease inhibitor cocktail (P8340, Sigma-Aldrich). Lysates were clarified by centrifugation at 20,000 x g at 4°C for 10 min and lysates were snap frozen in 5 µL aliquots in liquid nitrogen and stored at −80°C.

Actin polymerization and inhibition. Actin for the methyltransferase assay came from the following sources: rabbit skeletal muscle actin (Cytoskeleton, Inc., AKL95), bovine cardiac muscle actin (Cytoskeleton, Inc., AD99), chicken gizzard smooth muscle actin (Cytoskeleton, Inc., AS99), β-actin human recombinant protein (OriGene, TP303643), and β-actin human recombinant protein (OriGene, TP720518)]. Actin purified from rabbit skeletal muscle was natively purified and gifted by the Higgs lab was polymerized at X in 10 mM Tris-HCl (pH 7.5), 2 mM MgCl2, 50 mM KCl, and 1 mM ATP. Latrunculin A was also gifted from the Higgs lab and inhibited actin polymerization.

2.6 References

Akella, Jyothi S., Dorota Wloga, Jihyun Kim, Natalia G. Starostina, Sally Lyons-Abbott, Naomi S. Morrissette, Scott T. Dougan, Edward T. Kipreos, and Jacek Gaertig. 2010. "MEC-17 Is an α-Tubulin Acetyltransferase." *Nature* 467 (7312): 218–22.

Alushin, Gregory M., Gabriel C. Lander, Elizabeth H. Kellogg, Rui Zhang, David Baker, and Eva Nogales. 2014. "High-Resolution Microtubule Structures Reveal the Structural Transitions in Ab -Tubulin upon GTP Hydrolysis." *Cell* 157 (5): 1117–29.

Aumeier, Charlotte, Laura Schaedel, Jérémie Gaillard, Karin John, Laurent Blanchoin, and Manuel Théry. 2016. "Self-Repair Promotes Microtubule Rescue." *Nature Cell Biology* 18 (10): 1054–64.

Ayscough, Kathryn R., Joel Stryker, Navin Pokala, Miranda Sanders, Phil Crews, and David G. Drubin. 1997. "High Rates of Actin Filament Turnover in Budding Yeast and Roles for Actin in Establishment and Maintenance of Cell Polarity Revealed Using the Actin Inhibitor Latrunculin-A." *The Journal of Cell Biology* 137 (2): 399–416.

Ayukawa, R., S. Iwata, H. Imai, S. Kamimura, and M. Hayashi. 2020. "GTP-Dependent Formation of Straight Oligomers Leads to Nucleation of Microtubules." *bioRxiv*. https://www.biorxiv.org/content/10.1101/2020.03.05.979989v1.abstract.

Baumgart, Johannes, Marcel Kirchner, Stefanie Redemann, Alec Bond, Jeffrey Woodruff, Jean-Marc Verbavatz, Frank Jülicher, Thomas Müller-Reichert, Anthony A. Hyman, and Jan Brugués. 2019. "Soluble Tubulin Is Significantly Enriched at Mitotic Centrosomes." *The Journal of Cell Biology*, October, jcb.201902069.

Beghin, A., C. Galmarini, and C. Dumontet. 2007. "Tubulin Folding Pathways: Implication in the Regulation of Microtubule Dynamics." *Current Cancer Drug Targets*. https://doi.org/10.2174/156800907783220426.

Bitterman, Elizabeth, Ryan Liegel, Chelsea Menke, Andrew Timms, David Beier, Beth Kline-Fath, Howard M. Saal, Howard M. Saal, and Rolf Slottman. 2018. "Differential Requirements of Tubulin Genes in Mammalian Forebrain Development."

Blanchoin, Laurent, Rajaa Boujemaa-Paterski, Cécile Sykes, and Julie Plastino. 2014. "Actin Dynamics, Architecture, and Mechanics in Cell Motility." *Physiological Reviews* 94 (1): 235–63.

Boggs, Amanda E., Michele I. Vitolo, Rebecca A. Whipple, Monica S. Charpentier, Olga G. Goloubeva, Olga B. Ioffe, Kimberly C. Tuttle, et al. 2015. "α-Tubulin Acetylation Elevated in

Metastatic and Basal-like Breast Cancer Cells Promotes Microtentacle Formation, Adhesion, and Invasive Migration." *Cancer Research* 75 (1): 203–15.

Brants, Jan, Kostyantyn Semenchenko, Christine Wasylyk, Aude Robert, Annaick Carles, Alberto Zambrano, Karine Pradeau-Aubreton, et al. 2012. "Tubulin Tyrosine Ligase Like 12, a TTLL Family Member with SET- and TTL-Like Domains and Roles in Histone and Tubulin Modifications and Mitosis." Edited by Axel Imhof. *PloS One* 7 (12): e51258.

Buey, Rubén M., J. Fernando Díaz, and José M. Andreu. 2006. "The Nucleotide Switch of Tubulin and Microtubule Assembly: A Polymerization-Driven Structural Change." *Biochemistry* 45 (19): 5933–38.

Cermakova, Katerina, Eric A. Smith, Vaclav Veverka, and H. Courtney Hodges. 2019. "Dynamics of Transcription-Dependent H3K36me3 Marking by the SETD2:IWS1:SPT6 Ternary Complex." *bioRxiv*. https://doi.org/10.1101/636084.

Chen, Kun, Juan Liu, Shuxun Liu, Meng Xia, Xiaomin Zhang, Dan Han, Yingming Jiang, Chunmei Wang, and Xuetao Cao. 2017. "Methyltransferase SETD2-Mediated Methylation of STAT1 Is Critical for Interferon Antiviral Activity." *Cell* 170 (3): 492–506.e14.

Chiang, Yun-Chen, In Young Park, W. Kimryn Rathmell, Cheryl Lyn Walker, and Ryoma Ohi. 2018. "SETD2 Haploinsufficiency for Microtubule Methylation Is an Early Driver of Genomic Instability in Renal Cell Carcinoma." *Cancer Research* 78 (12): 3135–46.

Chin, Hang Gyeong, Pierre-Olivier Esteve, Cristian Ruse, Jiyoung Lee, Scott E. Schaus, Sriharsa Pradhan, and Ulla Hansen. 2020. "The Microtubule-Associated Histone Methyltransferase SET8, Facilitated by Transcription Factor LSF, Methylates α-Tubulin." *The Journal of Biological Chemistry*. https://doi.org/10.1074/jbc.RA119.010951.

Chu, C-W, F. Hou, J. Zhang, L. Phu, A. V. Loktev, D. S. Kirkpatrick, P. K. Jackson, Y. Zhao, and H. Zou. 2011. "A Novel Acetylation of -Tubulin by San Modulates Microtubule Polymerization via down-Regulating Tubulin Incorporation." *Molecular Biology of the Cell* 22 (4): 448–56.

Coombes, Courtney, Ami Yamamoto, Mark McClellan, Taylor A. Reid, Melissa Plooster, G. W. Gant Luxton, Joshua Alper, Jonathon Howard, and Melissa K. Gardner. 2016. "Mechanism of Microtubule Lumen Entry for the α-Tubulin Acetyltransferase Enzyme αTAT1." *Proceedings of the National Academy of Sciences of the United States of America* 113 (46): E7176–84.

Cooper, Geoffrey M. 2000. "Structure and Organization of Actin Filaments." *The Cell: A Molecular Approach* 2.

Coué, M., S. L. Brenner, I. Spector, and E. D. Korn. 1987. “Inhibition of Actin Polymerization by Latrunculin A.” *FEBS Letters*. 213(2)

Davenport, Andrew M., Leslie N. Collins, Hui Chiu, Paul J. Minor, Paul W. Sternberg, and André Hoelz. 2014. “Structural and Functional Characterization of the α-Tubulin Acetyltransferase MEC-17.” *Journal of Molecular Biology* 426 (14): 2605–16.

Desai, Arshad, and Timothy J. Mitchison. 1997. “MICROTUBULE POLYMERIZATION DYNAMICS.” Vol. 13.

Dimitrov, Ariane, Mélanie Quesnoit, Sandrine Moutel, Isabelle Cantaloube, Christian Poüs, and Franck Perez. 2008. “Detection of GTP-Tubulin Conformation in Vivo Reveals a Role for GTP Remnants in Microtubule Rescues.” *Science* 322 (5906): 1353–56.

Dorgan, Kathleen M., Whitney L. Wooderchak, Donraphael P. Wynn, Erin L. Karschner, Joshua F. Alfaro, Yinqiu Cui, Zhaohui Sunny Zhou, and Joan M. Hevel. 2006. “An Enzyme-Coupled Continuous Spectrophotometric Assay for S-Adenosylmethionine-Dependent Methyltransferases.” *Analytical Biochemistry* 350 (2): 249–55.

Dye, R. B., P. F. Flicker, and D. Y. Lien. 1992. “End-stabilized Microtubules Observed in Vitro: Stability, Subunit Interchange, and Breakage.” *Cell Motility and the Cytoskeleton*. 21(3):171-186.

Edmunds, John W., Louis C. Mahadevan, and Alison L. Clayton. 2008. “Dynamic Histone H3 Methylation during Gene Induction: HYPB/Setd2 Mediates All H3K36 Trimethylation.” *The EMBO Journal* 27 (2): 406–20.

Ems-McClung, S.C, and Walczak, C.E. 2010. “Kinesin-13 in mitosis: Key players in the spatial and temporal organization of spindle microtubules. *Neuron* 89:449-460.

Eom, Gwang Hyon, Kee-Beom Kim, Jin Hee Kim, Ji-Young Kim, Ju-Ryung Kim, Hae Jin Kee, Dong-Wook Kim, et al. 2011. “Histone Methyltransferase SETD3 Regulates Muscle Differentiation.” *The Journal of Biological Chemistry* 286:34733-42/

Eram, Mohammad S., Ekaterina Kuznetsova, Fengling Li, Evelyne Lima-fernandes, Steven Kennedy, Irene Chau, Cheryl H. Arrowsmith, Matthieu Schapira, and Masoud Vedadi. 2015. “Biochimica et Biophysica Acta Kinetic Characterization of Human Histone H3 Lysine 36.” *BBA - General Subjects* 1850 (9): 1842–48.

Eshun-Wilson, Lisa, Rui Zhang, Didier Portran, Maxence V. Nachury, Dan Toso, Thomas Lohr, Michele Vendruscolo, Massimiliano Bonomi, James S. Fraser, and Eva Nogales. 2019. “Effects

of Alpha-Tubulin Acetylation on Microtubule Structure and Stability," *Proceedings of the National Academy of Sciences af the United States of America*. 116(21):10366-71.

Ferreira, Luísa T., Bernardo Orr, Girish Rajendraprasad, António J. Pereira, Carolina Lemos, Joana T. Lima, Clàudia Guasch Boldú, Jorge G. Ferreira, Marin Barisic, and Helder Maiato. 2020. "α-Tubulin Detyrosination Impairs Mitotic Error Correction by Suppressing MCAK Centromeric Activity." *The Journal of Cell Biology* 219 (4). https://doi.org/10.1083/jcb.201910064.

Forges, Hélène de, Antoine Pilon, Isabelle Cantaloube, Antoine Pallandre, Anne Marie Haghiri-Gosnet, Franck Perez, and Christian Poüs. 2016. "Localized Mechanical Stress Promotes Microtubule Rescue." *Current Biology: CB* 26 (24): 3399–3406.

Fujiwara, Ikuko, Mark E. Zweifel, Naomi Courtemanche, and Thomas D. Pollard. 2018. "Latrunculin A Accelerates Actin Filament Depolymerization in Addition to Sequestering Actin Monomers." *Current Biology: CB* 28 (19): 3183–92.e2.

Gadadhar, Sudarshan, Satish Bodakuntla, Kathiresan Natarajan, and Carsten Janke. 2017. "The Tubulin Code at a Glance." *Journal of Cell Science* 130 (8): 1347–53.

Garnham, Christopher P., Annapurna Vemu, Elizabeth M. Wilson-Kubalek, Ian Yu, Agnieszka Szyk, Gabriel C. Lander, Ronald A. Milligan, and Antonina Roll-Mecak. 2015. "Multivalent Microtubule Recognition by Tubulin Tyrosine Ligase-Like Family Glutamylases HHS Public Access Molecular Basis for Specificity among the Enzymes Primarily Responsible for Chemically Diversifying Cellular Microtubules." *Cell* 161 (5): 1112–23.

Guo, Qiong, Shanhui Liao, Sebastian Kwiatkowski, Weronika Tomaka, Huijuan Yu, Gao Wu, Xiaoming Tu, Jinrong Min, Jakub Drozak, and Chao Xu. 2019. "Structural Insights into SETD3-Mediated Histidine Methylation on β-Actin." *eLife* 8 (February). https://doi.org/10.7554/eLife.43676.

Hacker, Kathryn E., Catherine C. Fahey, Stephen A. Shinsky, Yun-Chen J. Chiang, Julia V. DiFiore, Deepak Kumar Jha, Andy H. Vo, et al. 2016. "Structure/Function Analysis of Recurrent Mutations in SETD2 Protein Reveals a Critical and Conserved Role for a SET Domain Residue in Maintaining Protein Stability and Histone H3 Lys-36 Trimethylation." *The Journal of Biological Chemistry* 291 (40): 21283–95.

Janke, Carsten, and Maria M. Magiera. 2020. "The Tubulin Code and Its Role in Controlling Microtubule Properties and Functions." *Nature Reviews. Molecular Cell Biology* 21 (6): 307–26.

Hu, Ming, Xiao-Jian Sun, Yuan-Liang Zhang, Ying Kuang, Chao-Quan Hu, Wei-Li Wu, Shu-Hong Shen, et al. 2010. "Histone H3 Lysine 36 Methyltransferase Hypb/Setd2 Is Required for Embryonic Vascular Remodeling." *Proceedings of the National Academy of Sciences of the United States of America* 107 (7): 2956–61.

Johnson, Vinu, Pelin Ayaz, Patrick Huddleston, and Luke M. Rice. 2011. "Design, Overexpression, and Purification of Polymerization-Blocked Yeast αβ-Tubulin Mutants." *Biochemistry* 50 (40): 8636–44.

Jordan, M. A., D. Thrower, and L. Wilson. 1992. "Effects of Vinblastine, Podophyllotoxin and Nocodazole on Mitotic Spindles. Implications for the Role of Microtubule Dynamics in Mitosis." *Journal of Cell Science* 102 (3).

Kanu, N., E. Grönroos, P. Martinez, R. A. Burrell, X. Yi Goh, J. Bartkova, A. Maya-Mendoza, et al. 2015. "SETD2 Loss-of-Function Promotes Renal Cancer Branched Evolution through Replication Stress and Impaired DNA Repair." *Oncogene* 34 (46): 5699–5708.

Kaul, Neha, Virupakshi Soppina, and Kristen J. Verhey. 2014. "Effects of α-Tubulin K40 Acetylation and Detyrosination on Kinesin-1 Motility in a Purified System." *Biophysical Journal* 106 (12): 2636–43.

Kearns, Sarah, Frank M. Mason, W. Kimryn Rathmell, In Young Park, Cheryl Walker, Kristen A. Verhey, and Michael A. Cianfrocco. 2020 "Molecular Determinants for α-Tubulin Methylation by SETD2." https://doi.org/10.1101/2020.10.21.349365.

Kizer, Kelby O., Hemali P. Phatnani, Yoichiro Shibata, Hana Hall, Arno L. Greenleaf, and Brian D. Strahl. 2005. "A Novel Domain in Set2 Mediates RNA Polymerase II Interaction and Couples Histone H3 K36 Methylation with Transcript Elongation." *Molecular and Cellular Biology* 25 (8): 3305–16.

Kormendi, Vasilisa, Agnieszka Szyk, Grzegorz Piszczek, and Antonina Roll-Mecak. 2012. "Crystal Structures of Tubulin Acetyltransferase Reveal a Conserved Catalytic Core and the Plasticity of the Essential N Terminus." *The Journal of Biological Chemistry* 287 (50): 41569–75.

Leandro-García, Luis J., Susanna Leskelä, Iñigo Landa, Cristina Montero-Conde, Elena López-Jiménez, Rocío Letón, Alberto Cascón, Mercedes Robledo, and Cristina Rodríguez-Antona. 2010. "Tumoral and Tissue-Specific Expression of the Major Human ??-Tubulin Isotypes." *Cytoskeleton* 67 (4): 214–23.

LeDizet, M., and G. Piperno. 1987. “Identification of an Acetylation Site of Chlamydomonas Alpha-Tubulin.” *Proceedings of the National Academy of Sciences of the United States of America* 84 (16): 5720–24.

Lee, Cheng Che, Yun Ching Cheng, Chi Yen Chang, Chi Min Lin, and Jang Yang Chang. 2018. “Alpha-Tubulin acetyltransferase/MEC-17 Regulates Cancer Cell Migration and Invasion through Epithelial–mesenchymal Transition Suppression and Cell Polarity Disruption.” *Scientific Reports* 8 (1). https://doi.org/10.1038/s41598-018-35392-6.

Lewis, Sally A., Guoling Tian, and Nicholas J. Cowan. 1997. “The α-and β-Tubulin Folding Pathways.” *Trends in Cell Biology* 7 (12): 479–84.

L’Hernault, Steven W., and Joel L. Rosenbaum. 1985. “Chlamydomonas .alpha.-Tubulin Is Posttranslationally Modified by Acetylation on the .epsilon.-Amino Group of a Lysine.” *Biochemistry*. https://doi.org/10.1021/bi00323a034.

Li, Faxiang, Yingjie Hu, Shutao Qi, Xuelian Luo, and Hongtao Yu. 2019. “Structural Basis of Tubulin Detyrosination by Vasohibins.” *Nature Structural & Molecular Biology* 26 (7): 583–91.

Li, Faxiang, Yang Li, Xuecheng Ye, Haishan Gao, Zhubing Shi, Xuelian Luo, Luke M. Rice, and Hongtao Yu. 2020. “Cryo-EM Structure of VASH1-SVBP Bound to Microtubules.” *eLife* 9 (August). https://doi.org/10.7554/eLife.58157.

Li, Ming-Ming, Anja Nilsen, Yue Shi, Markus Fusser, Yue-He Ding, Ye Fu, Bo Liu, et al. 2013. “ALKBH4-Dependent Demethylation of Actin Regulates Actomyosin Dynamics.” *Nature Communications*. https://doi.org/10.1038/ncomms2863.

Liu, Xi, Hao Wang, Jinying Zhu, Yongchao Xie, Xin Liang, Zeliang Chen, Yue Feng, and Yi Zhang. 2019. “Structural Insights into Tubulin Detyrosination by Vasohibins-SVBP Complex.” *Cell Discovery* 5 (December): 65.

Lu, Michelle S., and Christopher A. Johnston. 2013. “Molecular Pathways Regulating Mitotic Spindle Orientation in Animal Cells.” *Development* 140 (9): 1843–56.

Ly, Nathalie, Nadia Elkhatib, Enzo Bresteau, Olivier Piétrement, Mehdi Khaled, Maria M. Magiera, Carsten Janke, Eric Le Cam, Andrew D. Rutenberg, and Guillaume Montagnac. 2016. “αtAT1 Controls Longitudinal Spreading of Acetylation Marks from Open Microtubules Extremities.” *Scientific Reports* 6 (September): 1–10.

Maiato, Helder, Ana Margarida Gomes, Filipe Sousa, and Marin Barisic. 2017. "Mechanisms of Chromosome Congression during Mitosis." *Biology* 6 (1). https://doi.org/10.3390/biology6010013.

Manka, Szymon W., and Carolyn A. Moores. 2018. "Microtubule Structure by Cryo-EM: Snapshots of Dynamic Instability." *Essays in Biochemistry*, 20180031.

Matthews, L. 2009. "Post Chaperonin Tubulin Folding Pathway." *Reactome - a Curated Knowledgebase of Biological Pathways*. https://doi.org/10.3180/react_16889.1.

McHugh, T., Zou, J., Volkov, V.A., Bertin, A., Talapatra, S.K., Rarrsilber, J., Dogterom, M., Welburn, J.P.I. 2019. "The depolymerase activivty of MCAK shows a graded response to Aurora B kinase phosphorylation through allosteric regulation." *Journal Cell Science.* 132: jcs228353.

Minoura, Itsushi, You Hachikubo, Yoshihiko Yamakita, Hiroko Takazaki, Rie Ayukawa, Seiichi Uchimura, and Etsuko Muto. 2013. "Overexpression, Purification, and Functional Analysis of Recombinant Human Tubulin Dimer." *FEBS Letters* 587 (21): 3450–55.

Mitchison, T., L. Evans, E. Schulze, and M. Kirschner. 1986. "Sites of Microtubule Assembly and Disassembly in the Mitotic Spindle." *Cell* 45 (4): 515–27.

Mitchison, T. J. 1989. "Polewards Microtubule Flux in the Mitotic Spindle: Evidence from Photoactivation of Fluorescence." *The Journal of Cell Biology* 109 (2): 637–52.

Monroy, Brigette Y., Tracy C. Tan, Janah May Oclaman, Jisoo S. Han, Sergi Simó, Shinsuke Niwa, Dan W. Nowakowski, Richard J. McKenney, and Kassandra M. Ori-McKenney. 2020. "A Combinatorial MAP Code Dictates Polarized Microtubule Transport." *Developmental Cell* 53. https://doi.org/10.1101/731604.

Musacchio, Andrea. 2015. "The Molecular Biology of Spindle Assembly Checkpoint Signaling Dynamics." *Current Biology: CB* 25 (20): R1002–18.

Ohi, Ryoma, Claire Strothman, and Marija Zanic. 2021. "Impact of the 'tubulin Economy' on the Formation and Function of the Microtubule Cytoskeleton." *Current Opinion in Cell Biology*. https://doi.org/10.1016/j.ceb.2020.09.005.

Ojima, I., S. Chakravarty, T. Inoue, S. Lin, L. He, S. B. Horwitz, S. D. Kuduk, and S. J. Danishefsky. 1999. "A Common Pharmacophore for Cytotoxic Natural Products That Stabilize Microtubules." *Proceedings of the National Academy of Sciences of the United States of America* 96 (8): 4256–61.

Ori-McKenney, Kassandra M., Richard J. McKenney, Hector H. Huang, Tun Li, Shan Meltzer, Lily Yeh Jan, Ronald D. Vale, Arun P. Wiita, and Yuh Nung Jan. 2016. "Phosphorylation of β-Tubulin by the Down Syndrome Kinase, Minibrain/DYRK1a, Regulates Microtubule Dynamics and Dendrite Morphogenesis." *Neuron* 90 (3): 551–63.

O'Toole, Eileen, Mary Morphew, and J. Richard McIntosh. 2019. "Electron Tomography Reveals Aspects of Spindle Structure Important for Mechanical Stability at Metaphase." Edited by Fred Chang. *Molecular Biology of the Cell*, December, mbc.E19–07 – 0405.

Park, In Young, Reid T. Powell, Durga Nand Tripathi, Ruhee Dere, Thai H. Ho, T. Lynne Blasius, Yun Chen Chiang, et al. 2016. "Dual Chromatin and Cytoskeletal Remodeling by SETD2." *Cell* 166 (4): 950–62.

Petry, Sabine. 2016. "Mechanisms of Mitotic Spindle Assembly." *Annual Review of Biochemistry* 85 (June): 659–83.

Piedra, Felipe-Andrés, Tae Kim, Emily S. Garza, Elisabeth A. Geyer, Alexander Burns, Xuecheng Ye, and Luke M. Rice. 2016. "GDP-to-GTP Exchange on the Microtubule End Can Contribute to the Frequency of Catastrophe." *Molecular Biology of the Cell* 27 (22): 3515–25.

Piperno, G., M. LeDizet, and X. J. Chang. 1987. "Microtubules Containing Acetylated Alpha-Tubulin in Mammalian Cells in Culture." *The Journal of Cell Biology* 104 (2): 289–302.

Portran, Didier, Laura Schaedel, Zhenjie Xu, Manuel Théry, and Maxence V. Nachury. 2017. "Tubulin Acetylation Protects Long-Lived Microtubules against Mechanical Ageing." *Nature Cell Biology* 19 (4): 391–98.

Prota, Andrea E., Maria M. Magiera, Marijn Kuijpers, Katja Bargsten, Daniel Frey, Mara Wieser, Rolf Jaussi, et al. 2013. "Structural Basis of Tubulin Tyrosination by Tubulin Tyrosine Ligase." *The Journal of Cell Biology*. https://doi.org/10.1083/jcb.201211017.

Raybin, D., and M. Flavin. 1977. "Modification of Tubulin by Tyrosylation in Cells and Extracts and Its Effect on Assembly in Vitro." *The Journal of Cell Biology* 73 (2): 492–504.

Rebehmed, Joseph, Patrick Revy, Guilhem Faure, Jean-Pierre de Villartay, and Isabelle Callebaut. 2014. "Expanding the SRI Domain Family: A Common Scaffold for Binding the Phosphorylated C-Terminal Domain of RNA Polymerase II." *FEBS Letters* 588 (23): 4431–37.

Roll-Mecak, Antonina. 2019. "How Cells Exploit Tubulin Diversity to Build Functional Cellular Microtubule Mosaics." *Current Opinion in Cell Biology* 56 (February): 102–8.

Schaedel, Laura, Karin John, Jérémie Gaillard, Maxence V. Nachury, Laurent Blanchoin, and Manuel Théry. 2015. “Microtubules Self-Repair in Response to Mechanical Stress.” *Nature Materials* 14 (11): 1156–63.

Schindelin, Johannes, Ignacio Arganda-Carreras, Erwin Frise, Verena Kaynig, Mark Longair, Tobias Pietzsch, Stephan Preibisch, et al. 2012. “Fiji: An Open-Source Platform for Biological-Image Analysis.” *Nature Methods* 9 (7): 676–82.

Seervai, Riyad N. H., Rahul K. Jangid, Menuka Karki, Durga Nand Tripathi, Sung Yun Jung, Sarah E. Kearns, Kristen J. Verhey, et al. 2020. “The Huntingtin-Interacting Protein SETD2/HYPB Is an Actin Lysine Methyltransferase.” *Science Advances*. https://doi.org/10.1126/sciadv.abb7854.

Shida, Toshinobu, Juan G. Cueva, Zhenjie Xu, Miriam B. Goodman, and Maxence V. Nachury. 2010. “The Major α-Tubulin K40 Acetyltransferase αTAT1 Promotes Rapid Ciliogenesis and Efficient Mechanosensation.” *Proceedings of the National Academy of Sciences of the United States of America* 107 (50): 21517–22.

Silkworth, William T., and Daniela Cimini. 2012. “Transient Defects of Mitotic Spindle Geometry and Chromosome Segregation Errors.” *Cell Division* 7 (1): 19.

Spector, I., N. R. Shochet, Y. Kashman, and A. Groweiss. 1983. “Latrunculins: Novel Marine Toxins That Disrupt Microfilament Organization in Cultured Cells.” *Science* 219 (4584): 493–95.

Svitkina, Tatyana. 2018. “The Actin Cytoskeleton and Actin-Based Motility.” *Cold Spring Harbor Perspectives in Biology* 10 (1). https://doi.org/10.1101/cshperspect.a018267.

Szyk, Agnieszka, Alexandra M. Deaconescu, Grzegorz Piszczek, and Antonina Roll-Mecak. 2011. “Tubulin Tyrosine Ligase Structure Reveals Adaptation of an Ancient Fold to Bind and Modify Tubulin.” *Nature Structural & Molecular Biology* 18 (11): 1250–58.

Szyk, Agnieszka, Alexandra M. Deaconescu, Jeffrey Spector, Benjamin Goodman, Max L. Valenstein, Natasza E. Ziolkowska, Vasilisa Kormendi, Nikolaus Grigorieff, and Antonina Roll-Mecak. 2014. “Molecular Basis for Age-Dependent Microtubule Acetylation by Tubulin Acetyltransferase.” *Cell* 157 (6): 1405–15.

Terman, Jonathan R., and Anna Kashina. 2013. “Post-Translational Modification and Regulation of Actin.” *Current Opinion in Cell Biology* 25 (1): 30–38.

Ti, Shih-Chieh, Gregory M. Alushin, and Tarun M. Kapoor. 2018. “Human β-Tubulin Isotypes Can Regulate Microtubule Protofilament Number and Stability.” *Developmental Cell* 47 (September): 1–16.

Ti, Shih-Chieh, Michal Wieczorek, and Tarun M. Kapoor. 2020. “Purification of Affinity Tag-Free Recombinant Tubulin from Insect Cells.” *STAR Protocols*, June, 100011.

Triclin, Sarah, Daisuke Inoue, Jeremie Gaillard, Zaw Min Htet, Morgan De Santis, Didier Portran, Emmanuel Derivery, et al. 2018. “Self-Repair Protects Microtubules from Their Destruction by Molecular Motors.” *bioRxiv*, 499020.

Valenstein, M. L. and Roll-Mecak A. 2016. “Graded Control of Microtubule Severing by Tubulin Glutamylation.” *Cell* 164(5):836-837.

Varland, Sylvia, Joël Vandekerckhove, and Adrian Drazic. 2019. “Actin Post-Translational Modifications: The Cinderella of Cytoskeletal Control.” *Trends in Biochemical Sciences* 44 (6): 502–16.

Vemu, Annapurna, Ewa Szczesna, Elena A. Zehr, Jeffrey O. Spector, Nikolaus Grigorieff, Alexandra M. Deaconescu, and Antonina Roll-Mecak. 2018. “Severing Enzymes Amplify Microtubule Arrays through Lattice GTP-Tubulin Incorporation.” *Science* 361 (6404). https://doi.org/10.1126/science.aau1504.

Verhey, Kristen J., and Jacek Gaertig. 2007. “The Tubulin Code.” *Cell Cycle* 6 (17): 2152–60.

Vermeulen, Katrien, Dirk R. Van Bockstaele, and Zwi N. Berneman. 2003. “The Cell Cycle: A Review of Regulation, Deregulation and Therapeutic Targets in Cancer.” *Cell Proliferation* 36 (3): 131–49.

Walker, R. A., E. T. O ’brien, N. K. Pryer, M. E. Soboeiro, W. A. Voter, H. P. Erickson, and E. D. Salmon. 1988. “Dynamic Instability of Individual Microtubules Analyzed by Video Light Microscopy: Rate Constants and Transition Frequencies” 107 (October): 1437–48.

Weisenberg, R. C., W. J. Deery, and P. J. Dickinson. 1976. “Tubulin-Nucleotide Interactions during the Polymerization and Depolymerization of Microtubules.” *Biochemistry* 15 (19): 4248–54.

Wilkinson, Alex W., Jonathan Diep, Shaobo Dai, Shuo Liu, Yaw Shin Ooi, Dan Song, Tie-Mei Li, et al. 2018. “SETD3 Is an Actin Histidine Methyltransferase That Prevents Primary Dystocia.” *Nature*, December, 1.

Xu, Zhenjie, Laura Schaedel, Didier Portran, Andrea Aguilar, Jérémie Gaillard, M. Peter Marinkovich, Manuel Théry, and Maxence V. Nachury. 2017. “Microtubules Acquire Resistance from Mechanical Breakage through Intralumenal Acetylation.” *Science* 356 (6335): 328–32.

Yoh, Sunnie M., Helen Cho, Loni Pickle, Ronald M. Evans, and Katherine A. Jones. 2007. "The Spt6 SH2 Domain Binds Ser2-P RNAPII to Direct Iws1-Dependent mRNA Splicing and Export." *Genes and Development* 21 (2): 160–74.

Yu, Nuo, Luca Signorile, Sreya Basu, Sophie Ottema, Joyce H. G. Lebbink, Kris Leslie, Ihor Smal, Dick Dekkers, Jeroen Demmers, and Niels Galjart. 2016. "Isolation of Functional Tubulin Dimers and of Tubulin-Associated Proteins from Mammalian Cells." *Current Biology: CB* 26 (13): 1728–36.

Zhai, Y., P. J. Kronebusch, and G. G. Borisy. 1995. "Kinetochore Microtubule Dynamics and the Metaphase-Anaphase Transition." *The Journal of Cell Biology* 131 (3): 721–34.

Zheng, Yihui, Xingrun Zhang, and Haitao Li. 2020. "Molecular Basis for Histidine N3-Specific Methylation of Actin H73 by SETD3." *Cell Discovery* 6 (January): 3.

Zilberman, Y., C. Ballestrem, L. Carramusa, R. Mazitschek, S. Khochbin, and A. Bershadsky. 2009. "Regulation of Microtubule Dynamics by Inhibition of the Tubulin Deacetylase HDAC6." *Journal of Cell Science* 122 (19): 3531–41.

Chapter 3: Mutations in SETD2 Tune Substrate Binding

3.1 Forward

This chapter will introduce cancer mutations that impact histone and tubulin methylation, focusing on clear cell renal cell carcinoma mutations found in SETD2. This work identifies the mechanism of tubulin methylation by SETD2 and is published in Kearns 2020 *bioRiv* and submitted to *JBC*.

3.2 Introduction

Cancer is, in part, due to mutations in genes that result in aberrant cell division. Many cancers including kidney, lung, bladder, glioma, and leukemia have inactivating mutations in histone methylating proteins, like SETD2 (Fontebasso et al. 2013; Zhu et al. 2014; Mar et al. 2017; Kim et al. 2019). SETD2 is an S-adenosyl-methionine (SAM)-dependent lysine methyltransferase, which on chromatin is responsible for histone-3 lysine 36 trimethylation (H3K36me3), a mark associated with gene transcription (Edmunds, Mahadevan, and Clayton 2008; J. Li, Duns, Westers, Sijmons, Van Den Berg, et al. 2016). Loss of SETD2 is embryonic lethal in part because its ability to trimethylate H3K36 is non-redundant (Hu et al. 2010). In clear cell renal cell carcinoma (ccRCC), SETD2 is the second most frequent mutation and is estimated to contribute to 10-15% of all ccRCC cases (Dalgliesh et al. 2010; Hakimi et al. 2013; Ho et al. 2014; W. Liu et al. 2015; J. Li, Duns, Westers, Sijmons, Van Den Berg, et al. 2016). For example, an arginine-to-cysteine mutation at position 1625 (R1625C), found within the catalytic SET domain, ablates methyltransferase activity and is thought to be pathogenic as it is associated with poor prognosis in the clinic. Another mutation, arginine-to-histidine at position 2510 (R2510H), occurs in the Set2-Rpb1-interacting (SRI)-domain at the C-terminus of SETD2 but does not result in loss of H3K36me3 (L. Liu et al., 2017.; Hacker et al. 2016; Park et al. 2016), suggesting that pathogenicity associated with this SRI domain mutation is not due to loss of histone methylation.

Our previous work demonstrated that SETD2 can methylate tubulin and that methylation occurs at Lysine 40 of α-tubulin (αTubK40me3) (Park et al. 2016; Kearns et al., 2020). In dividing cells, αTubK40me3 localizes to the minus ends of microtubules that form the mitotic spindle (Park et al. 2016). Loss of SETD2 in ccRCC and knock-out of SETD2 in cells results in genomic instability and mitotic defects such as multipolar spindles, lagging chromosomes during anaphase, chromosomal bridging during cytokinesis, and micronuclei (Park et al. 2016; Chiang et al. 2018). These phenotypes correlated with a drastic reduction in both H3K36me3 and αTubK40me3 methylation. Reintroduction of a truncated form of wild-type SETD2 (tSETD2) containing the SET and SRI domains rescued both histone and tubulin methylation as well as the mitotic defects (Park et al. 2016; Hacker et al. 2016). In contrast, expression of tSETD2 with the R2510H mutation in the SRI domain rescued histone methylation but was unable to rescue tubulin methylation or the mitotic defects (Park et al. 2016; Hacker et al. 2016) (Fig. 3.1A), suggesting that a loss of SETD2 activity can result in increased mitotic defects in a tubulin-dependent manner.

Here, I sought to understand how SETD2 methylation is regulated and how mutations in the enzyme alter activity by reconstituting tubulin methylation with ccRCC-associated SETD2 mutations. Utilizing binding and activity assays, I verified that tSETD2-R2510H cannot methylate tubulin, and identified that the lack of activity is due to ablated substrate binding. I generated additional SRI-domain mutations and tested if any of these residues were also important for tubulin binding. Interestingly, positively charged residues within the SRI domain are more important for tubulin binding where aromatic residues are more critical for RNA Pol II binding. Surprisingly, none of these residues impact actin binding, suggesting an alternative mechanism for actin substrate recognition. Together, these start to provide a mechanistic basis for the regulation of SETD2 amongst its various substrates.

3.3 Results

3.3.1 ccRCC-associated SRI domain mutant cannot methylate or bind tubulin

We started investigating the two most common ccRCC mutations in SETD2 by generating the associated point mutations in our tSETD2-FLAG construct (described in Ch. 2) to make either the SET-domain mutation, R1625C, or the SRI-domain mutation, R2510H (Fig. 3.1A). These constructs were then expressed and purified from mammalian cells, as with the WT enzyme described in Chapter 2 (Fig. 3.1B-C). tSETD2-FLAG constructs, either the R1615C or R2510H,

were expressed in COS-7 cells and immunostained to identify cellular localization (Fig. 3.2). Both mutants typically localize in the nucleus during interphase (Fig. 3.2C) and are cytoplasmic during mitosis (Fig. 3.2D). The nuclei with mutant overexpression, especially R2510H, have a different morphology than WT full length or truncated SETD2-FLAG, being less round and having more patchy DNA and FLAG staining. This could be due to the genomic instability that both mutants confer when dominantly expressed in cells, either due to the lack of histone or tubulin methylation by these mutants. Together, the purification (Fig 3.1) and expression (Fig 3.2) experiments show that we have intact and properly-localizing protein to use in our biochemical experiments.

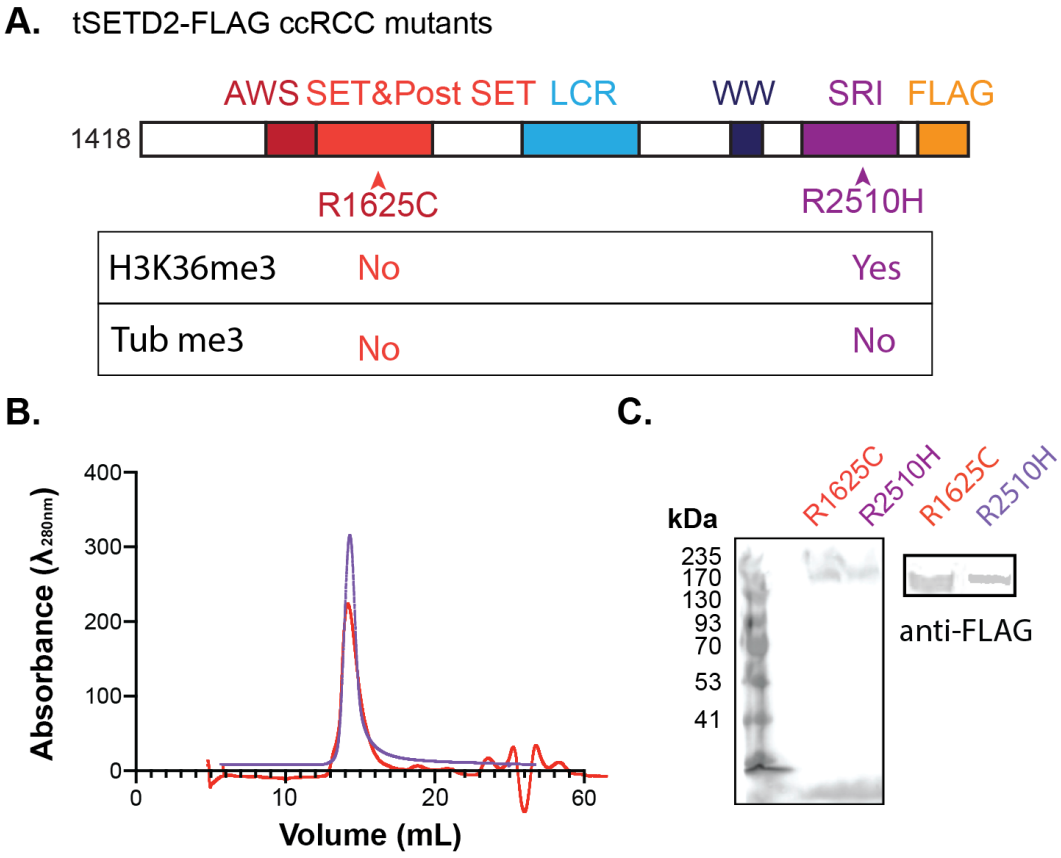

Fig. 3.1 Purification of ccRCC point mutations in tSETD2-FLAG A) Schematic of tSETD2-FLAG domain architecture highlighting the two main ccRCC mutations, R1625C in the SET domain (red) and R2510H in the SRI domain (purple). Previous in vivo studies show that R1625C rescues neither histone nor tubulin methylation, but R2510H mutation retains histone and loses tubulin methylation. B) Size exclusion chromatogram of both mutants purified from HEK293 cells. C) Mutants analyzed by Coomassie gel electrophoresis and western blot analysis with anti-FLAG.

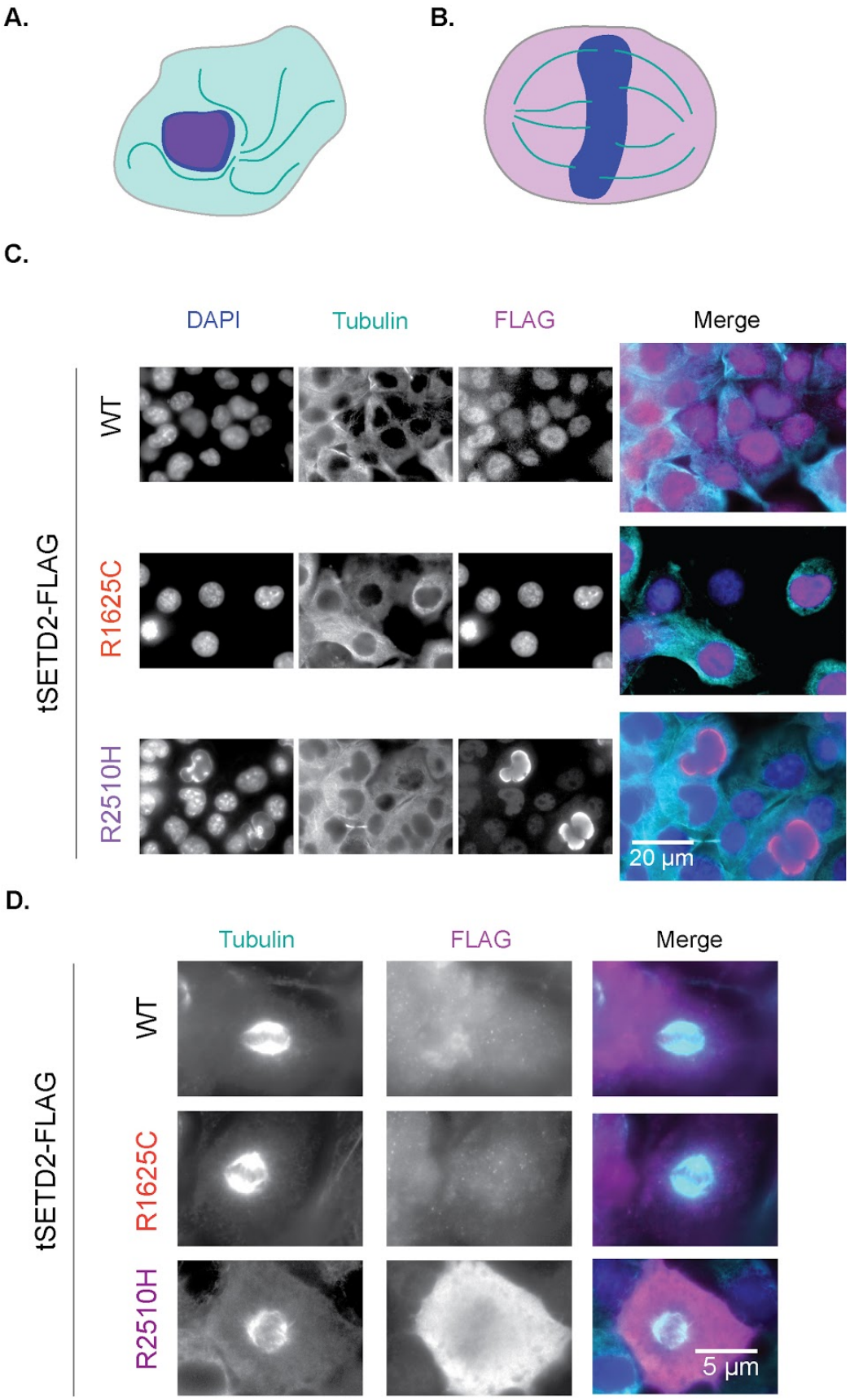

Fig. 3.2 ccRCC in tSETD2-FLAG mutations localize to cytoplasm during cell division. A-B) Cartoon schematic of fluorescent imaging results in A) interphase cells or B) mitotic cells, with DNA in blue, microtubules in cyan, and tSETD2-FLAG in pink. C-D) Representative images of tSETD2-FLAG WT, R1625C, and R2510H overexpression in COS-7 cells, stained with antibodies for DNA (DAPI 280nm), tubulin (Ms 488), and FLAG (Rb 680) in C) interphase cells or D) mitotic cells.

The ability of the mutant tSETD2 proteins to carry out methyltransferase activity was tested *in vitro* by utilizing the methyltransferase assay described in Chapter 2. Briefly, this assay works by monitoring the production of SAH, the byproduct of SAM-dependent methyl transfer, using fluorescence and then correlating the time-dependent fluorescence traces directly to methyltransferase activity. Using WT tSETD2-FLAG as a control, both the tSETD2(R1625C)-FLAG and tSETD2(R2510H)-FLAG mutant activities were tested with both histone H3 peptide (aa21-44) and porcine brain tubulin substrates. From the corrected fluorescence traces, the activity was calculated by determining the initial velocity using a linear fit over the first portion of the experiment. Compared to WT tSETD2-FLAG, tSETD2(R1625C)-FLAG had no methyltransferase activity with either tubulin protein or histone peptide substrate (Fig. 3.3A). This result was expected based on the literature (Hacker et al. 2016) as the R1625C mutation in the SET domain abolishes catalytic activity. For its histone substrate, this mutation within the catalytic domain is known to prevent proper positioning of a histone substrate with the methyl donor SAM in the binding pocket (Hacker et al. 2016). Compared to WT tSETD2-FLAG, tSETD2(R2510H)-FLAG shows no activity with tubulin but retains histone methylation, as expected (Hackler et al. 2016, Park et al. 2016). The fact that the R2510H mutation in the SRI domain does not abolish activity towards the histone peptide allows us to calculate Michaelis Menten kinetic values towards this substrate. Compared to WT tSETD2-FLAG, the R2510H mutant has a slightly higher v_{max} (9.49±1.255 vs 41±048 for the WT protein), a lower k_{cat} (7.08±0.97 vs 9.41±0.84 for the WT protein), yet comparable K_M (0.45±0.22 vs 0.45±0.32. for the WT protein) (Fig. 3.3B). This means that, despite a similar affinity for the H3 peptide, the R2510H mutant leads to a different turn-over rate than WT SETD2.

A.

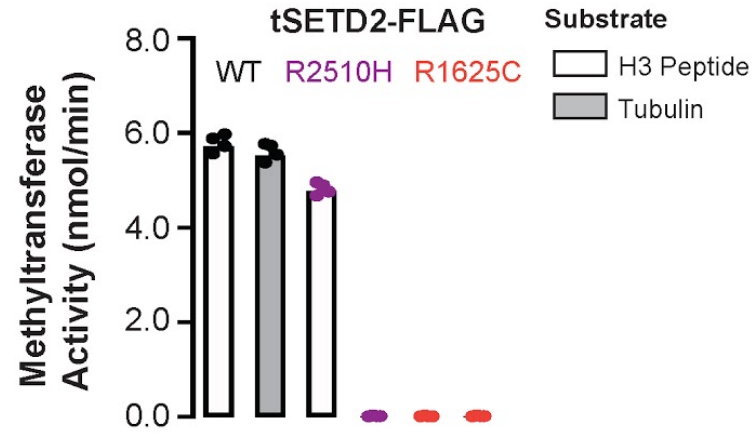

B.

Reaction (tSETD2-FLAG: Substrate)	WT: H3 peptide	WT: Tubulin	R1510H: H3 peptide
V_{max} (nmol/min)	5.41 ± 0.48	3.98 ± 0.12	9.49 ± 1.25
K_M (μM)	0.45 ± 0.32	0.75 ± 0.06	0.45 ± 0.22
K_{cat} (hr^{-1})	9.41 ± 0.84	3.68 ± 0.22	7.08 ± 0.97

C.

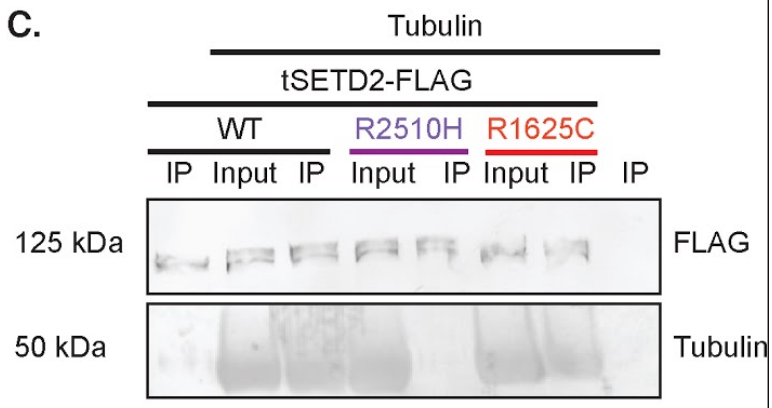

D.

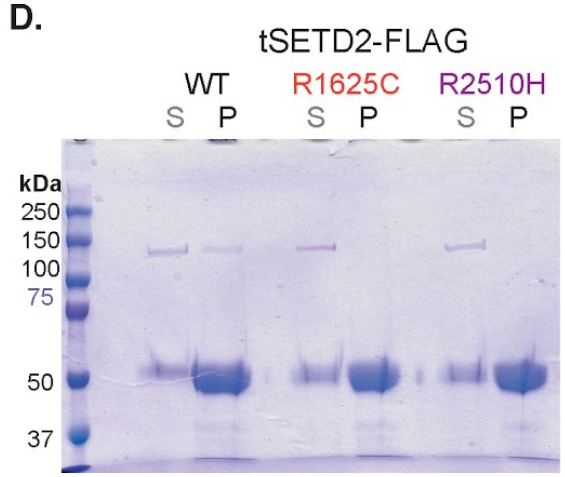

Fig. 3.3 R2510H ccRCC mutant cannot bind or methylate tubulin. A) Methyltransferase activity of tSETD2-FLAG WT (black dots), R1625C (red dots), and R2510H (purple dots), against histone H3 peptide (white bars) and tubulin dimers (grey bars) at 5 uM substrate concentration. Each dot indicates the average of a single experiment and the bar represents the average±SD methyltransferase activity across n=4 experiments. B) Kinetic constants measured by varying substrate concentration and performing Michaelis-Menton analysis. C) Co-immunoprecipitation of tubulin protein with WT, R1625C, and R2510H tSETD2-FLAG. The input and anti-FLAG pellet (IP) fraction were blotted with antibodies against FLAG tag (top) and β-tubulin E7 (bottom). D) Sedimentation assay of tSETD2-FLAG WT, R1625C, and R2510H with microtubules. The supernatant and pellet fractions were separate by SDS-PAGE and imaged by Coomassie gel. Proteins bound to microtubules are found in the pellet (P) fraction.

We hypothesized that the reduction in tubulin methylation by the R2510 mutation in the SRI domain could be due to reduced or abolished ability to bind the tubulin substrate. To test this, we performed pull-down assays to assess the interaction of WT, R1625C, and R2510H tSETD2-FLAG proteins with tubulin. We found that both WT and the SET domain mutant R1625C bound to tubulin but that the SRI domain mutant R2510H abolished the ability to bind tubulin (Fig. 3.3C). Likewise, we performed a co-sedimentation assay to see if these mutants are able to bind microtubules. Here we found that both mutants have reduced ability to bind to microtubules, (Fig. 3.3D). These results suggest that the ccRCC-associated mutation of R2510H in the SRI domain abolishes the ability of tSETD2-FLAG to bind to and methylate tubulin as a substrate.

3.3.2 SRI of SETD2 domain important for tubulin binding

So far, our work suggests that the SRI domain of tSETD2-FLAG is critical for interaction with tubulin as a substrate. Previous work demonstrated that protein-protein interactions between the SRI-domain of SETD2 and the highly phosphorylated C-terminal domain (CTD) repeat of RNA Pol II recruits SETD2 to chromatin during transcription (M. Li et al. 2005; Rebehmed et al. 2014). Performing a sequence alignment of all SRI-domains annotated in Pfam, we were able to identify highly conserved amino acids within the SRI domain (Fig. 3.4A). The structure shows that many conserved residues are hydrophobic and reside inside the core of the domain. We decided not to probe any of these hydrophobic residues because we hypothesized that disrupting these amino acids would drastically alter the fold of the domain. However, many residues along the outside of the helical bundle are not hydrophobic and are instead either positively charged or aromatic. Moreover, a handful of these residues are implicated in RNA Pol II binding. Previous structural studies using NMR took a purified human SRI domain and titrated peptides of the phosphorylated C-terminus of RNA Pol II and observed chemical shifts in residues V2483, F2505, K2506, R2510, and H2514 of the SRI domain (M. Li et al. 2005; Vojnic et al. 2006) (Fig. 3.4B). These shifts suggest that these residues undergo a conformational change upon RNA Pol II CTD binding. Our alignment coupled with previous NMR-based studies pointed to positions within the SRI domain we could probe to identify a mechanism between tubulin and RNA Pol II binding.

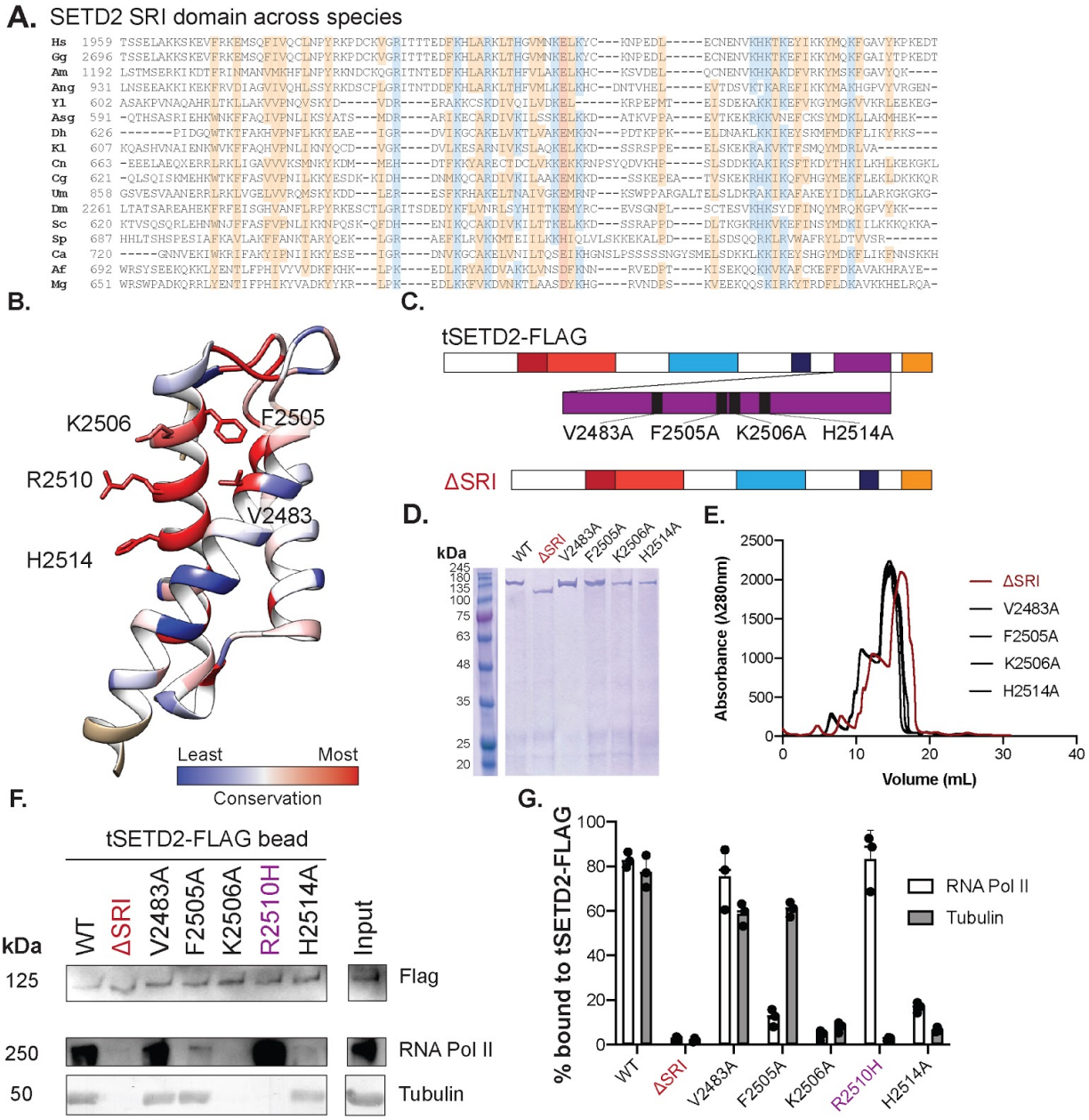

Fig. 3.4 The SRI domain of tSETD2 is critical for binding tubulin A) Sequence alignment of SETD2 SRI domain residues across species. Orange residues are hydrophobic residues important for three-helix bundle packing, blue are basic residues, and red is the acidic residue. B) Sequence conservation mapped onto the NMR structure of human SETD2 with most conserved residues colored in red and least in blue. Conserved residues that are not part of the hydrophobic packing are labeled. C) Some of the most conserved residues across species in the SRI domain (V2483, F2505, K2506, and H2514) were mutated to alanine, or the SRI domain was deleted. These constructs were expressed and purified D-E) and analyzed by D) Coomassie and E) size

exclusion chromatography. F) Purified WT, delSRI, or mutant versions of tSETD2-FLAG bound to anti-FLAG beads were incubated with either tubulin protein or HEK293 lysate. The presence of tSETD2-FLAG variant, tubulin, and RNA Pol II in the bead pellet was analyzed by western blotting with antibodies to the FLAG tag, α-tubulin, and phosphorylated RNA Pol II, respectively. The far right-column shows the input for the reaction with WT tSETD2-FLAG. G) Quantification of RNA Pol II (wihte) and porcine brain tubulin (grey) co-pelleting with tSETD2-FLAG as a percentage of the input reaction. Each dot indicates the percent bound from one experiment and the bar represents the average±SD across n=3 experiments.

We thus generated tSETD2-Flag variants with alanine mutations to V2483, F2505, K2506, R2510, and H2514. We also generated a construct lacking the SRI-domain (ΔSRI) as a control (Fig. 3.4C). The mutant and deletion variants of tSETD2-Flag were purified from mammalian cells as before and analyzed by Coomassie gel and size exclusion chromatography (Fig. 3.4D-E). We tested the ability of the purified mutant and deletion tSETD2-Flag proteins to bind to Pol II and tubulin using a co-immunoprecipitation assay (Fig. 3.4F-G). The tSETD2-Flag proteins bound to anti-FLAG beads were incubated with either porcine brain tubulin or HEK293 cell lysates containing endogenous RNA Pol II. As expected, deletion of the SRI domain (ΔSRI) abolished the ability of tSETD2-Flag to bind to both RNA Pol II and tubulin substrates. Interestingly, the SRI-domain mutants varied in their ability to bind to the two substrates. The V2483A mutant retained binding to both substrates, the F2505A retained tubulin but not Pol II binding, the R2510H mutant retained Pol II but not tubulin binding, and the K2506A and H2514A mutants lost the ability to bind to both tubulin and Pol II. These results indicate that the SRI domain is involved in substrate recognition and that distinct residues in the SRI domain contribute to recognition of different substrates.

3.3.3 Actin binding mechanism distinct from tubulin

Lastly, we were curious to see if the SRI-domain of SETD2 is also important for actin binding and methylation. When compared to WT tSETD2-FLAG, little difference was observed in the ability of R2510H tSETD2-FLAG to methylate actin (Fig. 3.5A-E). While. the WT and R2510H proteins show similar Km values toward actin, the Vmax for tSETD2(R2510H) is lower than for WT, suggesting that the kcat, or the turnover rate, is also lower for R2510H mutant. To assess binding, a co-immunoprecipitation assay with actin and different SRI-domain mutants of SETD2 showed

that there are no impairments in actin binding with any of the SRI-domain mutations (Fig. 3.5F). As such, actin binding and methylation do not depend on the SRI-domain. This suggests an alternative mechanism for actin binding and methylation that is distinct from tubulin or RNA Pol II binding and does not leverage the electrostatic interactions of the positively charged residues within the SRI-domain of SETD2.

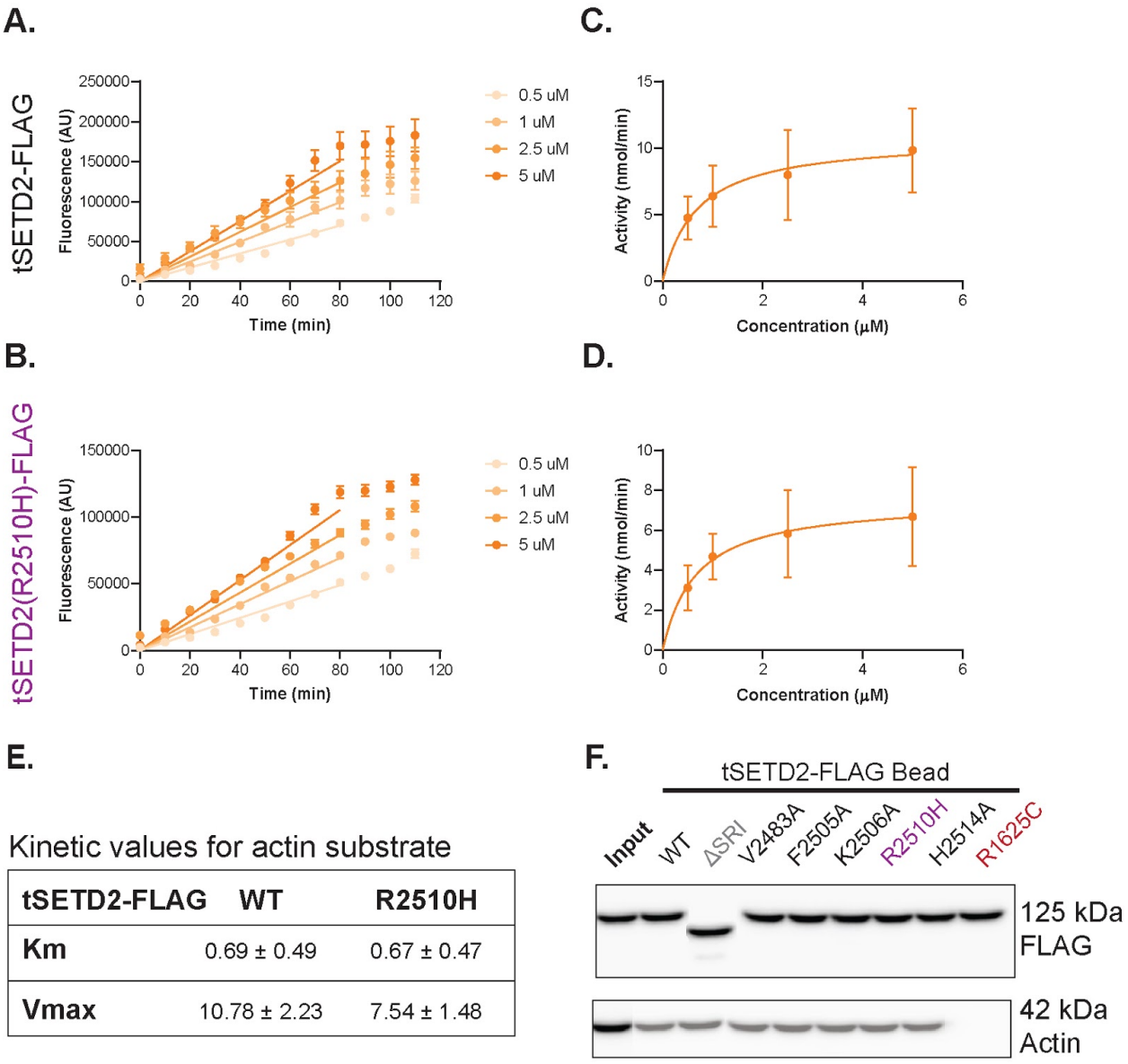

tSETD2-FLAG	WT	R2510H
Km	0.69 ± 0.49	0.67 ± 0.47
Vmax	10.78 ± 2.23	7.54 ± 1.48

Fig. 3.5 The SRI domain of tSETD2-FLAG is not important for actin binding or methylation.
A-B) Representative fluorescence traces of tSETD2-FLAG A) WT or B) R2510H with varying concentrations of actin. C-D) Michaelis-Menton kinetic plots of activity of tSETD2-FLAG C) WT

or D) R2510H. E) Kinetic constants calculated from C-D for WT and R2510H with actin substrate. E) Purified WT, delSRI, or mutant versions of tSETD2-FLAG bound to anti-FLAG beads were incubated with actin. The presence of tSETD2-FLAG variant and actin in the bead pellet was analyzed by western blotting with antibodies to the FLAG tag and actin, respectively. The far left-column shows the input for the reaction with WT tSETD2-FLAG.

3.4 Discussion

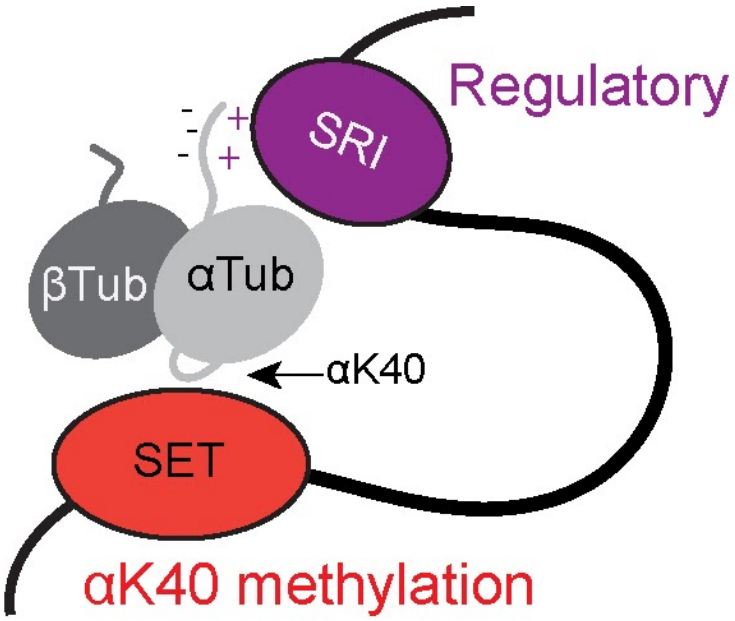

Fig. 3.6 Model of tubulin methylation by tSETD2. The SRI domain (purple) recognizes the negatively-charged CTT of α-tubulin (grey) and positions the SET domain (red) for methylation of α-tubulin at the K40 position.

3.4.1 Gotta keep 'em regulated

Work here shows that common ccRCC mutations in SETD2 tune binding and thus methylation of tubulin. In particular, mutations in the SRI domain alter binding for its tubulin and RNA Pol II binding partners, suggesting a regulation between tubulin and histone methylation substrates. Because positively-charged residues within the SRI domain are critical for tubulin binding, electrostatic interactions between the SRI domain and the negatively charged α-tubulin tail likely facilitate substrate recognition.

Tubulin binding that requires a functional SRI-domain appears to contradict previous work suggesting that the SET domain is sufficient for tubulin binding (Park et al. 2016). These discrepancies could be due to the use of different constructs and expression systems, as well as differences in experimental protocols. The fact that the interaction of RNA Pol II is less sensitive

than tubulin to the R2510H mutation may be related to the sequence and charge of these binding segments. Specifically, the CTD of Pol II contains 22 heptapeptide (YSPTSS) repeats, and is highly phosphorylated whereas the CTT of α-tubulin contains a short sequence of negatively-charged residues. Thus, the interaction between the SRI domain of SETD2 with RNA Pol II may better tolerate the R2510H mutation than the interaction of the SRI domain with α-tubulin. If so, caution should be taken when studying interactions with RNA Pol II CTD peptides containing fewer repeats which could produce different results than using full-length RNA Pol II. Nevertheless, these results provide strong support for the hypothesis that genomic instability in ccRCC can be driven by tubulin-dependent functions of SETD2 contributed by the SRI domain.

By mutagenesis of the SRI domain based on structural information in the literature (M. Li et al. 2005; Kizer et al. 2005), we were able to identify residues that further distinguish the ability of SETD2 to bind to tubulin versus Pol II. We demonstrate that the ability of tSETD2 to bind to tubulin requires not only the SRI domain residue R2510, but also K2506 and H2514. In contrast, the ability of tSETD2 to bind Pol II is influenced by F2505, K2506, and H2514. These results are largely consistent with previous studies using NMR structures of the SRI domain and titration experiments with phosphorylated Pol II peptides that implicated residues V2483, F2505, K2506, R2510, H2514 in forming part of the SRI-Pol II binding interface (M. Li et al. 2005; Vojnic et al. 2006; Rebehmed et al. 2014). However, while the isolated SRI domain with the R2510H point mutant showed decreased binding to RNA Pol II CTD peptides (M. Li et al. 2005), our results suggest that R2510H does not decrease the ability of tSETD2-FLAG to pull-down Pol II from cell lysates (Fig. 5C). These differences are likely due to differences in experimental conditions including the use of an isolated SRI domain versus tSETD2 and the use of Pol II peptides versus full-length CTD.

Our findings show that the positively-charged residues within the SRI domain make electrostatic interactions with the negatively-charged CTT of α-tubulin. Because the CTT of tubulins are often modified, tubulin PTMs could change substrate recognition. Especially polyglutamylation would add significantly more negative charge to the CTT and as such could increase binding affinity. Future work will have to look at the fine tuning of the SRI-domain as a tubulin PTM reader and how other modifications alter or crosstalk with methylation by SETD2. In addition, more work needs to be done to understand how mutations in the SRI impact histone methylation. We and others observed that methylation of histone peptides are also impacted by

SRI-domain mutations despite reactions lacking RNA-Pol II. As such, we suspect that there could be other histone-mediated interactions that could be required for proper H3K36 methylation by SETD2.

3.4.2 Role of cytoskeleton in cancer pathologies

Our findings provide further support for a role of SETD2 in writing the histone, tubulin, and actin codes. Here, we verified the *in vivo* studies (Hacker et al. 2016; Park et al. 2016) looking at two main kidney cancer mutations in SETD2, R1625C and R2510H, and found that both mutations abolish the ability of SETD2 to methylate tubulin. With binding assays, we expanded this model and found that the R2510H mutation cannot bind tubulin, thus launching an investigation whether the SRI domain regulates methylation by SETD2. As mutations in SETD2 continue to be identified in a growing list of tumor types (J. Li, Duns, Westers, Sijmons, van den Berg, et al. 2016; Chiang et al. 2018), it will be important to discern the relative roles of histone versus tubulin methylation in contributing to the underlying mechanisms of particular cancer phenotypes. A better understanding between histone, tubulin, and actin methylation by SETD2 could also drive anti-cancer drug development and thus could provide new therapeutic targets to help cancer patients.

Some of the SRI domain mutations we made probing RNA Pol II and tubulin binding are also found in other types of cancer. For example, the missense mutation of F2505L is found in patients with acute leukemia (Zhu et al. 2014), and blocks binding of SETD2 to RNA Pol II, and as such loses H3K36me3 (M. Li et al. 2005; Rebehmed et al. 2014). In general, similar missense mutations in SETD2 account for ~10% of genetic abnormalities of leukemia patients, though the mechanism of many of these mutations remains unclear since some do not impact histone methylation. Additionally, truncation mutations, K2469 and V2516, have also been identified in ccRCC patients, though similarly the mechanism remains unknown (Network 2013). These studies suggest that other residues within the SRI-domain may play a role in substrate recognition. Our data suggest that cytoskeletal methylation, in particular tubulin modifications, should be studied to understand leukemia- and kidney cancer-driving pathologies.

Other tubulin code factors beyond tubulin methylation have been shown to impact mitotic progression and may also underlie cancer phenotypes. A disruption of α-tubulin detyrosination leads to reduced chromosome congression and increased errors of kinetochore-microtubule attachment (Peris et al. 2009; Barisic et al. 2015; Liao et al. 2019; Ferreira et al. 2020). Moreover,

deregulation of the detyrosination-tyrosination cycle influences tumorigenesis (Mialhe et al. 2001; Kato et al. 2004; Souček et al. 2006). Additionally, tubulin glutamylation changes throughout the cell cycle, where levels increase during mitosis on both centriole and spindle microtubules, especially kinetochore microtubules (Bobinnec et al. 1998). The combination of detyrosination and polyglutamylation, mediated through septin, are important to recruit microtubule associated proteins to the microtubule lattice, where the inhibition of tyrosination and polyglutamylation leads to taxane-resistance (Froidevaux-Klipfel et al. 2015). With taxanes, like Taxol® commonly used in cancer treatment, these studies suggest a fine-tuning of tubulin modifications that can drive drug-resistant tumors in cancer patients. In addition to chemical modifications, tubulin isotypes also play a role in cancer, where an increase or decrease in expression levels of particular β-tubulin isotypes correlate to specific tumor types (Parker et al. 2017). For example, increased expression of Tubβ3 is implicated in lung, ovarian, breast, gastric, and prostate cancers and has a poor response to taxane treatment due to emerged drug resistance (Kavallaris, Burkhart, and Horwitz 1999; Hari et al. 2003; Akasaka et al. 2009; McCarroll et al. 2015). Further investigations into tubulin PTMs and their modifying enzymes are required to understand the nuanced interaction tubulin writers and readers and their implications for cancer progression.

Our findings showed that actin at lysine 68 can also be methylated by SETD2, and the lack of actin methylation impairs actin dynamics at the cell periphery. Similarly, arginine methylation of H73 of actin by SETD3 also is associated with actin polymerization (Nyman et al. 2002). Actin plays a significant role in cancer because oftentimes cancer cells are extremely motile (Yamaguchi, Wyckoff, and Condeelis 2005; Condeelis, Singer, and Segall 2005). As such, actin in cancer cells are typically more dynamic and have distinct cytoskeletal reorganization compared to non-cancer cells, contributing to metastasis. Compared with our findings that actin dynamics decrease without methylation, it suggests a disease-driving mechanism distinct from highly motile cells. That said, we found that actin methylation depends on HTT and the actin-binding protein HIP1R. HTT associates with SETD2 alters methylation activity by sequestration of the methyltransferase (Passani et al. 2000; Gao et al. 2014) in neurons, which also may have implications in Huntington's Disease since mutant HTT could promote abnormal interactions with other proteins. Additionally, HTT, SETD2, and actin can all localize in the nucleus, and nuclear actin regulates transcription and DNA repair (Hyrskyluoto and Vartiainen 2020). As such, SETD2, HTT, and actin could interact within the nucleus to additionally regulate cellular processes. However, without a better

understanding of how these proteins associate and bind, regulation of SETD2 methylation of actin remains unknown.

3.5 Materials & Methods

Plasmids.

An active truncated SETD2 construct (1418-2564) with a FLAG affinity tag (tSETD2-FLAG) for mammalian pInducer expression was gifted by the Walker Lab. Single isoform αTub1B/βTub3 plasmid was obtained from the Kapoor lab for insect cell expression (Ti, Wieczorek, and Kapoor 2020). Point mutations and domain deletions were generated using QuickChange site-directed mutagenesis with Q5 Polymerase (NEB). All plasmids were verified by DNA sequencing.

Purification.

SETD2. tSETD2-FLAG and all its variants was purified as described in Chapter 2.

αTub1B/βTub3 tubulin. Single isotype tubulin, in addition to the tail-less tubulin, was purified as described in Chapter 2.

Methyltransferase assay.

Activity of tSETD2-Flag constructs was surveyed using a Methyltransferase Fluorescence Assay Kit (Cayman Chemical, 700150) as described in Chapter 2.

Immunohistochemistry.

COS7 cells transiently expressing tSETD2-FLAG constructs were imaged as described in Chapter 2.

Microtubule polymerization.

GMPCPP-stabilized. αTub1B/βTub3 microtubules were prepared as described in Chapter 2.

Pull-down assay. FLAG M2 beads were blocked with 3% BSA in PBS for 1 hour and equilibrated in the reaction buffer (tSETD2-Flag size-exclusion buffer, described previously). tSETD2-Flag protein (WT or variants) was added at 20 μM with a putative binding partner for 2 hours in the

presence of SAM. For tubulin, 0.25 mg/mL of porcine tubulin (Cytoskeleton, Inc.) was used, for actin, 0.25 mg/mL of rabbit actin (Cytoskeleton, Inc. AKL99) was used, and for RNA Polymerase II, 10 μL of HEK293 Freestyle clarified lysate was used. Beads were spun down and the supernatant was collected as the fraction of unbound substrate. The beads were then resuspended in the reaction buffer to the total reaction volume, and the same amount of supernatant and beads were added to SDS-PAGE gel. Analysis of binding was conducted by western blot with the following antibodies: anti-FLAG (Sigma Aldrich, A9469, 1:1000), anti-tubulin antibodies E7 (DSHB, AB_528499, 1:1000) and/or TU-01 (Abcam, ab7750, 1:1000), anti-RNA Polymerase II (Abcam, ab193468, 1:1000), and anti-actin (Fisher Scientific, MS1295P0), with secondary antibody anti-mouse (Enzo Life Science, ADI-SAB-100-J, 1:1000) or anti-rabbit (Enzo Life Science, ADI-SAB-300-J, 1:1000), respectively. Binding was quantified by measuring the background-subtracted intensity of each band with Fiji ImageJ (Schindelin et al. 2012) as a fraction of the input intensity. Each experiment was performed three times, independently.

Sedimentation. Microtubules were polymerized by incubating 2.5 mg/mL porcine brain tubulin (Cyotskeleton Inc, #) with 0.1 mM GTP and 0.2 mM MgCl2 in BRB80 buffer and incubated at 37C for one hour. These microtubules were taxol stabilized by adding 100 uL of 2 mM taxol in BRB80 buffer and incubating at 37C for 30 minutes. Taxol stabilized microtubules were spun down at 15K rpm at room temperature for 10 minutes, before incubating with 5 uM tSETD2-FLAG. Reactions were incubated for one hour at room temperature, before 100 uL of cushion buffer, 2 mM taxol with 60% glycerol in BRB80, was added and the reaction was centrifuged at 100K xg at room temperature for 40 minutes. The uppermost layer of the supernatant was removed and the pellet was resuspended in 50 uL of 2uM taxol BRB80 buffer. Supernatant and pellet of each reaction was analyzed by Coomassie gel electrophoresis.

Sequence alignment. All SRI-domain containing proteins identified in Pfam (Finn et al. 2014) were aligned using Clustal Omega (Sievers and Higgins 2018). Alignments were imported into Chimera (Yang et al. 2012) and mapped onto the NMR structure of the human SETD2 SRI domain (M. Li et al. 2005).

3.6 References

Akasaka, Kiyomi, Chihaya Maesawa, Masahiko Shibazaki, Fumihiko Maeda, Kazuhiro Takahashi, Toshihide Akasaka, and Tomoyuki Masuda. 2009. "Loss of Class III Beta-Tubulin Induced by Histone Deacetylation Is Associated with Chemosensitivity to Paclitaxel in Malignant Melanoma Cells." *The Journal of Investigative Dermatology* 129 (6): 1516–26.

Barisic, Marin, Ricardo Silva e Sousa, Suvranta K. Tripathy, Maria M. Magiera, Anatoly V. Zaytsev, Ana L. Pereira, Carsten Janke, Ekaterina L. Grishchuk, and Helder Maiato. 2015. "Mitosis. Microtubule Detyrosination Guides Chromosomes during Mitosis." *Science* 348 (6236): 799–803.

Bobinnec, Y., M. Moudjou, J. P. Fouquet, E. Desbruyeres, B. Eddé, and M. Bornens. 1998. "Glutamylation of Centriole and Cytoplasmic Tubulin in Proliferating Non-Neuronal Cells." *Cell Motility and the Cytoskeleton* 39 (3): 223–32.

Chiang, Yun-Chen, In Young Park, W. Kimryn Rathmell, Cheryl Lyn Walker, and Ryoma Ohi. 2018. "SETD2 Haploinsufficiency for Microtubule Methylation Is an Early Driver of Genomic Instability in Renal Cell Carcinoma." *Cancer Research* 78 (12): 3135–46.

Condeelis, John, Robert H. Singer, and Jeffrey E. Segall. 2005. "The Great Escape: When Cancer Cells Hijack the Genes for Chemotaxis and Motility." *Annual Review of Cell and Developmental Biology* 21: 695–718.

Dalgliesh, Gillian L., Kyle Furge, Chris Greenman, Lina Chen, Graham Bignell, Adam Butler, Helen Davies, et al. 2010. "Systematic Sequencing of Renal Carcinoma Reveals Inactivation of Histone Modifying Genes." *Nature* 463 (7279): 360–63.

Edmunds, John W., Louis C. Mahadevan, and Alison L. Clayton. 2008. "Dynamic Histone H3 Methylation during Gene Induction: HYPB/Setd2 Mediates All H3K36 Trimethylation." *The EMBO Journal* 27 (2): 406–20.

Ferreira, Luísa T., Bernardo Orr, Girish Rajendraprasad, António J. Pereira, Carolina Lemos, Joana T. Lima, Clàudia Guasch Boldú, Jorge G. Ferreira, Marin Barisic, and Helder Maiato. 2020. "α-Tubulin Detyrosination Impairs Mitotic Error Correction by Suppressing MCAK Centromeric Activity." *The Journal of Cell Biology* 219 (4). https://doi.org/10.1083/jcb.201910064.

Finn, Robert D., Alex Bateman, Jody Clements, Penelope Coggill, Ruth Y. Eberhardt, Sean R. Eddy, Andreas Heger, et al. 2014. "Pfam: The Protein Families Database." *Nucleic Acids Research* 42 (Database issue): D222–30.

Fontebasso, Adam M., Jeremy Schwartzentruber, Dong-Anh Khuong-Quang, Xiao-Yang Liu, Dominik Sturm, Andrey Korshunov, David T. W. Jones, et al. 2013. “Mutations in SETD2 and Genes Affecting Histone H3K36 Methylation Target Hemispheric High-Grade Gliomas.” *Acta Neuropathologica* 125 (5): 659–69.

Froidevaux-Klipfel, Laurence, Benjamin Targa, Isabelle Cantaloube, Hayat Ahmed-Zaïd, Christian Poüs, and Anita Baillet. 2015. “Septin Cooperation with Tubulin Polyglutamylation Contributes to Cancer Cell Adaptation to Taxanes.” *Oncotarget* 6 (34): 36063–80.

Gao, Yong-Guang, Hui Yang, Jian Zhao, Ya-Jun Jiang, and Hong-Yu Hu. 2014. “Autoinhibitory Structure of the WW Domain of HYPB/SETD2 Regulates Its Interaction with the Proline-Rich Region of Huntingtin.” *Structure* 22 (3): 378–86.

Hacker, Kathryn E., Catherine C. Fahey, Stephen A. Shinsky, Yun-Chen J. Chiang, Julia V. DiFiore, Deepak Kumar Jha, Andy H. Vo, et al. 2016. “Structure/Function Analysis of Recurrent Mutations in SETD2 Protein Reveals a Critical and Conserved Role for a SET Domain Residue in Maintaining Protein Stability and Histone H3 Lys-36 Trimethylation.” *The Journal of Biological Chemistry* 291 (40): 21283–95.

Hakimi, A. Ari, Ying-Bei Chen, James Wren, Mithat Gonen, Omar Abdel-Wahab, Adriana Heguy, Han Liu, et al. 2013. “Clinical and Pathologic Impact of Select Chromatin-Modulating Tumor Suppressors in Clear Cell Renal Cell Carcinoma.” *European Urology* 63 (5): 848–54.

Hari, Malathi, Hailing Yang, Changqing Zeng, Martin Canizales, and Fernando Cabral. 2003. “Expression of Class III β-Tubulin Reduces Microtubule Assembly and Confers Resistance to Paclitaxel.” *Cell Motility and the Cytoskeleton* 56 (1): 45–56.

Ho, Thai Huu, Toni K. Choueiri, Anthony D’Amelio, James Hsieh, Paul L. De Souza, Keith C. Deen, Peter B. Langmuir, Yuan Liu, and Robert J. Motzer. 2014. “The Effect of *SETD2* Mutation (mts) on Histone 3 Lysine 36 Tri-Methylation (H3K36me3) and Correlation with Clinical Outcome in Patients (pts) with Metastatic Clear Cell Renal Cell Carcinoma (ccRCC) Enrolled in COMPARZ.” *Journal of Clinical Oncology: Official Journal of the American Society of Clinical Oncology* 32 (15_suppl): 4583–4583.

Hu, Ming, Xiao-Jian Sun, Yuan-Liang Zhang, Ying Kuang, Chao-Quan Hu, Wei-Li Wu, Shu-Hong Shen, et al. 2010. “Histone H3 Lysine 36 Methyltransferase Hypb/Setd2 Is Required for Embryonic Vascular Remodeling.” *Proceedings of the National Academy of Sciences of the United States of America* 107 (7): 2956–61.

Hyrskyluoto, Alise, and Maria K. Vartiainen. 2020. “Regulation of Nuclear Actin Dynamics in Development and Disease.” *Current Opinion in Cell Biology* 64 (June): 18–24.

Kato, Chiaki, Kou Miyazaki, Atsuko Nakagawa, Miki Ohira, Yohko Nakamura, Toshinori Ozaki, Toshio Imai, and Akira Nakagawara. 2004. “Low Expression of Human Tubulin Tyrosine Ligase and Suppressed Tubulin Tyrosination/detyrosination Cycle Are Associated with Impaired Neuronal Differentiation in Neuroblastomas with Poor Prognosis.” *International Journal of Cancer*. https://doi.org/10.1002/ijc.20431.

Kavallaris, M., C. A. Burkhart, and S. B. Horwitz. 1999. “Antisense Oligonucleotides to Class III Beta-Tubulin Sensitize Drug-Resistant Cells to Taxol.” *British Journal of Cancer* 80 (7): 1020–25.

Kearns, Sarah, Frank M. Mason, W. Kimryn Rathmell, In Young Park, Cheryl Walker, Kristen A. Verhey, and Michael A. Cianfrocco. 2020 “Molecular Determinants for α-Tubulin Methylation by SETD2.” https://doi.org/10.1101/2020.10.21.349365.

Kim, In-Kyu, Justine N. McCutcheon, Guanhua Rao, Stephen V. Liu, Yves Pommier, Marcin Skrzypski, Yu-Wen Zhang, and Giuseppe Giaccone. 2019. “Acquired SETD2 Mutation and Impaired CREB1 Activation Confer Cisplatin Resistance in Metastatic Non-Small Cell Lung Cancer.” *Oncogene* 38 (2): 180–93.

Kizer, Kelby O., Hemali P. Phatnani, Yoichiro Shibata, Hana Hall, Arno L. Greenleaf, and Brian D. Strahl. 2005. “A Novel Domain in Set2 Mediates RNA Polymerase II Interaction and Couples Histone H3 K36 Methylation with Transcript Elongation.” *Molecular and Cellular Biology* 25 (8): 3305–16.

Liao, Shanhui, Girish Rajendraprasad, Na Wang, Susana Eibes, Jun Gao, Huijuan Yu, Gao Wu, et al. 2019. “Molecular Basis of Vasohibins-Mediated Detyrosination and Its Impact on Spindle Function and Mitosis.” *Cell Research*, June, 1.

Li, Jun, Gerben Duns, Helga Westers, Rolf Sijmons, Anke van den Berg, and Klaas Kok. 2016. “SETD2: An Epigenetic Modifier with Tumor Suppressor Functionality.” *Oncotarget* 7 (31): 50719–34.

Li, Jun, Gerben Duns, Helga Westers, Rolf Sijmons, Anke Van Den Berg, and Klaas Kok. 2016. “SETD2: An Epigenetic Modifier with Tumor Suppressor Functionality.” *Oncotarget* 7 (31).

Li, Ming, Hemali P. Phatnani, Ziqiang Guan, Harvey Sage, Arno L. Greenleaf, and Pei Zhou. 2005. “Solution Structure of the Set2–Rpb1 Interacting Domain of Human Set2 and Its Interaction with

the Hyperphosphorylated C-Terminal Domain of Rpb1." *Proceedings of the National Academy of Sciences of the United States of America* 102 (49): 17636–41.

Liu, Lei, Renbo Guo, Xiang Zhang, Yiran Liang, Feng Kong, Jue Wang, and Zhonghua Xu. 2017 "Loss of SETD2, but Not H3K36me3, Correlates with Aggressive Clinicopathological Features of Clear Cell Renal Cell Carcinoma Patients." https://doi.org/10.5582/bst.2016.01228.

Liu, Weisi, Qiang Fu, Huimin An, Yuan Chang, Weijuan Zhang, Yu Zhu, Le Xu, and Jiejie Xu. 2015. "Decreased Expression of SETD2 Predicts Unfavorable Prognosis in Patients With Nonmetastatic Clear-Cell Renal Cell Carcinoma." *Medicine* 94 (45): e2004.

Mar, Brenton G., S. Haihua Chu, Josephine D. Kahn, Andrei V. Krivtsov, Richard Koche, Cecilia A. Castellano, Jacob L. Kotlier, et al. 2017. "SETD2 Alterations Impair DNA Damage Recognition and Lead to Resistance to Chemotherapy in Leukemia." *Blood* 130 (24): 2631–41.

McCarroll, Joshua A., George Sharbeen, Jie Liu, Janet Youkhana, David Goldstein, Nigel McCarthy, Lydia F. Limbri, et al. 2015. "βIII-Tubulin: A Novel Mediator of Chemoresistance and Metastases in Pancreatic Cancer." *Oncotarget* 6 (4): 2235–49.

Mialhe, A., L. Lafanechère, I. Treilleux, N. Peloux, C. Dumontet, A. Brémond, M. H. Panh, et al. 2001. "Tubulin Detyrosination Is a Frequent Occurrence in Breast Cancers of Poor Prognosis." *Cancer Research* 61 (13): 5024–27.

Network, The Cancer Genome Atlas Research. 2013. "Comprehensive Molecular Characterization of Clear Cell Renal Cell Carcinoma." *Nature* 499 (7456): 43–49.

Nyman, Tomas, Herwig Schüler, Elena Korenbaum, Clarence E. Schutt, Roger Karlsson, and Uno Lindberg. 2002. "The Role of MeH73 in Actin Polymerization and ATP Hydrolysis." *Journal of Molecular Biology* 317 (4): 577–89.

Parker, Amelia L., Wee Siang Teo, Joshua A. McCarroll, and Maria Kavallaris. 2017. "An Emerging Role for Tubulin Isotypes in Modulating Cancer Biology and Chemotherapy Resistance." *International Journal of Molecular Sciences* 18 (7). https://doi.org/10.3390/ijms18071434.

Park, In Young, Reid T. Powell, Durga Nand Tripathi, Ruhee Dere, Thai H. Ho, T. Lynne Blasius, Yun Chen Chiang, et al. 2016. "Dual Chromatin and Cytoskeletal Remodeling by SETD2." *Cell* 166 (4): 950–62.

Passani, L. A., M. T. Bedford, P. W. Faber, K. M. McGinnis, A. H. Sharp, J. F. Gusella, J. P. Vonsattel, and M. E. MacDonald. 2000. "Huntingtin's WW Domain Partners in Huntington's Disease Post-

Mortem Brain Fulfill Genetic Criteria for Direct Involvement in Huntington's Disease Pathogenesis." *Human Molecular Genetics* 9 (14): 2175–82.

Peris, Leticia, Michael Wagenbach, Laurence Lafanechère, Jacques Brocard, Ayana T. Moore, Frank Kozielski, Didier Job, Linda Wordeman, and Annie Andrieux. 2009. "Motor-Dependent Microtubule Disassembly Driven by Tubulin Tyrosination." *The Journal of Cell Biology* 185 (7): 1159–66.

Rebehmed, Joseph, Patrick Revy, Guilhem Faure, Jean-Pierre de Villartay, and Isabelle Callebaut. 2014. "Expanding the SRI Domain Family: A Common Scaffold for Binding the Phosphorylated C-Terminal Domain of RNA Polymerase II." *FEBS Letters* 588 (23): 4431–37.

Schindelin, Johannes, Ignacio Arganda-Carreras, Erwin Frise, Verena Kaynig, Mark Longair, Tobias Pietzsch, Stephan Preibisch, et al. 2012. "Fiji: An Open-Source Platform for Biological-Image Analysis." *Nature Methods* 9 (7): 676–82.

Sievers, Fabian, and Desmond G. Higgins. 2018. "Clustal Omega for Making Accurate Alignments of Many Protein Sequences." *Protein Science: A Publication of the Protein Society* 27 (1): 135–45.

Souček, Karel, Andrés Kamaid, Anh D. Phung, Lukáš Kubala, J. Chloë Bulinski, Richart W. Harper, and Jason P. Eiserich. 2006. "Normal and Prostate Cancer Cells Display Distinct Molecular Profiles of α-Tubulin Posttranslational Modifications." *The Prostate* 66 (9): 954–65.

Ti, Shih-Chieh, Michal Wieczorek, and Tarun M. Kapoor. 2020. "Purification of Affinity Tag-Free Recombinant Tubulin from Insect Cells." *STAR Protocols*, June, 100011.

Vojnic, Erika, Bernd Simon, Brian D. Strahl, Michael Sattler, and Patrick Cramer. 2006. "Structure and Carboxyl-Terminal Domain (CTD) Binding of the Set2 SRI Domain That Couples Histone H3 Lys36 Methylation to Transcription." *The Journal of Biological Chemistry* 281 (1): 13–15.

Yamaguchi, Hideki, Jeffrey Wyckoff, and John Condeelis. 2005. "Cell Migration in Tumors." *Current Opinion in Cell Biology* 17 (5): 559–64.

Yang, Zheng, Keren Lasker, Dina Schneidman-Duhovny, Ben Webb, Conrad C. Huang, Eric F. Pettersen, Thomas D. Goddard, Elaine C. Meng, Andrej Sali, and Thomas E. Ferrin. 2012. "UCSF Chimera, MODELLER, and IMP: An Integrated Modeling System." *Journal of Structural Biology* 179 (3): 269–78.

Zhu, Xiaofan, Fuhong He, Huimin Zeng, Shaoping Ling, Aili Chen, Yaqin Wang, Xiaomei Yan, et al. 2014. "Identification of Functional Cooperative Mutations of SETD2 in Human Acute Leukemia." *Nature Genetics* 46 (3): 287–93.

Chapter 4: Future Directions

4.1 Structure of tubulin with SETD2

My data shows first and foremost that the histone lysine methyltransferase SETD2 has a wider substrate scope than just histones and can modify cytoskeletal elements tubulin and actin *in vitro*. For tubulin methylation, I found that positive residues on the SRI domain of SETD2 make electrostatic interactions with a-tubulin CTT. This allows the SET domain to wrap around tubulin and methylate the aK40 site. SETD2 is able to methylate both tubulin dimers in solution in addition to microtubule polymers but has higher activity with the former. For actin methylation, we found that SETD2 methylates K68, which is accessible in both monomer and filamentous actin populations, and as such can methylate both with equal activity. Our cartoon model of tubulin methylation by SETD2 accurately summarizes what our studies have found (Fig. 3.6), but it certainly lacks high resolution data. Further understanding into how the SRI domain binds tubulin, or how the SET domain interacts with the K40 loop of α-tubulin, requires higher resolution information about the structure. Due to the high flexibility and large size of the tubulin-tSETD2 complex, we would turn to cryoEM and perform single particle analysis.

When considering the microtubule and tubulin dimer substrates of SETD2, my data suggests that the tSETD2-tubulin dimer complex (Fig. 4.1A) is likely to be a better structural target based on activity and binding assays. However, a small amount of tSETD2-FLAG remains in complex with tubulin when performing size exclusion chromatography (Fig. 4.1B), and moreover this complex dissociates or aggregates on cryoEM grids (Fig. 4.1C). tSETD2-FLAG itself also has a lot of flexibility and the domains that have structural features are too small compared to the whole protein to be able to find particles. To try and get a structure of tSETD2, with or without tubulin, crosslinkers may have to be used to stabilize the structure. By exposing macromolecular complexes to a low concentration of chemical cross-linkers during sedimentation, the gradient fixation (GraFix) can stabilize individual particles (Kastner et al. 2008; Stark 2010). During the cross-linking process, covalent bonds are formed between functional groups, thus making the protein complex less flexible and more stable. Centrifuging helps prevent aggregation and

precipitation due to the increased pressure during the hard spin. To use GraFix on the tSETD2-tubulin structure, the chemical cross-linker and buffer would have to be optimized, in addition to any glycerol removal before grid application. But optimization of parameters could result in a stable complex which would help obtain the structure of tubulin with SETD2. In addition, because full length SETD2 is autoinhibited, and not to mention much larger, crosslinking may be able to stabilize the autoinhibited protein.

One thing that would be helpful is knowing the structure of the tubulin dimer. Historically, the tubulin dimer structure has been difficult to solve due to its small size of ~100 kDa. In the late 1990s, a structure of the tubulin dimer within the lattice was determined using electron crystallography, where the addition of zinc ions induced anti-parallel protofilaments sheets (Nogales, Wolf, and Downing 1998). This resulted in a 3.7 Å model, a feat at the time but not useful in answering questions about tubulin dimer state in solution. More recent microscopy and structural studies have looked at tubulin dimers within the microtubule lattice using cryoEM, for example identifying the motor binding site and longitudinal contacts within the lattice (Arnal et al. 1996; Nogales et al. 1999; Meurer-Grob, Kasparian, and Wade 2001). With the "resolution revolution" and better data processing software and pipelines, more details can be observed in the lattice structure, for example how nucleotide state, tubulin isotypes, protein binding, and small molecules impact the lattice (Li et al. 2002; Alushin et al. 2014; Zhang et al. 2015; Kellogg et al. 2017; Zhang, LaFrance, and Nogales 2018; Kellogg et al. 2018; Ti, Alushin, and Kapoor 2018). Despite the advances and detail into the microtubule polymer, the tubulin dimer structure remains unknown. Some recent work has looked at tubulin oligomers, and found that straight oligomers promote nucleation and polymerization of microtubules (Ayukawa et al. 2020). However, the mechanism of plus-end growth of microtubules has been contested (McIntosh et al. 2018; Mickolajczyk et al. 2019). Knowing the conformation of tubulin dimers in solution (straight or bent, elongated or compact) will make clear the role of nucleotide state on polymerization, and how proteins interacting with dimers alters polymerization dynamics at a structural level.

Our preliminary studies looking at just tubulin dimers have focused on sample preparation, because, to our knowledge, this structure has not been attempted since better detectors were developed. Because porcine tubulin in a microtubule buffer contains high background and either promotes aggregation (Fig. 4.1E) or polymerization (Fig. 4.1F), we turned to a recombinant yeast tubulin that contains mutations in β-tubulin that block polymerization (Johnson et al. 2011) (Fig.

4.1G). We collected a full dataset of yeast tubulin on gold grids (Fig. 4.1H-I), combining tilted and untitled micrographs in the attempt to overcome preferred orientation. However, we were unable to overcome preferred orientation during data processing and were stuck at an ~10 Å map. Switching to carbon grids, we were able to obtain more side views of the tubulin dimer (Fig. 4.1J-K). From this half-day of screening, we were able to obtain an 6.7 Å map using particles picked by Warp (Tegunov and Cramer 2019) and processed in cryoSPARC (Punjani et al. 2017) (Fig. 4.1L). Molecular docking of previously solved tubulin structure (pdbid: 1tub, Fig. 4.1M) suggests that our dimer structure has a straight and uncompressed conformation. However, more work will need to be done to get this structure to high resolution, perhaps through more data collection or better particle picking. Limitations so far have been preferred orientation and thick ice on the grid, so different grids, such as graphene oxide, could be used to obtain thin ice and overcome preferred particle orientation.

If we had the structures of both tubulin dimers and the SETD2-tubulin complex, we would be able to more specifically identify how the SRI-domain of SETD2 recognizes and binds to tubulin in addition to finding other domains that are important for substrate recognition. While studies have shown the WW domain flanking the SRI-domain is important for autoinhibition of full length SETD2, it could be the case that the WW domain plays other roles in protein-protein interactions with tubulin (or other substrates). Seeing the structure of SETD2 bound to substrate would show us what other domains are important for tubulin binding and methylation. Moreover, SETD2 bound to actin would allow us to elucidate how these proteins interact because our biochemical data so far has shown us negative results. Comparing structures of SETD2 with different substrates would highlight the nuanced difference in substrate specificity and recognition. Because histone, tubulin, and actin methylation all have different outcomes in the cell, fine-tuning the structure through small molecule drugs could alter activity specifically. As such, a structure of SETD2 with its various substrates could enable structure-based drug design.

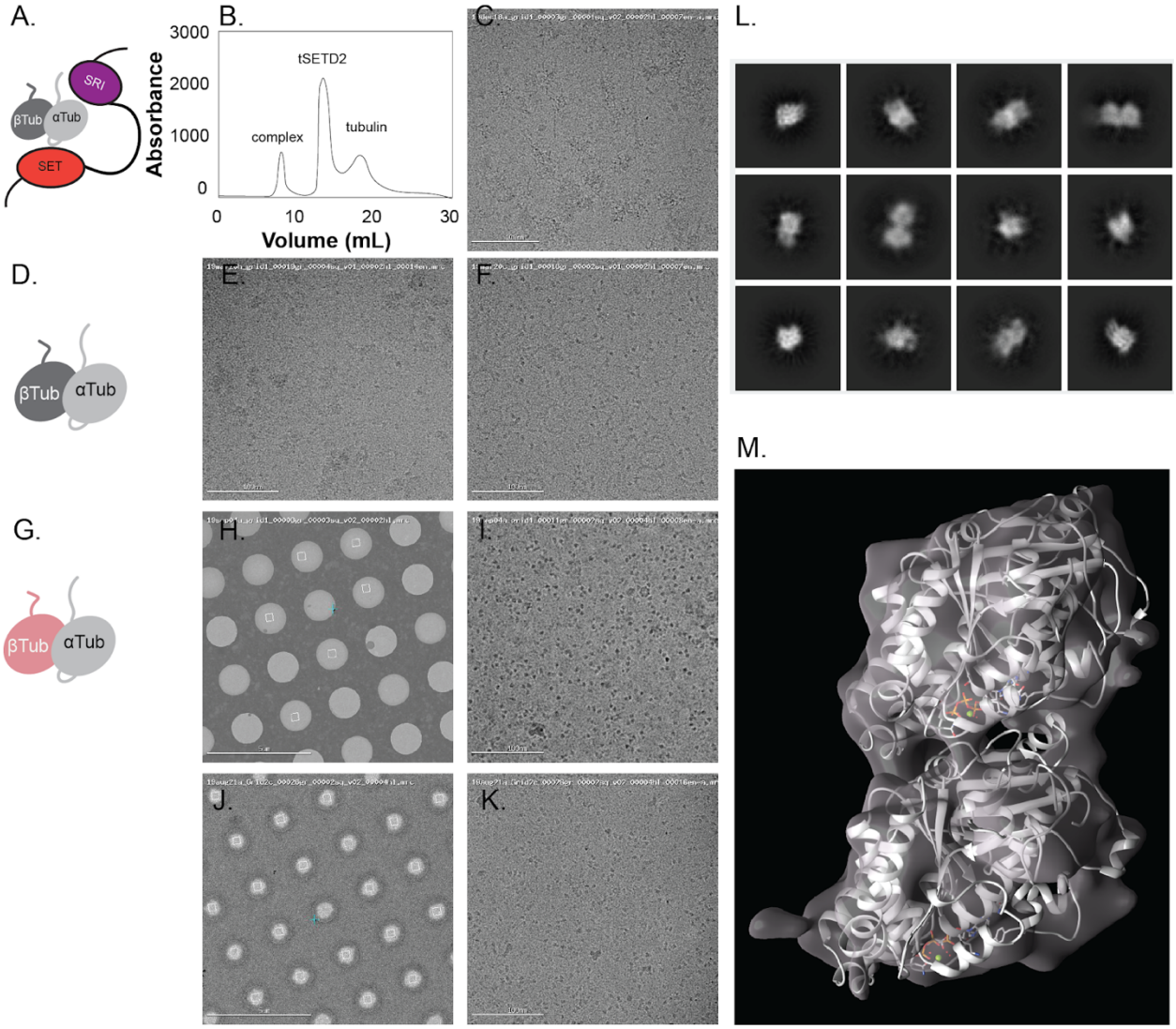

Fig. 4.1 Efforts into getting the tubulin dimer structure. A-C) tSETD2-FLAG in complex with tubulin A) schematic B) size-exclusion chromatography of the tSETD2-FLAG complex C) micrograph of complex aggregated on a grid. D-F) Single isotype tubulin D) schematic E) aggregation on a grid F) oligomer formation on a grid G-K) yeast tubulin with β-tubulin mutations that block polymerization G) schematic, β-tubulin in red to signify mutation H) gold grid at hole level I) micrograph at exposure level of preferred orientation particles on gold grid J) carbon grid at the hole level K) micrograph at exposure level of particles on carbon grid L) Subset of 2D classes M) 3D refinement with tubulin dimer docked.

4.2 Image tubulin methylation on mitotic spindles

In addition to obtaining the structure of tSETD2-FLAG with tubulin dimer, we would want to further observe the enzyme's localization in cells. Our studies show that tSETD2-FLAG is dispersed throughout the cytoplasm during mitosis, but when and how it specifically goes to the centrioles to methylate tubulin in growing mitotic spindles remains unclear. Moreover, how methylated tubulin is incorporated into the mitotic spindle, and when and how the mark is removed upon successful cell division, is also unknown. Recent advances in imaging techniques could answer some of these questions. Due to the dynamic nature of the spindle, light microscopy has remained to be the main tool to observe the microtubules involved in cell division (Maddox et al. 2012). Fluorescence imaging adds specificity to the molecules being observed. Thus far, immunofluorescence imaging has shown co-localization of methylation and tubulin at the minus ends of the mitotic spindle during cell division.

Visualizing the mark using antibodies has thus far been difficult because the modification is temporal in the cell and thus difficult to isolate in addition to being low in abundance. Moreover, a limitation of immunofluorescence imaging of methylated tubulin is the lack of a specific antibody that recognizes tubulin methylation specifically rather than methylation in general (Park et al. 2016; Chiang et al. 2018). As such, we need to develop an antibody that has an epitope against methylated tubulin. Once we have a specific antibody for methylated tubulin, we could perform experiments that allow us to image cells and tubulin methylation directly without other methylation signals. Fluorescent imaging with cells (over-) expressing tSETD2-FLAG could be coupled and imaged with antibodies for both FLAG and methylated tubulin. These cells would be synchronized and then fixed to monitor across a cell cycle where SETD2 and methylated tubulin are during interphase and mitosis.

Moreover, we could combine fluorescence microscopy with electron microscopy using correlative light electron microscopy (CLEM) and cryo-electron tomography (cryoET), the combination cryoCLEM. By combining whole cell visualization of individual fluorescent proteins in living cells, with spatial imaging of that same cell frozen in its native environment (Plitzko, Rigort, and Leis 2009; Schwartz 2008). Because cryoET is limited to a sample thickness of under 500 um, thinner than most cells, samples typically must be prepared using focused-ion-beam (FIB) milling (Villa et al. 2013). While CLEM can help identify where to FIB mill, the procedure and

protocols are extremely challenging. Attempting to image a mitotic cell, as such, would provide an even bigger challenge even when CLEM highlights where to make the "windows into the cell." Nevertheless, as protocols for FIB-milling and cryoET become more common, the structure of methylated tubulin by SETD2 on the mitotic spindle could be determined, along with many other interesting cell-division-based structures like the kinetochore.

4.3 Regulation of SETD2

SETD2 methylates histones, tubulin, and actin, but outstanding is how this methyltransferase is regulated and localized for it to modify its various substrates. Our collaborators have identified SETD2 in the cytoplasm even during interphase (Seervai et al. 2020), but how it gets there without being degraded or transported back into the nucleus remains a mystery. Additionally, how SETD2 seems to methylate actin during interphase in sufficient quantities to alter cell migration, yet not methylate tubulin while it's cytosolic, is also unknown. More work doing live cell imaging will show us where and how SETD2 gets to the cell periphery to methylate actin, the minus ends of microtubules to methylate tubulin, and the nucleus to methylate histones during transcription. Imaging alone, however, only shows us where SETD2 is localized, rather than actually carrying out methyltransferase activity. As such, cells expressing SETD2 could be synchronized and fixed at different time points during mitosis and re-entering interphase, then stained with DAPI, FLAG, tubulin, and general methylation antibodies to correlate where SETD2 is with methyltransferase activity. We would expect that during mitosis SETD2 would localize to the centrioles and we would observe an increase in methylation signal in the cytoplasm surrounding the centrioles, and then have the methylation signal become incorporated into the mitotic spindle. After cell division, we would try and observe where SETD2 goes and if any methylation signal increases near the cell periphery. These types of time course imaging experiments would help us see how and where SETD2 goes in the cell to methylate its various substrates.

Given our findings that tubulin methylation is found on the inside of the microtubule, and that tSETD2-FLAG can methylate microtubules, another outstanding question is how SETD2 accesses the K40 loop despite it being a large protein. Chapter 2 discussed two possible mechanisms: either the enzyme can enter the lumen like the tubulin acetyltransferase, αTAT, or it enters the lumen through lattice defects. Microtubule lattice self-repair in structurally damaged

sites, for example where microtubules cross each other or have been damaged by other proteins, is responsible for the rescue of microtubule growth (Aumeier et al. 2016). This model is supported by the observation of "GTP islands" that are detected in microtubule lattices, far from polymerizing ends, where GTP-tubulin is incorporated in otherwise GDP-tubulin lattice (Dimitrov et al. 2008; de Forges et al. 2016; Bollinger et al. 2020). However, whether and how modifying enzymes like SETD2 enzymatically alter tubulin before, during, or after microtubule rescue remains unknown. We could try and figure this out by fixing distressed microtubules and staining for FLAG, methylation, and GTP tubulin. Perhaps this experiment could determine when and where tSETD2-FLAG is and whether or not it methylates at areas of distorted and broken microtubule lattice. We anticipate that, while SETD2 may methyate microtubules at these exposed areas, this would not be terribly relevant in the context of the mitotic spindle.

Additionally, SETD2 is highly regulated by a number of other proteins. RNA Pol II, along with Iws1, and Spt6 are critical for proper histone 3 lysine 36 methylation (Yoh, Lucas, and Jones 2008; Rebehmed et al. 2014), and Huntington protein (HTT) along with the actin-binding adapter HIP1R in complex with SETD2 regulate actin methylation (Seervai et al. 2020). More work needs to be done to identify whether and which proteins mediate tubulin methylation in cells. This could be done using BioID, a screening method to identify protein-protein interactions that occur in living cells (Roux, Kim, and Burke 2013; Sears, May, and Roux 2019). By tethering a promiscuous biotin ligase to tSETD2, expression in cells leads to biotinylation of interacting and proximal proteins. Then, the biotinylated proteins can then be purified using affinity beads and identified with mass spectrometry. Using our different tSETD2 mutants described in Chapter 3, differences in protein-protein interactions could be teased apart and could hint at methylation regulation in cells. A similar experiment could be conducted with synchronized cells to identify differential interactions in mitotic and interphase cells, perhaps also determining a mechanism for how SETD2 remains cytoplasmic during interphase. These experiments could also be conducted using the full length SETD2, which is autoinhibited. Performing BioID and comparing binding partners between truncated and full length SETD2 may play a role in substrate binding and activation of the enzyme. Moreover, identifying binding partners throughout the cell cycle could pose more questions and find more avenues of biological questions.

4.4 References

Alushin, Gregory M., Gabriel C. Lander, Elizabeth H. Kellogg, Rui Zhang, David Baker, and Eva Nogales. 2014. “High-Resolution Microtubule Structures Reveal the Structural Transitions in Ab -Tubulin upon GTP Hydrolysis.” *Cell* 157 (5): 1117–29.

Arnal, I., F. Metoz, S. DeBonis, and R. H. Wade. 1996. “Three-Dimensional Structure of Functional Motor Proteins on Microtubules.” *Current Biology: CB* 6 (10): 1265–70.

Aumeier, Charlotte, Laura Schaedel, Jérémie Gaillard, Karin John, Laurent Blanchoin, and Manuel Théry. 2016. “Self-Repair Promotes Microtubule Rescue.” *Nature Cell Biology* 18 (10): 1054–64.

Ayukawa, R., S. Iwata, H. Imai, S. Kamimura, and M. Hayashi. 2020. “GTP-Dependent Formation of Straight Oligomers Leads to Nucleation of Microtubules.” *bioRxiv*. https://www.biorxiv.org/content/10.1101/2020.03.05.979989v1.abstract.

Bollinger, Jonathan A., Zachary I. Imam, Mark J. Stevens, and George D. Bachand. 2020. “Tubulin Islands Containing Slowly Hydrolyzable GTP Analogs Regulate the Mechanism and Kinetics of Microtubule Depolymerization.” *Scientific Reports* 10 (1): 13661.

Chiang, Yun-Chen, In Young Park, W. Kimryn Rathmell, Cheryl Lyn Walker, and Ryoma Ohi. 2018. “SETD2 Haploinsufficiency for Microtubule Methylation Is an Early Driver of Genomic Instability in Renal Cell Carcinoma.” *Cancer Research* 78 (12): 3135–46.

Dimitrov, A., M. Quesnoit, S. Moutel, I. Cantaloube, C. Pous, and F. Perez. 2008. “Detection of GTP-Tubulin Conformation in Vivo Reveals a Role for GTP Remnants in Microtubule Rescues.” *Science*. https://doi.org/10.1126/science.1165401.

Forges, Hélène de, Antoine Pilon, Isabelle Cantaloube, Antoine Pallandre, Anne Marie Haghiri-Gosnet, Franck Perez, and Christian Poüs. 2016. “Localized Mechanical Stress Promotes Microtubule Rescue.” *Current Biology: CB* 26 (24): 3399–3406.

Johnson, Vinu, Pelin Ayaz, Patrick Huddleston, and Luke M. Rice. 2011. “Design, Overexpression, and Purification of Polymerization-Blocked Yeast αβ-Tubulin Mutants.” *Biochemistry* 50 (40): 8636–44.

Kastner, Berthold, Niels Fischer, Monika Mariola Golas, Bjoern Sander, Prakash Dube, Daniel Boehringer, Klaus Hartmuth, et al. 2008. “GraFix: Sample Preparation for Single-Particle Electron Cryomicroscopy.” *Nature Methods* 5 (1): 53–55.

Kellogg, Elizabeth H., Nisreen M. A. Hejab, Stuart Howes, Peter Northcote, John H. Miller, J. Fernando Díaz, Kenneth H. Downing, and Eva Nogales. 2017. “Insights into the Distinct Mechanisms of Action of Taxane and Non-Taxane Microtubule Stabilizers from Cryo-EM Structures.” *Journal of Molecular Biology* 429 (5): 633–46.

Kellogg, Elizabeth H., Nisreen M. A. Hejab, Simon Poepsel, Kenneth H. Downing, Frank DiMaio, and Eva Nogales. 2018. “Near-Atomic Model of Microtubule-Tau Interactions.” *Science* 360 (6394): 1242–46.

Li, Huilin, David J. DeRosier, William V. Nicholson, Eva Nogales, and Kenneth H. Downing. 2002. “Microtubule Structure at 8 Å Resolution.” *Structure* 10 (10): 1317–28.

Maddox, Paul S., Anne-Marie Ladouceur, Rajesh Ranjan, Jonas Dorn, Hery Ratsima, Damien D’Amours, and Amy S. Maddox. 2012. “Imaging the Mitotic Spindle.” *Methods in Enzymology* 505: 81–103.

McIntosh, J. Richard, Eileen O’Toole, Garry Morgan, Jotham Austin, Evgeniy Ulyanov, Fazoil Ataullakhanov, and Nikita Gudimchuk. 2018. “Microtubules Grow by the Addition of Bent Guanosine Triphosphate Tubulin to the Tips of Curved Protofilaments.” *The Journal of Cell Biology* 217 (8): 2691–2708.

Meurer-Grob, Patricia, Jérôme Kasparian, and Richard H. Wade. 2001. “Microtubule Structure at Improved Resolution †” 40: 23.

Mickolajczyk, Keith J., Elisabeth A. Geyer, Tae Kim, Luke M. Rice, and William O. Hancock. 2019. “Direct Observation of Individual Tubulin Dimers Binding to Growing Microtubules.” *Proceedings of the National Academy of Sciences of the United States of America* 116 (15): 7314–22.

Nogales, E., M. Whittaker, R. A. Milligan, and K. H. Downing. 1999. “High-Resolution Model of the Microtubule.” *Cell*. https://www.sciencedirect.com/science/article/pii/S0092867400809617.

Nogales, E., S. G. Wolf, and K. H. Downing. 1998. “Structure of the Alpha Beta Tubulin Dimer by Electron Crystallography.” *Nature* 391 (6663): 199–203.

Park, In Young, Reid T. Powell, Durga Nand Tripathi, Ruhee Dere, Thai H. Ho, T. Lynne Blasius, Yun Chen Chiang, et al. 2016. “Dual Chromatin and Cytoskeletal Remodeling by SETD2.” *Cell* 166 (4): 950–62.

Plitzko, Jürgen M., Alexander Rigort, and Andrew Leis. 2009. "Correlative Cryo-Light Microscopy and Cryo-Electron Tomography: From Cellular Territories to Molecular Landscapes." *Current Opinion in Biotechnology* 20 (1): 83–89.

Punjani, Ali, John L. Rubinstein, David J. Fleet, and Marcus A. Brubaker. 2017. "cryoSPARC: Algorithms for Rapid Unsupervised Cryo-EM Structure Determination." *Nature Methods* 14 (3): 290–96.

Rebehmed, Joseph, Patrick Revy, Guilhem Faure, Jean-Pierre de Villartay, and Isabelle Callebaut. 2014. "Expanding the SRI Domain Family: A Common Scaffold for Binding the Phosphorylated C-Terminal Domain of RNA Polymerase II." *FEBS Letters* 588 (23): 4431–37.

Roux, Kyle J., Dae In Kim, and Brian Burke. 2013. "BioID: A Screen for Protein-Protein Interactions." *Current Protocols in Protein Science / Editorial Board, John E. Coligan ... [et Al.]*, no. SUPPL.74: 1–14.

Schwartz, C. L. 2008. "Cryo-Fluorescence: A Tool for Correlative Cryo-Light and Cryo-Electron Microscopy." *Microscopy and Microanalysis*. https://doi.org/10.1017/s143192760808522x.

Sears, Rhiannon M., Danielle G. May, and Kyle J. Roux. 2019. "BioID as a Tool for Protein-Proximity Labeling in Living Cells." In *Enzyme-Mediated Ligation Methods*, edited by Timo Nuijens and Marcel Schmidt, 299–313. New York, NY: Springer New York.

Seervai, Riyad N. H., Rahul K. Jangid, Menuka Karki, Durga Nand Tripathi, Sung Yun Jung, Sarah E. Kearns, Kristen J. Verhey, et al. 2020. "The Huntingtin-Interacting Protein SETD2/HYPB Is an Actin Lysine Methyltransferase." *Science Advances*. https://doi.org/10.1126/sciadv.abb7854.

Stark, Holger. 2010. "GraFix: Stabilization of Fragile Macromolecular Complexes for Single Particle Cryo-EM." *Methods in Enzymology* 481: 109–26.

Tegunov, Dimitry, and Patrick Cramer. 2019. "Real-Time Cryo-Electron Microscopy Data Preprocessing with Warp." *Nature Methods* 16 (11): 1146–52.

Ti, Shih-Chieh, Gregory M. Alushin, and Tarun M. Kapoor. 2018. "Human β-Tubulin Isotypes Can Regulate Microtubule Protofilament Number and Stability." *Developmental Cell* 47 (September): 1–16.

Villa, Elizabeth, Miroslava Schaffer, Jürgen M. Plitzko, and Wolfgang Baumeister. 2013. "Opening Windows into the Cell: Focused-Ion-Beam Milling for Cryo-Electron Tomography." *Current Opinion in Structural Biology* 23 (5): 771–77.

Yoh, S. M., J. S. Lucas, and K. A. Jones. 2008. “The Iws1:Spt6:CTD Complex Controls Cotranscriptional mRNA Biosynthesis and HYPB/Setd2-Mediated Histone H3K36 Methylation.” *Genes & Development*. https://doi.org/10.1101/gad.1720008.

Zhang, Rui, Gregory M. Alushin, Alan Brown, and Eva Nogales. 2015. “Mechanistic Origin of Microtubule Dynamic Instability and Its Modulation by EB Proteins.” *Cell* 162 (4): 849–59.

Zhang, Rui, Benjamin LaFrance, and Eva Nogales. 2018. “Separating the Effects of Nucleotide and EB Binding on Microtubule Structure.” *Proceedings of the National Academy of Sciences* 115 (27): E6191–6200.

Appendix A[1]: Cilia maintenance by KIF3A/KIF3B

A.1 Forward

This chapter will introduce some adjacent work I've conducted researching kinesin motors in primary cilia. Some of this work was published in Engelke, *et al.* (2019) *Current Biology* with then-postdoctoral fellow Martin Engelke leading the project in collaboration with Dr. Benjamin Allen's lab.

A.2 Introduction

Imagine yourself as a bird flying above a suburban city. You'd see cars driving towards and away the city center, bike trails through the forest, and pedestrians walking along sidewalks and paths. Farther away, perhaps you hear the interstate highway system, with cars and trucks zooming to get to their destination. Much like this little city, each cell in our body has a similar network of structural elements used for transportation called the cytoskeleton. Microtubules and actin fibers work together to form this cytoskeleton, where the former are for long-range transport like highways and the latter are more like local side streets. Depending on the type of road, there are particular molecular vehicles and pedestrians that transport intracellular cargo. These different roads have distinct motor proteins that "walk" on them in a processive foot-over-foot manner: myosin motors move along actin fibers and kinesin and dynein motors on microtubules.

On the microtubules, kinesin motors are largely responsible for anterograde transport to the cell periphery and dynein motors perform retrograde transport back to the cell center (R. Vale,

[1] *The following appendices highlight some work I've been a part of beyond my main thesis work surrounding the narrative of cytoskeletal methylation. Appendix A discusses work I conducted during my rotation in the Verhey lab, and Appendix B shows a combination of cryoEM data collection and processing techniques in the Cianfrocco lab.*

Reese, and Sheetz 1985; Gibbons and Rowe 1965; R. D. Vale, Soll, and Gibbons 1989). Focusing here on the kinesin superfamily of proteins (a.k.a. KIFs), kinesin motors are divided up into 15 families based on phylogenetic analyses (Lawrence et al. 2004; Hirokawa and Takemura 2004). In general, in terms of domain architecture, kinesins have an N-terminal motor ATPase domain and dimerize with a coil-coiled stalk. There are some cases of a C-terminal motor domain that move in the opposite, or minus-end, direction and some motors with a central domain destabilize microtubules rather than move along their surface. There are also some cases of single-headed kinesin motors carrying cargo in teams (Schimert et al. 2019). Typically functioning as dimers however, kinesin enzymes use the energy-providing molecule ATP to generate power to walk on microtubules. This nucleotide binds in the ATPase domain of kinesin and then converts the chemical energy of ATP hydrolysis to ADP into mechanical energy and force production. Additionally, a flexible 12-18 amino acid sequence called the neck linker (NL) adjacent to the ATPase domain serves as a structural element for force generation and directed motility. With the addition of ATP, the NL docks and the rear motor head will swing forward, where subsequent ATP hydrolysis will complete NL docking and induces microtubule binding by the other motor head (Shang et al. 2014; Phillips et al. 2016; Budaitis et al. 2019). At this stage, kinesin will either complete a mechanical step by binding to the next microtubule site and releasing ADP, or will fall off the microtubule if it prematurely releases phosphate (Milic et al. 2014).

The diversity across these different kinesin motors is indicative of their various roles throughout the cell depending on the family. For example, kinesin-1 motors are important for vesicle, organelle, and mRNA transport, kinesin-2 for intraflagellar transport in cilia, and kinesin-4 and -5 for chromosome positioning and spindle pole separation in mitosis. How the many different kinesin motors are regulated depends on many factors including activation, cargo adaptors, and cell cycle state. To prevent needless ATP hydrolysis and clear up space on crowded microtubules, motor activity must be deactivated where kinesin is regulated by auto-inhibition (Hammond et al. 2010; Kaan, Hackney, and Kozielski 2011; Ren et al. 2018). Such folding requires hinge sections within the coil-coil domain, where the C-terminal cargo adaptor interacts with the N-terminal motor. With kinesin-1 as the canonical kinesin as an example, the QIAKPIRP-containing tail domain directly contacts a helix in the motor domain that acts like a switch to prevent ADP release from the nucleotide pocket (Dietrich et al. 2008; Verhey and Hammond 2009). Cargo binding can subsequently activate kinesin motors for microtubule-based transport.

For example, fasciculation and elongation protein-ζ1 (FEZ1) and Jun N-terminal kinase interacting protein (JIP1) are required in cells to bind to the inhibitory regions of the molecule for activation, KHC tail and the KLC, respectively (Blasius et al. 2007). Adding complexity, the cargo adaptor that activates kinesins depends on the motor, the cargo itself, and the presence of adaptor or scaffold proteins (Hirokawa et al. 2009).

Cilia formation and maintenance by kinesin-2 motors

Cilia are microtubule-based organelles that protrude from the surface of almost every human cell. Cilia consist of a core called the axoneme, which is constructed from nine parallel doublet microtubules (A- and B-tubules) that project from a basal body and is surrounded by a specialized ciliary membrane which is an extension of the plasma membrane. Particular types of cells have distinct ciliary functions like a sperm's flagellar tail, or the respiratory tract's cilia that helps move liquids over the surface of organs. Both of these examples are of motile cilia. Primary cilia, on the other hand, are largely immotile and instead function as cellular antennae to sense extracellular stimuli. For example, vertebrate Hedgehog (Hh) signaling depends on the presence of a primary cilium for proper gene transcription. Given this critical role particularly for development, incorrect ciliary formation gives rides to a collection of diseases, termed ciliopathies, like midline defects, neural tube defects, polydactyly, and lung hypoplasia (Wheway, Nazlamova, and Hancock 2018).

Cilium biogenesis requires a process of cargo transport to the tip and back down to the basal body, called intraflagellar transport (IFT). Motor proteins, particularly kinesin-2 and dynein-2, are responsible for antero- and retro-grade transport, respectively, of multiprotein complexes called IFT trains. These protein assemblies are divided into A and B complexes (which have six and sixteen proteins) and deliver axoneme precursors to the site of incorporation at the axoneme tip and could be rearranged themselves. These IFT train complexes also contribute to ciliary maintenance by carrying cargo, like free tubulin, to be incorporated into the axoneme (Craft et al. 2015; Lechtreck et al. 2017). With regard to ciliary-cell signaling pathways, like Hedgehog signaling, IFT trains are also thought to move membrane-associated signaling complexes (Wang, Pan, and Snell 2006). Anterograde transport of IFT trains occurs predominately on B-tubules and retrograde transport on A-tubules, perhaps to avoid collisions in a very busy and compact organelle (Kuhns and Blacque 2016; Prevo, Scholey, and Peterman 2017; Bertiaux et al. 2018; Webb,

Mukhopadhyay, and Roberts 2020). As such, IFT is an organized process that occurs within the cilium.

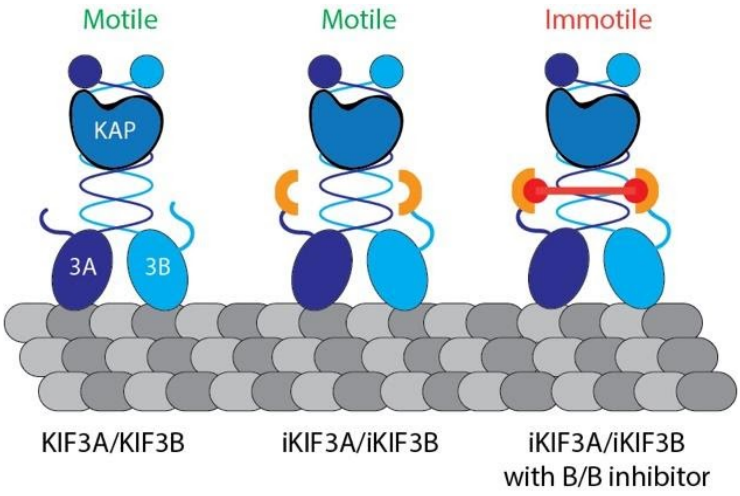

Figure A1. Inhibitable kinesin-2 motor, KIF3A/KIF3B. Left: endogenous heterotrimeric KIF3A/KIF3B/KAP. Middle: Engineered inhibitable motor with DmrB domains (orange) on the N-terminus of KIF3A and KIF3B (iKIF3A/iKIF3B). Right: inhibitable motor with small molecule inhibitor B/B homodimerizer (B/B, red) yielding an immotile motor.

A.3 Results

Models of IFT had been based on invertebrate model systems such as *C. elegans* and *Chlamydomonas*. However, these organisms are inadequate to describe mammalian functions due to both inconsistencies and a lack of homologs: Klp20/Kpl11/Kap is required in *Chlamydomonas*, but not in *C. elegans*, OSM-3 is required in *C. elegans*, but not in *Chlamydomonas* and the homolog KIF17 in mice seems dispensable. Instead, knock-outs of kinesin-2 heterodimeric protein KIF3A/KIF3B in mouse models are lethal due to a lack of cilia formation. Given that knock-down or -out approaches lead to off-target effects, to understand how mammalian cilia formation and maintenance occurs, a post-doc in Verhey lab used a chemical-genetic strategy to engineer an inhibitable version of this heterodimeric protein (Engelke et al. 2016). This strategy fused a DmrB domain, and a short linker, to the N-terminal motor domains of KIF3A and KIF3B such that when a small molecule B/B homodimerizer (B/B) is added the kinesin motor can no longer take a step forward, much like tying someone's sneaker shoelaces together (Fig. A1). In addition, a KIF3A/KIF3B CRISPR-Cas9 knock-out cell line in NIH-3T3 cells was generated. Typically, NIH-3T3 cells generate primary cilia which we observed by immunofluorescence staining for ciliary marker ARL13B. In double knockout KIF3A-/- KIF3B-/- cells, primary cilia only form when KIF3A and KIF3B are transiently expressed. When the inhibitable constructs are transfected, cells

are also able to generate primary cilia, but when the B/B inhibitor is added, cilia are absent (Fig. A2). The combination of double-knockout cells and an inhabitable iKIF3A/iKIF3B allowed us to probe and monitor cilia maintenance and disassembly processes.

A.3.2 Kinesin-2 KIF3A/3B is necessary for cilia formation and maintenance

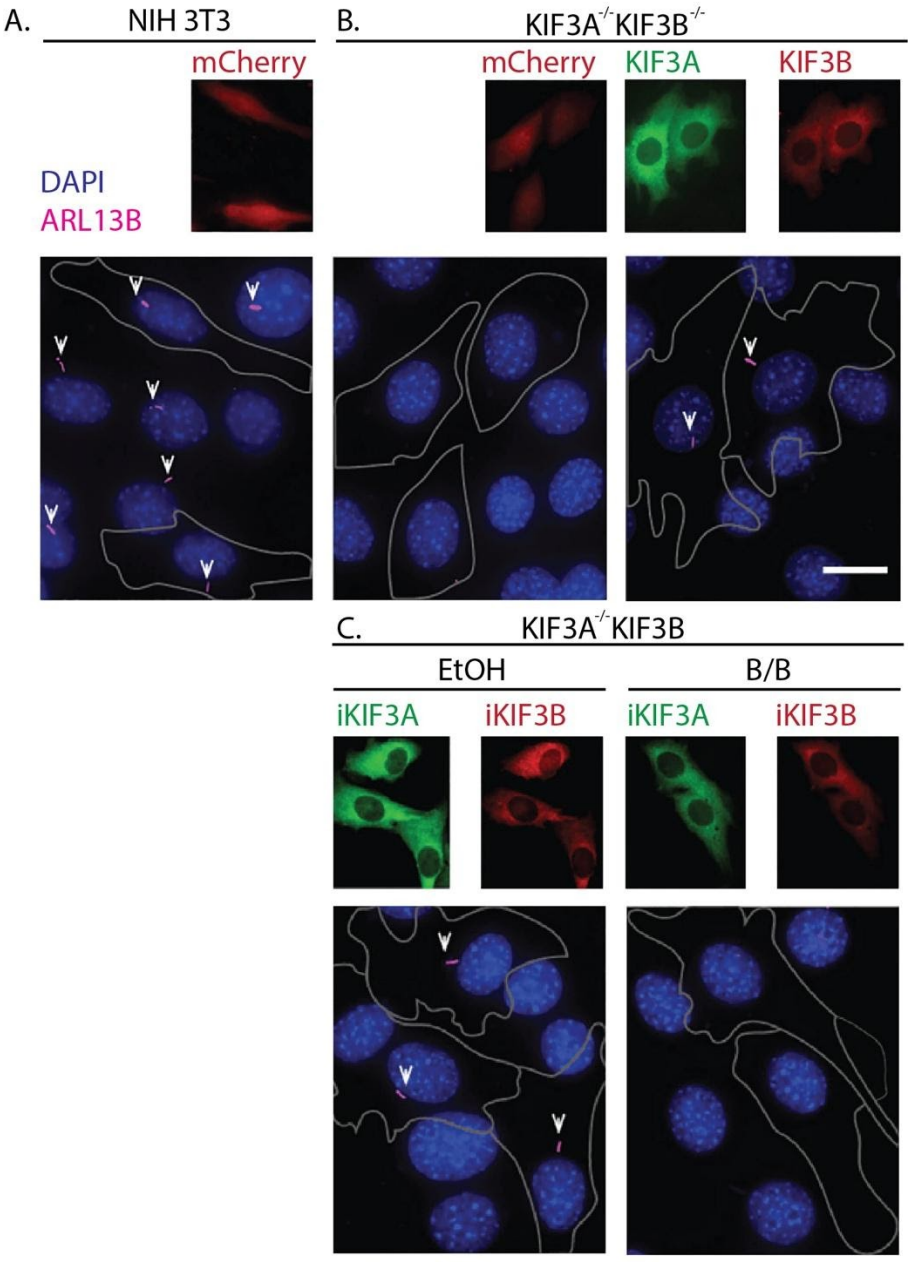

Figure A2. Kinesin-2 KIF3A/KIF3B necessary to form cilia. A) In NIH3T3 cells with vehicle mCherry vector, have proper cilia formation as determined by ciliary marker ARL13B. B) In KIF3A/KIF3B CRISPR-Cas knock down cell line, left: there is no cilia formation, right: transfecting in WT KIF3A/KIF3B rescues cilia formation in transfected cells. C) Inhibitable motor left: recuse cilia formation, right: when inhibited with B/B, cilia do not form. Experiments performed by Martin Engelke.

We hypothesized that KIF3A/3B are responsible for ciliary maintenance because they carry IFT trains within the cilia. To understand the role of kinesin-2 motors, we expressed iKIF3A-

neonGreen and iKIF3B-mCherry in the double knockout cells and allowed them to generate primary cilia. Two days after transfection, we added B/B inhibitor at different times to measure the impact of inhibited KIF3A/3B over a time course (Fig. A3A). These cells were fixed and stained with antibodies against axonemal marker acetylated α-tubulin and the ciliary membrane marker Arl13B. Treatment with B/B inhibitor resulted in a decrease in the percentage of cells that contained a primary cilium as early as 1 hour after treatment, and the percentage of ciliated cells continued to decrease over the next 8 hours of experimentation (Fig. A3B). A similar, albeit less dramatic, trend was also seen in the length of the cilia. As KIF3A/KIF3B inhibition results in a decrease in the percentage of ciliated cells over time, the cilium length measurements at a later point are based on only a few cilia (Fig A3C). Taken together, these data suggest that inhibiting kinesin-2 KIF3A/3B contributes to the disassembly of primary cilia, thus suggesting that KIF3A/KIF3B.KAP function is critical for cilium maintenance.

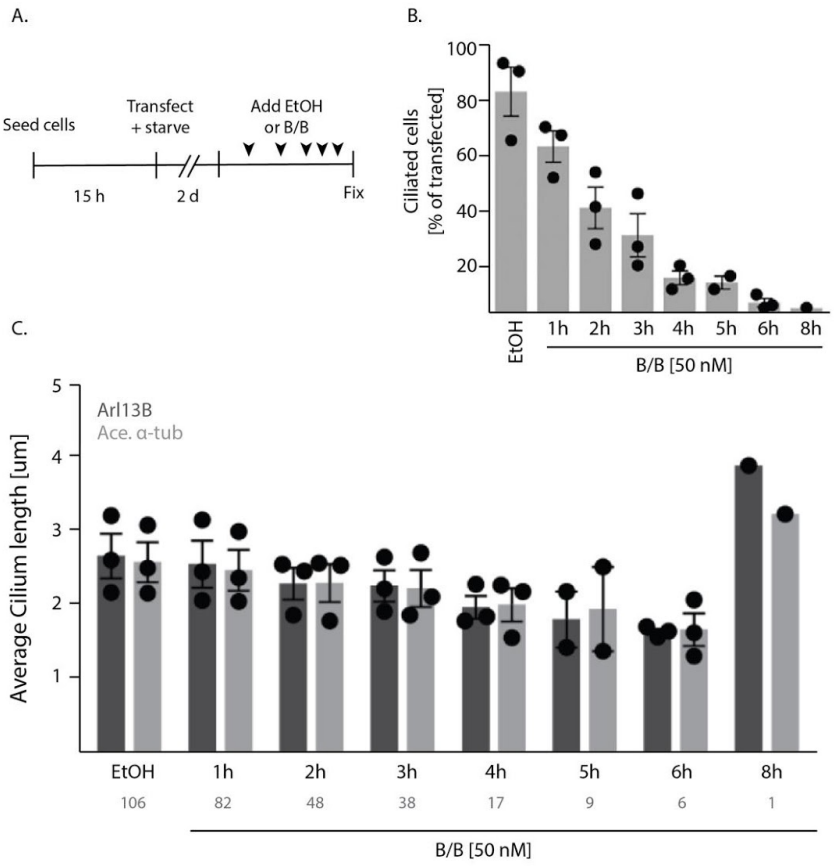

Figure A3. Inhibiting iKIF3A/iKIF3B reduces the number and length of ciliated cells. A) Schematic of time-point experiment B) Analysis of the number of ciliated cells compared to the amount of transfected cells treated with B/B inhibitor overtime. C) Average length of cilia over B/B inhibitor time course looking at cilia markers ARL13B and acetylated tubulin.

Because non-eukaryotic cells seem to require kinesin-2 motor KIF17, similar experiments expressing KIF3A/3B and KIF17 motors in knock-out cell lines were conducted. Adding the B/B inhibitor over a time course, the presence and persisting maintenance of a primary cilium would suggest that KIF17 does play a role. However, in these double-knockout cells, KIF17 rescue also did not produce any cilia (Fig. A4A-B). Moreover, treating cells with the B/B inhibitor yielded the same results between KIF17 over- and endogenously-expressed cells, and cilium length additionally followed the same trend (Fig. A4C-D). Taken together, this suggests that KIF17 does not play an important role and at least is not sufficient for cilia formation and maintenance.

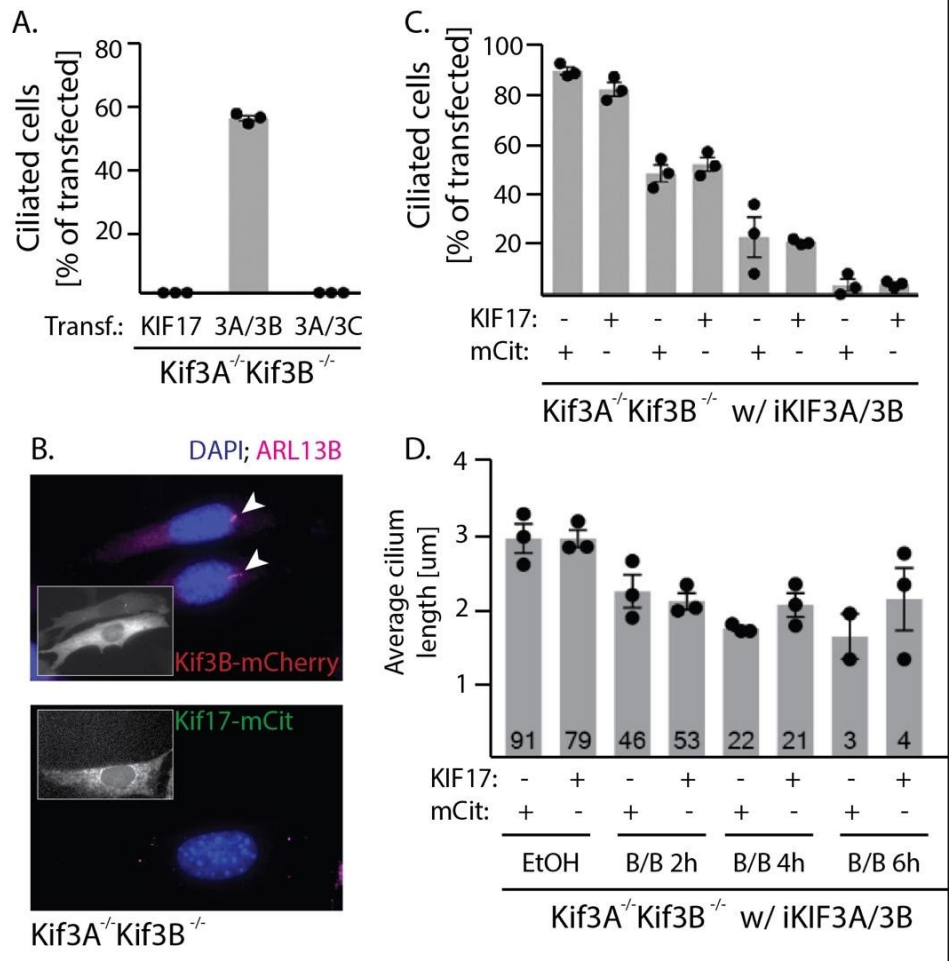

Figure A4. KIF17 is not sufficient to make or maintain a primary cilium. A) In double knockout cells, only KIF3A/KIF3B can rescue cilia formation, not KIF17 or KIF3A/3C. B) Immunofluorescence of top: knock down cells rescued with KIF3A/3B, bottom: rescued with KIF17. C) Percent of ciliated cells in double knockout cells expressing i3A/i3B with and without KIF17. D) Average length of cilia in double knockout cells expressing i3A/i3B with and without KIF17 over a time course of KIF3A/KIF4B inhibition with B/B. These experiments were performed by Martin Engelke.

A.3.3 Ciliary disassembly mechanism still outstanding

To begin to understand the mechanism of cilia disassembly, we utilized the iKIF3A/iKIF3B expression and inhibition in double knock-

out cells to instigate cilium disassmbly and then tested the effect of small molecules that modify the microtubules. In seeing how cilium disassembly was impacted by different drug treatments, we could make comparisons and inferences into the mechanism of disassembly at the microtubule level. As before, the percentage of ciliated cells along with the intensity of ciliary markers ARL13B (green) and acetylated tubulin (purple) staining were quantified to monitor the disassembly process (Fig. A5A-C, left column).

The first small molecule we tested was paclitaxel (taxol). Discovered through a collaboration between the US Department of Agriculture and the National Cancer Institute, this compound, originally extracted from the Pacific yew, blocks cancer cell growth by stopping cell division (Wani 1971; Schiff and Horwitz 1980; Arnal and Wade 1995; Horwitz 2019). Indeed, it stops non-cancer cell division by binding to microtubules in the mitotic spindle, halting chromosomal separation. Adding taxol to microtubules stabilizes the polymers such that they do not undergo dynamic instability. In our double-knockout cells, we noticed that adding taxol had. no effect on the percentage of cells with primary cilia (Fig. A5A, blue columns). When cilium disassembly was induced by addition of B/B inhibitor, taxol seemed to be a partial rescue because more cilia remained when taxol was supplemented with B/B inhibitor (Fig. A5A, purple columns). Looking at the intensities of ARL13B and acetylated tubulin, it seems that the longer the cell has been treated with taxol, the intensity of acetylated tubulin increases (Fig. A5A, right). As such, we find that taxol can slow down ciliary disassembly, likely by stabilizing microtubules.

Next, we looked at the impacts of nocodazole upon ciliary disassembly (Fig. A5B). When bound to soluble tubulin dimers, nocodazole inhibits polymerization because it binds along the β-tubulin interface and it thereby results in the depolymerization of microtubules. As such, we expected that adding nocodazole to our double-knockout cells would accelerate ciliary disassembly. However, the addition of nocodazole did not accelerate ciliary disassembly driven by the inhibtion of KIF4A/KIF3B/KAP (Fig. A5B, green columns). Looking at ARL13B and acetylated tubulin intensities within the cilia, we also did not observe an appreciable difference upon nocodazole treatment (Fig. A5B, right graph). These data suggest that inhibiting polymerization does not facilitate ciliary disassembly.

Lastly, we were curious if altering acetylated tubulin levels would impact ciliary maintenance. Tubulin acetylation is often a marker for stable microtubules (Cambray-Deakin et al. 1987, Janke et al. 2017) and antibodies raised against acetylated microtubules are a visual

marker for the primary cilium in cells. As such, we wanted to find out if promoting acetylation would impact cilia dynamics, so we treated our double-knockout cells with tubacin, a small molecule that inhibits deacetylase activity of HDAC6 (Namdar et al. 2010) Surprisingly, we found that tubacin treatment alone (yellow) resulted in ciliary disassembly but that the ciliary

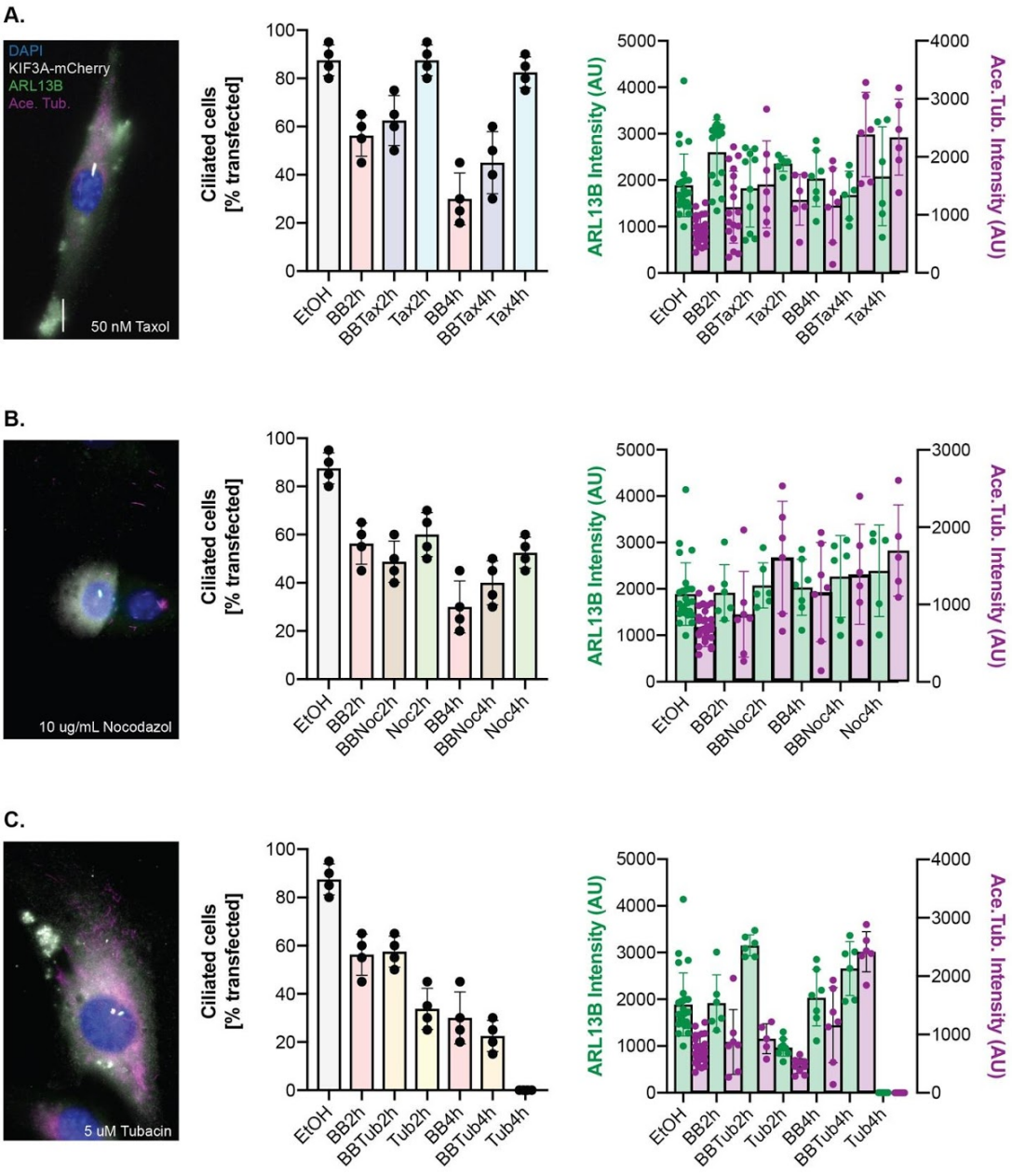

Figure A5. Cilia on drugs. NIH-3T3 double knockout cells were transfected with iKIF3A/iKIF3B-mCherry and treated with small molecules B/B with and without A) taxol, B) nocodozol, or C) tubacin. Left column) Cells were then permeabilized and fixed for immunofluorescence - DNA (DAPI-280), ciliary marker ARL13B (Rb-488), and acetylated tubulin (Ms-680). Middle column) We measured the amount of ciliated cells as a percentage of the total transfected (bars showing the mean of four different transfections), and Right column) the intensity of signal ARL13 and acetylated tubulin in the cilia (measured by line tracing the cilia in ImageJ and subtracting background signal in each channel, bars showing the mean intensity for the n-number of cells imaged from the four transfection experiments).

disassembly induced by inhibition of KIF3A/KIF3B was not affected by the tubacin treatment

(Fig. A5C, left graph). The effects of tubacin in this experiment are unclear, however, as the expected increase in acetylated tubulin staining was not observed (Fig. A5C, right graph).

From all these experiments, it's safe to say that the mechanism of ciliary disassembly remains a mystery that treating cells with a combination of small molecules did not solve.

A.4 Discussion

A.4.1 KIF3A/KIF3B is responsible for soluble tubulin entering cilia by IFT

We engineered an inhibitable version of the heterotrimeric KIF3A/KIF3B/KAP kinesin-2 motor that allows for specific inhibition of this motor and thus identifying its role in primary cilia. We observed a rapid block to IFT upon inhibition of the inhibitable motor in primary cilia. Without the B/B inhibitor, we found that IFT88 moves processively along the length of the cilium and anterograde and retrograde directions as expected (Williams et al. 2014; Ye, Nager, and Nachury 2018). Addition of the B/B inhibitor resulted in a rapid block of IFT within two minutes, and disassembly of the cilia overtime. When trying to rescue with KIF17, cilia are not able to form suggesting that this motor is not sufficient to make or maintain primary cilia. Taken together, our findings show that kinesin-2 motors KIF3A/KIF3B are critical for cilia formation in mammalian cells.

The most dramatic effect of i3A/i3B inhibition is a rapid block to new IFT trains entering the cilium. One possibility is that the B/B inhibitor crosslinks and stops i3A/i3B/KPA motors once they are activated by cargo binding at the base of the cilium. It is also possible that B/B inhibitor crosslinks the motor domains of soluble and autoinhibited kinesin-2 motors, thereby depleting the pool of active kinesin-2 that can be recruited to the IFT trains at the base of the cilium. These possibilities are not mutually exclusive, given that IFT trains are assembled at the basal body (Wingfield et al. 2017). Unlike most organelles, the ciliary membrane is continuous with the plasma membrane, rather than being a contained organelle like a mitochondria or vacuole. However, the base of the cilia has a transition zone that serves as a permeable barrier (Verhey, Dishinger, and Kee 2011). So far, there is no evidence of protein synthesis within a cilia and as such any protein within this organelle must be transported there and pass through the transition zone. Small proteins (<40 kDa) can diffuse through and some proteins have a cilia localization sequence, but most ciliary proteins are carried through the transition zone by the BBSome on IFT

trains (Nakayama and Katoh 2018). In Chlamydomonas, α-tubulin can enter the cilia by diffusion, but also as IFT cargo. During ciliary growth, IFT concentrates soluble tubulin in the cilia, therefore promoting microtubule growth (Craft et al. 2015). Additionally, kinesin-2 tails, particularly KIF3A, can bind soluble tubulin, preferentially for α-tubulin isotypes (Girotra et al. 2017). Interaction between kinesin tail domains and tubulin has also been documented for kinesin-1 and the N-terminal tail of kinesin-14, both promote microtubule stability which mediate microtubule gliding in cells (Karabay and Walker 1999; Seeger and Rice 2010). As such, inhibiting KIF3A/KIF3B could prevent soluble tubulin entering the cilia.

A.4.2 Ciliary disassembly corresponds to lack of IFT

After kinesin-2 was inhibited, thus blocking IFT, there was a rapid decrease in the number of ciliated cells. Within six hours of kinesin-2 inhibition, there was nearly a complete loss of cilia. As such, the assembly and maintenance of cilia depend on protein transport mediated by IFT. Without functional IFT, the ciliary structure does not form and cannot be retained. Surprisingly, the average cilium length of the remaining cilia decreased only slowly and moderately over the time course of kinesin-2 inhibition. It could also be the case that the lack of soluble tubulin in the cilia also prevents any rescue of axoneme microtubules, the tubulin either a part of the IFT trains, or carried by KIF3A/3B.

Our findings link functional IFT to cilia maintenance, and thus suggests some mechanisms for ciliary disassembly. Without KIF3A/3B, there is a progressive shortening of the cilia over time, caused by a decrease in IFT-mediated tubulin delivery. Without enough soluble tubulin near the tips of cilia, the rate of disassembly overcomes the rate of assembly and as such the ciliary microtubules begin to depolymerize. This so called “balance point” model of microtubule and ciliary maintenance has been mathematically simulated based on microtubule turnover and experimentally observed in *Chlamydomonas* flagellum, and suggests a simple steady-state model for regulating the cilia that’s length dependent (Wallace F. Marshall et al. 2005; W. F. Marshall and Rosenbaum 2001). When we treated the cells with Ciliobrevin D, a dynein inhibitor, we saw that both anterograde and retrograde IFT stops within five minutes, but primary cilium remained (Engelke et al. 2018). This further supports our model that IFT-mediated transport of tubulin into the cilia is critical for maintenance.

However, there are other models of cilia disassembly, including mitogenic signals resulting in tip shedding (Phua et al. 2019), or the loss of microtubule stability (Mirvis, Stearns, and Nelson 2018). To try and see if ciliary disassembly relies on the latter, we treated cells with a combination of KIF3A/3B inhibitor and small molecules that alter tubulin stability: taxol, nocodazole, and tubacin. Unsurprisingly, taxol was able to rescue the effects of the B/B inhibitor, suggesting that ciliary disassembly could be driven by increasing microtubule instability. This is supported by our finding that nocodazole treatment and B/B inhibitors have additive effects. However, we observed that adding tubacin, an HDAC inhibitor, proved to be fairly toxic to the cells and resulted in a drastic reduction in cilia. This seems counterintuitive to previous studies identifying acetylation to be important for cilia structure (Pitaval et al. 2017; L'Hernault and Rosenbaum 1985a, 1983; Ran et al. 2015; L'Hernault and Rosenbaum 1985b). It could be possible that other modifications, like tyrosination, glycylation, and polyglutamylation are also critical for proper cilia formation (Rocha et al. 2014; Wloga et al. 2009; Gadadhar et al. 2017; Kubo et al. 2015), and more work needs to be done looking at the role of post-translational modifications in the context of cilia disassembly.

A.5 Materials and Methods

Plasmids. KIFi3A/KIFi3B were generated as described in (Engelke et al. 2018).

Immunohistochemistry. Parental NIH-3T3 Flp-In cells (Thermo Fisher Scientific; RRID: CVCL_U422) and derived Kif3a-/-;Kif3b-/- cells were cultured in D-MEM (Gibco) with 10% Fetal Clone III (HyClone) and GluteMAX (Gibco) at 37°C and 5% CO2. See (Engelke et al. 2018) for CRISPR/Cas9-mediated genome editing. Both cell lines were transfected using Lipofectamine 2000 (Life Technologies) according to the manufacturer's protocol. Double knockout cells (Kif3a-/-;Kif3b-/-) were generated by sequentially engineering the Kif3a and Kif3b gene loci. Double knockout cells transiently expressing kinesin motors were fixed with 4% formaldehyde in PBS, treated with 50 mM NH4Cl in PBS to quench unreacted formaldehyde and permeabilized with 0.2% Triton X-100 in PBS. Subsequently, cells were blocked in blocking solution (0.2% fish skin gelatin in PBS). Primary and secondary antibodies were applied in blocking solution at room temperature for 1 h each. Cells were incubated 3x for 5 min in blocking solution to remove unbound antibodies. Antibodies used: polyclonal antibodies reacting with ARL13B (1:1000,

Protein Tech Group, 17711-1-AP), IFT88 (1:500, Protein Tech Group, 13967-1-AP), and monoclonal antibodies reacting with ARL13B (1:200, NeuroMAB, 73-287), acetylated tubulin (1:10.000, Sigma, T6793), KIF3A (K2.4, 1:300, Abcam, ab24626), and polyglutamylated tubulin (1:1000, Adipogen Life Sciences, GT335). Nuclei were stained with 10.9 mM40,6-diamidino-2-phenylindole (DAPI) and cover glasses were mounted in ProlongGold (Life Technologies).

Microscopy. Images were collected on an inverted epifluorescence microscope (Nikon TE2000E) equipped with a 60x, 1.40 numerical aperture (NA) oil-immersion objective and a 1.5x tube lens on a Photometrics CoolSnapHQ camera driven by NIS-Elements (Nikon) software. Images of KIF3A-mNG in cilia were captured by a Nikon A1 confocal system with 603 oil immersion objective (NA 1.40) on a high sensitivity GaAsP detector. To measure IFT88-mNG or i3A-mNG content of cilia, a region of interest (ROI) was drawn around the cilium shaft (identified by ARL13B) and the base of the cilium in ImageJ (NIH) and the average fluorescence intensity in the cilium shaft and at the cilium base was measured and the population average was calculated using Excel (and plotted in Prism).

Ciliogenesis rescue and disassembly assays. To assess the effect of B/B inhibitor on ciliogenesis, cells were seeded on cover glasses and 12 h later, the culture medium was switched to 1% Fetal Clone III (serum-starvation). Vehicle (0.1% ethanol final) or 50 nM B/B homodimerizer (Clonetech, 635060) was added followed by the transfection complexes. Two days later the cells were fixed and stained. To assess the effect of B/B inhibitor or Ciliobrevin D on fully-formed cilia, cells were seeded on cover glasses and serum-starved and transfected 12 h later. Two days later, vehicle (0.1% ethanol final) or 50 nM B/B homodimerizer or 30 mM Ciliobrevin D (Sigma, 250401) was added for the indicated times and cells were fixed and stained. Image analysis was performed using ImageJ (NIH). Cells expressing mCherry, or mCherry- and mNeonGreen-tagged inhibitable motors were selected and analyzed for the presence of a cilium, as judged by an ARL13B-positive filament that was R 10 pixel (R1.1 mm). We noted that cells that express low levels of the KIF3B and KIF3A constructs had the highest probability to generate cilia. Thus cells expressing high levels of transfected proteins were excluded from analysis.

A.6 References

Arnal, Isabelle, and Richard H. Wade. 1995. "How Does Taxol Stabilize Microtubules?" *Current Biology: CB* 5 (8): 900–908.

Bakhoum, Samuel F., Giulio Genovese, and Duane A. Compton. 2009. "Deviant Kinetochore Microtubule Dynamics Underlie Chromosomal Instability." *Current Biology: CB* 19 (22): 1937–42.

Bangs, Fiona, and Kathryn V. Anderson. 2017. "Primary Cilia and Mammalian Hedgehog Signaling." *Cold Spring Harbor Perspectives in Biology* 9 (5): 1–22.

Bertiaux, Eloïse, Adeline Mallet, Cécile Fort, Thierry Blisnick, Serge Bonnefoy, Jamin Jung, Moara Lemos, et al. 2018. "Bidirectional Intraflagellar Transport Is Restricted to Two Sets of Microtubule Doublets in the Trypanosome Flagellum." *The Journal of Cell Biology* 217 (12): 4284–97.

Blasius, T. Lynne, Dawen Cai, Gloria T. Jih, Christopher P. Toret, and Kristen J. Verhey. 2007. "Two Binding Partners Cooperate to Activate the Molecular Motor Kinesin-1." *The Journal of Cell Biology* 176 (1): 11–17.

Budaitis, Breane G., Shashank Jariwala, Dana N. Reinemann, Kristin I. Schimert, Guido Scarabelli, Barry J. Grant, David Sept, Matthew J. Lang, and Kristen J. Verhey. 2019. "Neck Linker Docking Is Critical for Kinesin-1 Force Generation in Cells but at a Cost to Motor Speed and Processivity." *eLife* 8: 1–28.

Cambray-Deakin, M.A., Burgoyne, R.D. 1987. "Acetylated and detyrosinated a-tubulins are co-localized in stable microtubules in rat meningeal fibroblasts." *Cell Motility.* 8(3)

Craft, Julie M., J. Aaron Harris, Sebastian Hyman, Peter Kner, and Karl F. Lechtreck. 2015. "Tubulin Transport by IFT Is Upregulated during Ciliary Growth by a Cilium-Autonomous Mechanism." *The Journal of Cell Biology* 208 (2): 223–37.

DeLuca, Jennifer G., Walter E. Gall, Claudio Ciferri, Daniela Cimini, Andrea Musacchio, and E. D. Salmon. 2006. "Kinetochore Microtubule Dynamics and Attachment Stability Are Regulated by Hec1." *Cell* 127 (5): 969–82.

Dietrich, Kristen A., Charles V. Sindelar, Paul D. Brewer, Kenneth H. Downing, Christine R. Cremo, and Sarah E. Rice. 2008. "The Kinesin-1 Motor Protein Is Regulated by a Direct Interaction of Its Head and Tail." *Proceedings of the National Academy of Sciences* 105 (26): 8938–43.

Engelke, Martin F., Bridget Waas, Sarah E. Kearns, Ayana Suber, Allison Boss, Benjamin L. Allen, and Kristen J. Verhey. 2018. "Acute Inhibition of Heterotrimeric Kinesin-2 Function Reveals Mechanisms of Intraflagellar Transport in Mammalian Cilia," 1–29.

Engelke, Martin F., Michael Winding, Yang Yue, Shankar Shastry, Federico Teloni, Sanjay Reddy, T. Lynne Blasius, et al. 2016. "Engineered Kinesin Motor Proteins Amenable to Small-Molecule Inhibition." *Nature Communications* 7: 1–12.

Gadadhar, Sudarshan, Hala Dadi, Satish Bodakuntla, Anne Schnitzler, Ivan Bièche, Filippo Rusconi, and Carsten Janke. 2017. "Tubulin Glycylation Controls Primary Cilia Length." *The Journal of Cell Biology* 216 (9): 2701–13.

Gibbons, I. R., and A. J. Rowe. 1965. "Dynein: A Protein with Adenosine Triphosphatase Activity from Cilia." *Science* 149 (3682): 424–26.

Girotra, Mukul, Shalini Srivastava, Anuttama Kulkarni, Ayan Barbora, Kratika Bobra, Debnath Ghosal, Pavithra Devan, et al. 2017. "The C-Terminal Tails of Heterotrimeric Kinesin-2 Motor Subunits Directly Bind to α-tubulin1: Possible Implications for Cilia-Specific Tubulin Entry." *Traffic* 18 (2): 123–33.

Gupta, Mohan L., Jr, Pedro Carvalho, David M. Roof, and David Pellman. 2006. "Plus End-Specific Depolymerase Activity of Kip3, a Kinesin-8 Protein, Explains Its Role in Positioning the Yeast Mitotic Spindle." *Nature Cell Biology* 8 (9): 913–23.

Hammond, Jennetta W., T. Lynne Blasius, Virupakshi Soppina, Dawen Cai, and Kristen J. Verhey. 2010. "Autoinhibition of the Kinesin-2 Motor KIF17 via Dual Intramolecular Mechanisms." *The Journal of Cell Biology* 189 (6): 1013–25.

Hammond, Jennetta W., Dawen Cai, T. Lynne Blasius, Zhe Li, Yuyang Jiang, Gloria T. Jih, Edgar Meyhofer, and Kristen J. Verhey. 2009. "Mammalian Kinesin-3 Motors Are Dimeric in Vivo and Move by Processive Motility upon Release of Autoinhibition." *PLoS Biology* 7 (3): 0650–63.

Hirokawa, Nobutaka, Yasuko Noda, Yosuke Tanaka, and Shinsuke Niwa. 2009. "Kinesin Superfamily Motor Proteins and Intracellular Transport." *Nature Reviews. Molecular Cell Biology* 10 (10): 682–96.

Hirokawa, Nobutaka, and Reiko Takemura. 2004. "Kinesin Superfamily Proteins and Their Various Functions and Dynamics." *Experimental Cell Research* 301 (1): 50–59.

Horwitz, Susan Band. 2019. "Reflections on My Life with Taxol." *Cell* 0 (0). https://doi.org/10.1016/j.cell.2019.03.031.

Idriss, Haitham T. 2004. “Defining a Physiological Role for the Tubulin Tyrosination Cycle.” *Electronic Journal of General Medicine*. https://doi.org/10.29333/ejgm/82183.

Janke, Carsten. 2014. “The Tubulin Code: Molecular Components, Readout Mechanisms, Functions.” *The Journal of Cell Biology* 206 (4): 461–72.

Janke, Carsten and Montagnac, Guillaume. 2017. “Causes and Consequences of Microtubule Acetylation.” *Current Biology.* 27(23):1287-1292.

Janke, Carsten, and Maria M. Magiera. 2020. “The Tubulin Code and Its Role in Controlling Microtubule Properties and Functions.” *Nature Reviews. Molecular Cell Biology* 21 (6): 307–26.

Jaqaman, Khuloud, Emma M. King, Ana C. Amaro, Jennifer R. Winter, Jonas F. Dorn, Hunter L. Elliott, Nunu McHedlishvili, et al. 2010. “Kinetochore Alignment within the Metaphase Plate Is Regulated by Centromere Stiffness and Microtubule Depolymerases.” *The Journal of Cell Biology* 188 (5): 665–79.

Kaan, Hung Yi Kristal, David D. Hackney, and Frank Kozielski. 2011. “The Structure of the Kinesin-1 Motor-Tail Complex Reveals the Mechanism of Autoinhibition.” *Science* 333 (6044): 883–85.

Kapoor, Tarun M., and Duane A. Compton. 2002. “Searching for the Middle Ground: Mechanisms of Chromosome Alignment during Mitosis.” *Journal of Cell Biology*. https://doi.org/10.1083/jcb.200202073.

Karabay, A., and R. A. Walker. 1999. “Identification of Microtubule Binding Sites in the Ncd Tail Domain.” *Biochemistry* 38 (6): 1838–49.

Kaul, Neha, Virupakshi Soppina, and Kristen J. Verhey. 2014. “Effects of α-Tubulin K40 Acetylation and Detyrosination on Kinesin-1 Motility in a Purified System.” *Biophysical Journal* 106 (12): 2636–43.

Kubo, Tomohiro, Masafumi Hirono, Takumi Aikawa, Ritsu Kamiya, and George B. Witman. 2015. “Reduced Tubulin Polyglutamylation Suppresses Flagellar Shortness in Chlamydomonas.” *Molecular Biology of the Cell*. https://doi.org/10.1091/mbc.e15-03-0182.

Kuhns, Stefanie, and Oliver E. Blacque. 2016. “Cilia Train Spotting.” *Developmental Cell* 37 (5): 395–96.

Lawrence, Carolyn J., R. Kelly Dawe, Karen R. Christie, Don W. Cleveland, Scott C. Dawson, Sharyn A. Endow, Lawrence S. B. Goldstein, et al. 2004. “A Standardized Kinesin Nomenclature.” *The Journal of Cell Biology* 167 (1): 19–22.

Lechtreck, Karl F., Julie C. Van De Weghe, J. Aaron Harris, and Peiwei Liu. 2017. "Protein Transport in Growing and Steady-State Cilia." *Traffic* 18 (5). https://doi.org/10.1111/tra.12474.

Lessard, Dominique V., Oraya J. Zinder, Takashi Hotta, Kristen J. Verhey, Ryoma Ohi, and Christopher L. Berger. 2019. "Polyglutamylation of Tubulin's C-Terminal Tail Controls Pausing and Motility of Kinesin-3 Family Member KIF1A." *The Journal of Biological Chemistry* 294 (16): 6353–63.

L'Hernault, S. W., and J. L. Rosenbaum. 1983. "Chlamydomonas Alpha-Tubulin Is Posttranslationally Modified in the Flagella during Flagellar Assembly." *The Journal of Cell Biology* 97 (1): 258–63.

———. 1985a. "Chlamydomonas Alpha-Tubulin Is Posttranslationally Modified by Acetylation on the Epsilon-Amino Group of a Lysine." *Biochemistry* 24 (2): 473–78.

———. 1985b. "Reversal of the Posttranslational Modification on Chlamydomonas Flagellar Alpha-Tubulin Occurs during Flagellar Resorption." *The Journal of Cell Biology* 100 (2): 457–62.

Li, Faxiang, Yingjie Hu, Shutao Qi, Xuelian Luo, and Hongtao Yu. 2019. "Structural Basis of Tubulin Detyrosination by Vasohibins." *Nature Structural & Molecular Biology* 26 (7): 583–91.

Marshall, Wallace F., Hongmin Qin, Mónica Rodrigo Brenni, and Joel L. Rosenbaum. 2005. "Flagellar Length Control System: Testing a Simple Model Based on Intraflagellar Transport and Turnover." *Molecular Biology of the Cell* 16 (1): 270–78.

Marshall, W. F., and J. L. Rosenbaum. 2001. "Intraflagellar Transport Balances Continuous Turnover of Outer Doublet Microtubules: Implications for Flagellar Length Control." *The Journal of Cell Biology* 155 (3): 405–14.

Mayr, Monika I., Stefan Hümmer, Jenny Bormann, Tamara Grüner, Sarah Adio, Guenther Woehlke, and Thomas U. Mayer. 2007. "The Human Kinesin Kif18A Is a Motile Microtubule Depolymerase Essential for Chromosome Congression." *Current Biology: CB* 17 (6): 488–98.

McKenney, Richard J., Walter Huynh, Ronald D. Vale, and Minhajuddin Sirajuddin. 2016. "Tyrosination of α-tubulin Controls the Initiation of Processive Dynein–dynactin Motility." *The EMBO Journal* 35 (11): 1175–85.

Milic, Bojan, Johan O. L. Andreasson, William O. Hancock, and Steven M. Block. 2014. "Kinesin Processivity Is Gated by Phosphate Release." *Proceedings of the National Academy of Sciences of the United States of America* 111 (39): 14136–40.

Mirvis, Mary, Tim Stearns, and W. James Nelson. 2018. “Cilium Structure, Assembly, and Disassembly Regulated by the Cytoskeleton.” *Biochemical Journal*. Portland Press Ltd. https://doi.org/10.1042/BCJ20170453.

Monroy, Brigette Y., Danielle L. Sawyer, Bryce E. Ackermann, Melissa M. Borden, Tracy C. Tan, and Kassandra M. Ori-Mckenney. 2018. “Competition between Microtubule-Associated Proteins Directs Motor Transport.” *Nature Communications* 9 (1): 1–12.

Monroy, Brigette Y., Tracy C. Tan, Janah May Oclaman, Jisoo S. Han, Sergi Simó, Shinsuke Niwa, Dan W. Nowakowski, Richard J. McKenney, and Kassandra M. Ori-McKenney. 2020. “A Combinatorial MAP Code Dictates Polarized Microtubule Transport.” *Developmental Cell* 53. https://doi.org/10.1101/731604.

Nakayama, Kazuhisa, and Yohei Katoh. 2018. “Ciliary Protein Trafficking Mediated by IFT and BBSome Complexes with the Aid of Kinesin-2 and Dynein-2 Motors.” *Journal of Biochemistry* 163 (3): 155–64.

Namdar, M., Perez, G., Ngo, L., Marks, P.A. 2010. “Selectine inhibition of histone deacetylase 6 (HDAC6) induces DNA damage and sensitizes transformed cells to anticancer agents.” *PNAS* 107(46):20003-8.

Pamula, Melissa C., Shih Chieh Ti, and Tarun M. Kapoor. 2016. “The Structured Core of Human β Tubulin Confers Isotype-Specific Polymerization Properties.” *The Journal of Cell Biology* 213 (4): 425–33.

Phillips, Rebecca K., Logan G. Peter, Susan P. Gilbert, and Ivan Rayment. 2016. “Family-Specific Kinesin Structures Reveal Neck-Linker Length Based on Initiation of the Coiled-Coil.” *The Journal of Biological Chemistry* 291 (39): 20372–86.

Phua, Siew Cheng, Shuhei Chiba, Masako Suzuki, Emily Su, Elle C. Roberson, Ganesh V. Pusapati, Stéphane Schurmans, et al. 2019. “Dynamic Remodeling of Membrane Composition Drives Cell Cycle through Primary Cilia Excision.” *Cell* 178 (1): 261.

Pitaval, Amandine, Fabrice Senger, Gaëlle Letort, Xavier Gidrol, Laurent Guyon, James Sillibourne, and Manuel Théry. 2017. “Microtubule Stabilization Drives 3D Centrosome Migration to Initiate Primary Ciliogenesis.” *The Journal of Cell Biology* 216 (11): 3713–28.

Prevo, Bram, Jonathan M. Scholey, and Erwin J. G. Peterman. 2017. “Intraflagellar Transport: Mechanisms of Motor Action, Cooperation, and Cargo Delivery.” *The FEBS Journal* 284 (18): 2905–31.

Prota, Andrea E., Maria M. Magiera, Marijn Kuijpers, Katja Bargsten, Daniel Frey, Mara Wieser, Rolf Jaussi, et al. 2013. "Structural Basis of Tubulin Tyrosination by Tubulin Tyrosine Ligase." *The Journal of Cell Biology*. https://doi.org/10.1083/jcb.201211017.

Ran, Jie, Yunfan Yang, Dengwen Li, Min Liu, and Jun Zhou. 2015. "Deacetylation of α-Tubulin and Cortactin Is Required for HDAC6 to Trigger Ciliary Disassembly." *Scientific Reports* 5 (1): 1–13.

Reed, Nathan A., Dawen Cai, T. Lynne Blasius, Gloria T. Jih, Edgar Meyhofer, Jacek Gaertig, and Kristen J. Verhey. 2006. "Microtubule Acetylation Promotes Kinesin-1 Binding and Transport." *Current Biology: CB* 16 (21): 2166–72.

Ren, Jinqi, Shuang Wang, Han Chen, Wenjuan Wang, Lin Huo, and Wei Feng. 2018. "Coiled-Coil 1-Mediated Fastening of the Neck and Motor Domains for Kinesin-3 Autoinhibition." *Proceedings of the National Academy of Sciences* 115 (51): E11933–42.

Rocha, Cecilia, Laura Papon, Wulfran Cacheux, Patricia Marques Sousa, Valeria Lascano, Olivia Tort, Tiziana Giordano, et al. 2014. "Tubulin Glycylases Are Required for Primary Cilia, Control of Cell Proliferation and Tumor Development in Colon." *The EMBO Journal* 33 (19): 2247–60.

Roll-Mecak, Antonina. 2019. "How Cells Exploit Tubulin Diversity to Build Functional Cellular Microtubule Mosaics." *Current Opinion in Cell Biology* 56 (February): 102–8.

Schiff, P. B., and S. B. Horwitz. 1980. "Taxol Stabilizes Microtubules in Mouse Fibroblast Cells." *Of the National Academy of Sciences*. https://www.pnas.org/content/77/3/1561.short.

Schimert, Kristin I., Breane G. Budaitis, Dana N. Reinemann, Matthew J. Lang, and Kristen J. Verhey. 2019. "Intracellular Cargo Transport by Single-Headed Kinesin Motors." *Proceedings of the National Academy of Sciences of the United States of America* 116 (13): 6152–61.

Seeger, Mark A., and Sarah E. Rice. 2010. "Microtubule-Associated Protein-like Binding of the Kinesin-1 Tail to Microtubules." *The Journal of Biological Chemistry* 285 (11): 8155–62.

Shang, Zhiguo, Kaifeng Zhou, Chen Xu, Roseann Csencsits, Jared C. Cochran, and Charles V. Sindelar. 2014. "High-Resolution Structures of Kinesin on Microtubules Provide a Basis for Nucleotide-Gated Force-Generation." *eLife* 3: 1–27.

Sirajuddin, Minhajuddin, Luke M. Rice, and Ronald D. Vale. 2014. "Regulation of Microtubule Motors by Tubulin Isotypes and Post-Translational Modifications." *Nature Cell Biology*. https://doi.org/10.1038/ncb2920.

Stumpff, Jason, George von Dassow, Michael Wagenbach, Charles Asbury, and Linda Wordeman. 2008. “The Kinesin-8 Motor Kif18A Suppresses Kinetochore Movements to Control Mitotic Chromosome Alignment.” *Developmental Cell* 14 (2): 252–62.

Stumpff, Jason, Yaqing Du, Chauca A. English, Zoltan Maliga, Michael Wagenbach, Charles L. Asbury, Linda Wordeman, and Ryoma Ohi. 2011. “A Tethering Mechanism Controls the Processivity and Kinetochore-Microtubule Plus-End Enrichment of the Kinesin-8 Kif18A.” *Molecular Cell* 43 (5): 764–75.

Szyk, Agnieszka, Alexandra M. Deaconescu, Grzegorz Piszczek, and Antonina Roll-Mecak. 2011. “Tubulin Tyrosine Ligase Structure Reveals Adaptation of an Ancient Fold to Bind and Modify Tubulin.” *Nature Structural & Molecular Biology* 18 (11): 1250–58.

Tas, Roderick P., Anaël Chazeau, Bas M. C. Cloin, Maaike L. A. Lambers, Casper C. Hoogenraad, and Lukas C. Kapitein. 2017. “Differentiation between Oppositely Oriented Microtubules Controls Polarized Neuronal Transport.” *Neuron* 96 (6): 1264–71.e5.

Ti, Shih-Chieh, Gregory M. Alushin, and Tarun M. Kapoor. 2018. “Human β-Tubulin Isotypes Can Regulate Microtubule Protofilament Number and Stability.” *Developmental Cell* 47 (September): 1–16.

Ti, Shih-Chieh, Michal Wieczorek, and Tarun M. Kapoor. 2020. “Purification of Affinity Tag-Free Recombinant Tubulin from Insect Cells.” *STAR Protocols*, June, 100011.

Vale, R. D., D. R. Soll, and I. R. Gibbons. 1989. “One-Dimensional Diffusion of Microtubules Bound to Flagellar Dynein.” *Cell* 59 (5): 915–25.

Vale, R., T. Reese, and M. Sheetz. 1985. “Identification of a Novel Force-Generating Protein, Kinesin, Involved in Microtubule-Based Motility.” *Cell* 42 (1): 39–50.

Varga, Vladimir, Jonne Helenius, Kozo Tanaka, Anthony A. Hyman, Tomoyuki U. Tanaka, and Jonathon Howard. 2006. “Yeast Kinesin-8 Depolymerizes Microtubules in a Length-Dependent Manner.” *Nature Cell Biology* 8 (9): 957–62.

Varga, Vladimir, Cecile Leduc, Volker Bormuth, Stefan Diez, and Jonathon Howard. 2009. “Kinesin-8 Motors Act Cooperatively to Mediate Length-Dependent Microtubule Depolymerization.” *Cell* 138 (6): 1174–83.

Verhey, Kristen J., John Dishinger, and Hooi Lynn Kee. 2011. “Kinesin Motors and Primary Cilia.” *Biochemical Society Transactions*. NIH Public Access. https://doi.org/10.1042/BST0391120.

Verhey, Kristen J., and Jacek Gaertig. 2007. “The Tubulin Code.” *Cell Cycle* 6 (17): 2152–60.

Verhey, Kristen J., and Jennetta W. Hammond. 2009. “Traffic Control: Regulation of Kinesin Motors.” *Nature Reviews. Molecular Cell Biology* 10 (11): 765–77.

Wang, Qian, Junmin Pan, and William J. Snell. 2006. “Intraflagellar Transport Particles Participate Directly in Cilium-Generated Signaling in Chlamydomonas.” *Cell* 125 (3): 549–62.

Wani, M. C. 1971. “The Isolation and Structure of Taxol, a Novel Antileukemic and Antitumor Agent from Taxus Brevifolia.” *Journal of the American Chemical Society* 93: 2325–27.

Webb, Stephanie, Aakash G. Mukhopadhyay, and Anthony J. Roberts. 2020. “Intraflagellar Transport Trains and Motors: Insights from Structure.” *Seminars in Cell & Developmental Biology* 107 (November): 82–90.

Wheway, Gabrielle, Liliya Nazlamova, and John T. Hancock. 2018. “Signaling through the Primary Cilium.” *Frontiers in Cell and Developmental Biology* 6 (February): 8.

Williams, Corey L., Jeremy C. McIntyre, Stephen R. Norris, Paul M. Jenkins, Lian Zhang, Qinglin Pei, Kristen Verhey, and Jeffrey R. Martens. 2014. “Direct Evidence for BBSome-Associated Intraflagellar Transport Reveals Distinct Properties of Native Mammalian Cilia.” *Nature Communications* 5 (1): 5813.

Wingfield, Jenna L., Ilaria Mengoni, Heather Bomberger, Yu-Yang Jiang, Jonathon D. Walsh, Jason M. Brown, Tyler Picariello, et al. 2017. “IFT Trains in Different Stages of Assembly Queue at the Ciliary Base for Consecutive Release into the Cilium.” *eLife* 6 (May). https://doi.org/10.7554/eLife.26609.

Wloga, Dorota, Danielle M. Webster, Krzysztof Rogowski, Marie-Hélène Bré, Nicolette Levilliers, Maria Jerka-Dziadosz, Carsten Janke, Scott T. Dougan, and Jacek Gaertig. 2009. “TTLL3 Is a Tubulin Glycine Ligase That Regulates the Assembly of Cilia.” *Developmental Cell* 16 (6): 867–76.

Ye, Fan, Andrew R. Nager, and Maxence V. Nachury. 2018. “BBSome Trains Remove Activated GPCRs from Cilia by Enabling Passage through the Transition Zone.” *The Journal of Cell Biology* 217 (5): 1847–68.

Yu, Ian, Christopher P. Garnham, and Antonina Roll-Mecak. 2015. “Writing and Reading the Tubulin Code.” *The Journal of Biological Chemistry* 290 (28): 17163–72.

Appendix B: Beam shift and accessible data improve cryoEM data collection and processing

B.1 Forward

This section describes the recent developments in the field of cryo electron microscopy (cryoEM) and our contributions to testing data collection and processing pipelines. Here we find that using beam-tilt increases the throughput of data collection at the cost of having to correct for aberrations at the data processing stage, this work published in (Cash et al. 2020). Additionally, this section will discuss the accessibility and future of cryoEM data processing, showing some ongoing work on cryoEDU, a cryoEM/ET education platform, in collaboration with the Herzik lab at UCSD, and Single Particle LLC. Accessible cryoEM data and education are critical as techniques make the technology more accessible, with some discussion and commentary published in (Kearns 2020).

B.2 Introduction

Cryogenic electron microscopy (cryoEM) allows for determining the three-dimensional shape and structure of biomacromolecules, like proteins and nucleic acids. By embedding biological samples in ice in native conditions, dynamics and conformational changes can be determined, two things that are difficult to see using other structural biology techniques like x-ray crystallography. The Nobel Prize in Chemistry in 2017 was awarded to Jacques Dubochet, Richard Henderson, and Joachim Frank for developing cryoEM (Henderson and Unwin 1975; Saxton and Frank 1977; Dubochet et al. 1988). Since their foundational establishments in the field, technical advances on numerous fronts, including direct electron detectors, which increases the amount of information collected per image, and algorithm developments allowing for motion-correction during imaging, have made data collection and processing go to higher resolution, thus being able to see structures in high detail (Campbell et al. 2012; Bai et al. 2013; Li et al. 2013). In addition,

automated data collection strategies and software for image analysis streamline many methods in cryoEM (Suloway et al. 2005; Grant et al. 2018; Scheres 2012; Punjani et al. 2017; Tegunov and Cramer 2019). As such, the combination of Nobel hype and technical advances has made cryoEM a go-to method for structural analysis.

To obtain a high-resolution structure using cryoEM, the sample of interest must first be applied to a small grid, which has a mesh made of conductive material and covered with a support film. The grid is usually polarized first such that the particles stick to the grid. Excess sample is blotted away from the grid to make sure the ice is thin when it's plunged into a bath of cryogen. Next, the grid is clipped such that the mechanical auto-loader in the microscope can pick it up and place it on the stage for imaging. Because the microscope contains a system of lenses and condensers, electrons shot out from the electron gun (at various voltages depending on the type of microscope) at the top of a column are directed towards the sample to produce an image that the direct electron detector can see. Data is collected in the form of short movies, and then aligned into a single image. From there, particles are picked and fed into various data processing software to determine the 3D map and build the atomic model.

In order to increase the throughput from cryo-EM instruments, many laboratories and facilities have begun using beam-image shift for data collection (Cheng et al. 2018). Using this approach, instead of moving the stage to each position on the cryo-EM grid, a process that requires precise movement, the beam is moved in conjunction with image adjustments. Without long waiting times of moving the stage, tilting the beam leads to a dramatic increase in the number of exposures per hour. As such, it is now routine to use beam-tilt to collect 100-300 exposures whereas previously it was only possible to collect 40-50 per hour. This throughput will continue to increase with the advent of direct detectors with faster frame rates, leading to hundreds of exposures per hour.

Even though users can collect two to three times the amount of data using beam-image shift, they must overcome an additional aberration induced by the beam-image shift: beam tilt (Glaeser et al. 2011). When using beam-image shift for collecting exposures, the resulting image will have both axial and off-axis beam tilt (or coma), aberrations that will dampen high-resolution (<3Å) information in the micrographs (Glaeser et al. 2011). Beam tilt aberrations can be corrected computationally for high-resolution structures, starting with the atomic-resolution structure of bacteriorhodopsin from 2D crystals (Henderson et al. 1986). Since its use 40 years ago, recent

advances in single-particle cryo-EM have led to the incorporation of beam tilt correction into software packages such as RELION (Zivanov et al. 2018; Zivanov, Nakane, and Scheres 2020; Herzik, Wu, and Lander 2017; Wu, Lander, and Herzik, 2020) which has lead to the widespread adoption of beam tilt correction in cryoEM data processing.

Even though beam-image shift data collection in combination with aberration correction has been implemented for datasets at 300 keV(Herzik, Wu, and Lander 2017; Wu, Lander, and Herzik, 2020), there is limited experimental data on the correction for beam tilt for data sets collected at 200 keV. Beam-image shift would likely induce coma, thus introducing optical aberrations and we wanted to determine if it can be overcome computationally. Given that the phase error caused by either axial or off-axis beam tilt scales with the wavelength squared (Glaeser et al. 2011), using a 200 keV microscope will result in worse phase error than a 300 keV microscope from both axial and off-axis beam tilt. In order to test the limits of computational correction of microscope aberrations at 200 keV, we collected and analyzed a dataset of aldolase using beam-image shift on a Talos-Arctica at 200 kV. Using this dataset, I was able to determine a 4.9Å structure of aldolase without aberration corrections. Following iterative rounds of axial beam tilt correction and particle polishing, we were able to determine a 2.8Å structure of aldolase. This indicates that beam-image shift can be an effective data collection strategy to increase the throughput on 200 keV cryo-EM instruments, where microscope aberrations can be corrected computationally.

By going through the process of data processing, we have also noticed a significant educational barrier required of new users. In order to start doing cryoEM, practitioners must understand concepts that range from biochemistry to physics of electron microscopes to computational image alignment algorithms. Although there are cryoEM workshops currently available to tackle such concepts with hands-on training, the limited capacity and intimate format results in substantial oversubscription and an inability to train cryoEM neophytes en masse. As such, there exists a significant gap in training materials and resources that help users understand, analyze, interpret, and validate cryoEM data and structure determination. Towards this end, we propose to build an educational platform focused on cryoEM/ET data processing called cryoEDU.

B.3 Results

B.3.1 Binning micrographs by beam-tilt groups

To increase the speed of data collection on the Talos-Arctica, we utilized beam-image shift instead of traditional stage movement. In order to test the impact of beam-image shift on data quality, we set up the automated data collection system to target 5x5 holes with beam-image shift (Fig. B1A). At medium magnification, we typically focused on the middle hole which was followed by beam-image shift with distances up to 5 μm away from the beam center. After collecting 2,111 micrographs over 18 hours at ten second exposures, we obtained a large range of beam-image shift micrographs that provided a near-continuous distribution across the 10 x 10 μm area (Fig. B1B). Interestingly, while many micrographs showed minimal objective astigmatism (Fig. B1C), a large percentage of the dataset showed exaggerated objective astigmatism (Fig. B1D).

Following data collection, the aldolase beam-image shift data were analyzed using standard single-particle processing.. This involved estimating the contrast transfer function (CTF) using CTFFIND4 (Rohou and Grigorieff 2015), which yielded CTF fits to higher than 4Å resolution for the majority of the micrographs (Fig. B1E). After selecting particles from class averages exhibiting high-resolution features, we performed 3D classification in order to obtain a homogenous population of aldolase particles with all four subunits intact (Fig. B1F). Using these selected particle coordinates, particles were re-extracted at the full pixel size (0.91 Å/pixel) and subjected to 3D refinement in RELION. The refined structure reached a resolution of only 4.9Å (Fig. B1G-H), which is significantly less than published work of ~3Å (Kim et al. 2018; Herzik, Wu, and Lander 2017). This suggested that the aberrations from beam tilt induced by beam-image shift data collection are likely limiting the resolution of the final structure.

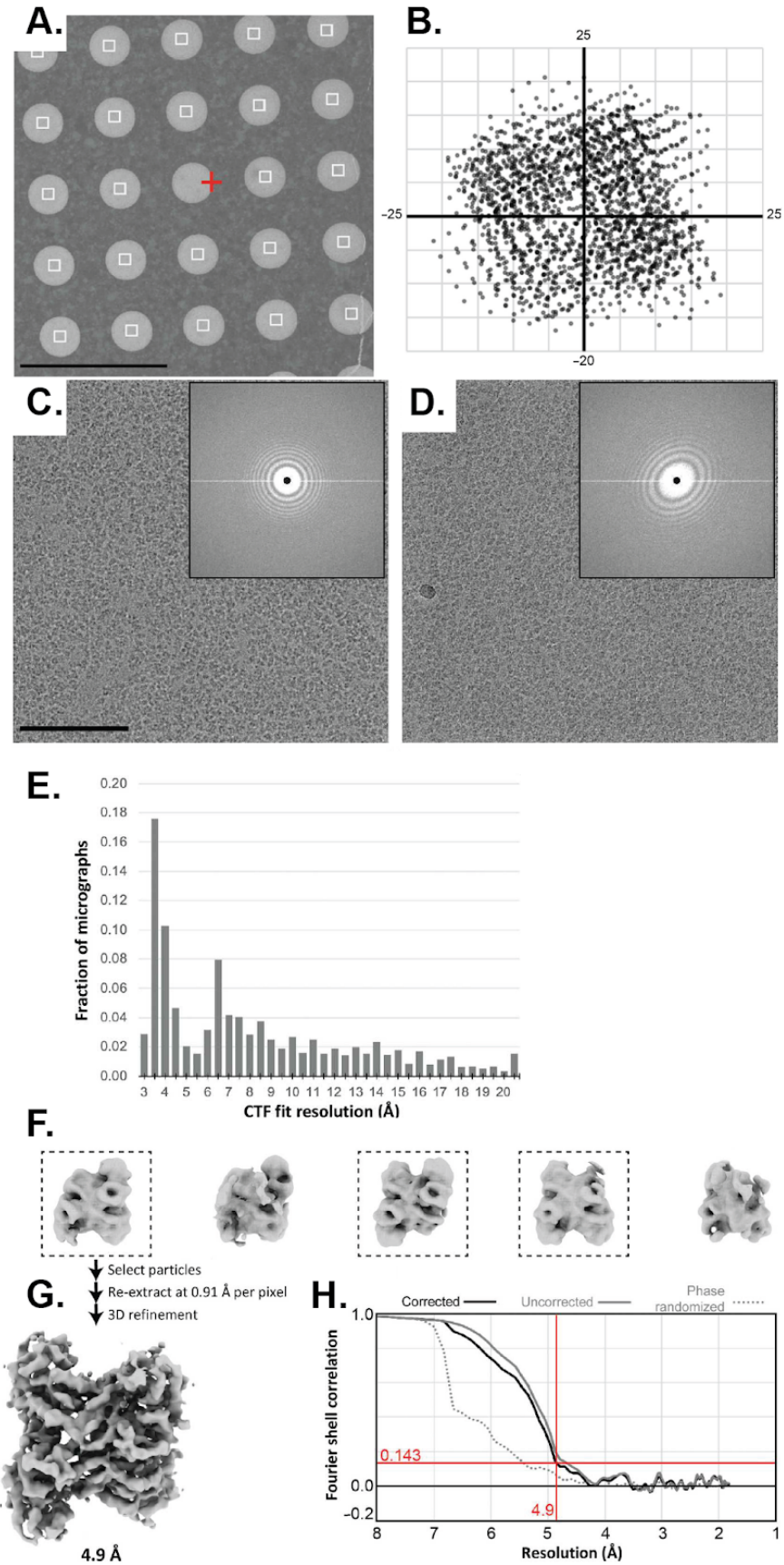

Fig. B1 Beam-tilt data-collection strategy and single particle analysis of aldolase without beam-tilt. A) Representative image at intermediate magnification. Red cross, focus area; white squares, exposures. The scale bar is 5 µm. Each exposure was collected with image-shift beam tilt. B) Overview of image-shift values from Leginon for the beam-tilt data set. The units shown are µm. C-D) Representative micrographs with minimal C) and obvious D) beam-tilt-induced objective astigmatism. Inset: cropped power spectrum. The scale bar is 100 nm. E) Histogram of CTF resolution limits across the data set using CTFFIND4. (c) Representative 2D class averages calculated using RELION. The scale bar is 200 Å. F) 3D classification results for selected particles after 2D classification. Dashed boxes indicate classes with particles used for subsequent 3D refinement. G) Sharpened reconstruction after 3D refinement using RELION filtered to 4.9 Å resolution. H) FSC curves for final reconstruction.

B.3.2 Iterative beam-tilt correction improves resolution

After determining a refined 3D structure of aldolase, we wanted to test whether the beam tilt refinement option in RELION 3.0 is capable of overcoming such a large degree of axial beam tilt. To use this feature of RELION, the micrographs must be grouped into beam tilt groups. Considering the near-continuously changing beam-image shift data collection for the entire dataset, beam-image shift values from Leginon were used in order to divide the micrographs into groups (Fig. B2A). This involved dividing data into groups of 25 (5x5), 100 (10x10), and 400 (20x20) based on the amount of beam-image shift in Leginon. For each grouping, the particles underwent beam tilt refinement, 3D refinement, and sharpening in RELION in order to determine the change in the final resolution of the structure. We saw that grouping into 5x5, 10x10, and 20x20 groups had a significant increase in the final resolution of 4.1Å, 4.0Å, and 3.8Å, respectively (Fig. B2B). This result indicates that the previously determined structure at 4.9Å (Fig. B2C) was limited in resolution due to beam tilt aberrations that could be partially overcome by grouping the data into beam tilt groups in RELION.

For the micrographs divided into 400 groups, the subsequently refined map showed improved density features and had a gold standard FSC value of 3.8Å (Fig. B2C-D). This indicates that beam tilt refinement improved the resolution of aldolase significantly from 4.9Å to 3.8Å in a single step. Further iterations of beam-tilt correction, in addition to Bayesian particle polishing, further increased the resolution to a final 2.8 Å map. The final structure at 2.8Å (Fig. B2E-F) shows dramatically improved density features compared to the original 4.9Å structure. Specifically, the significantly higher resolution provides unambiguous secondary structure tracing whereas the 4.9Å structure contained many more ambiguities. This structure demonstrates that computational correction of microscope aberrations and particle motion allows for sub-3Å structure determination.

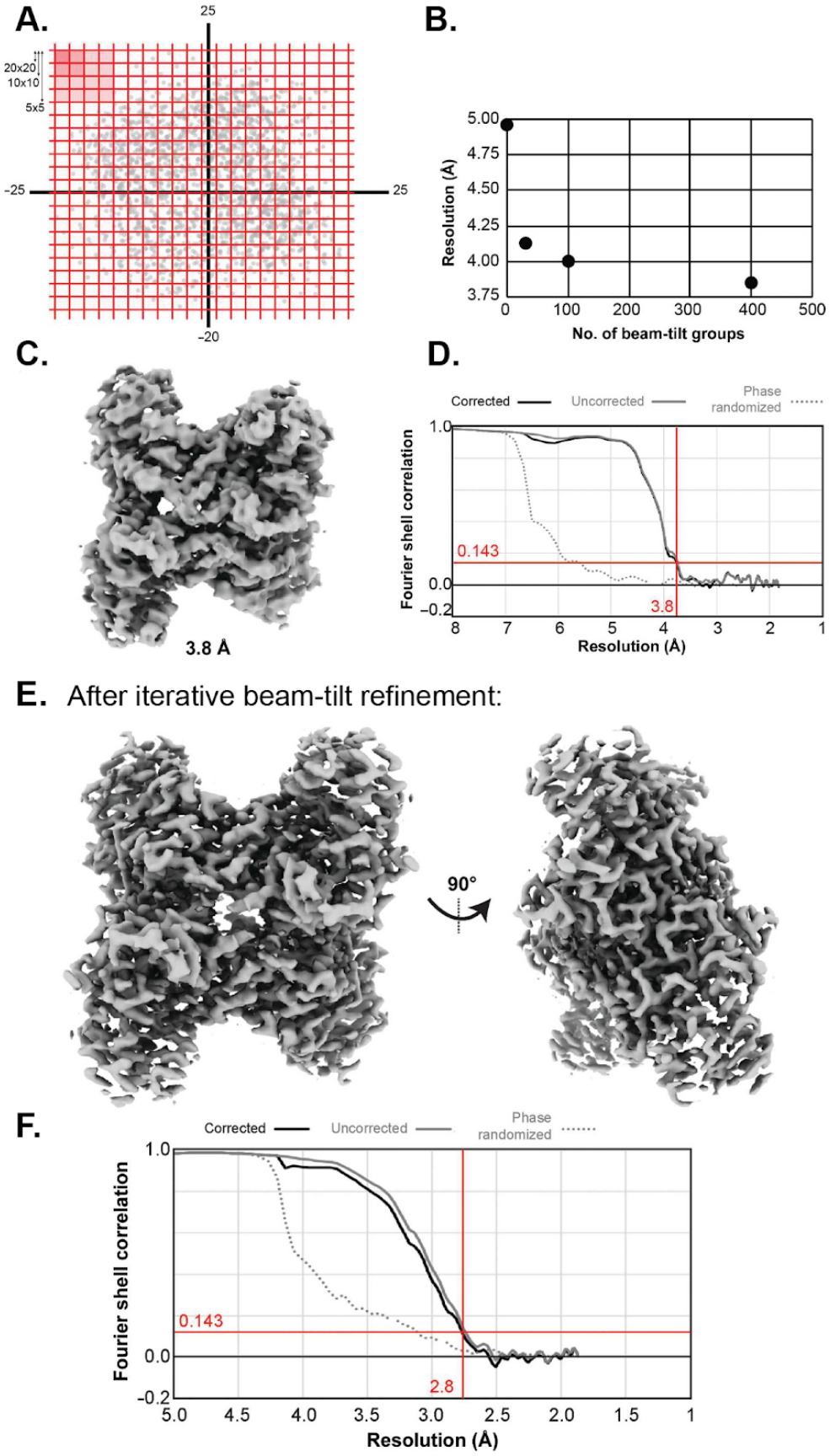

Fig. B2 Improved resolution using beam-tilt refinement. A) Strategy for grouping micrographs. Micrographs were grouped into 25 groups (5 × 5), 100 groups (10 × 10) and 400 groups (20 × 20). B) The effect of group size on beam-tilt refinement and subsequent resolution estimation for refined 3D structures. C) Sharpened 3D reconstruction for particles placed into 400 micrograph groups filtered to 3.8 Å resolution. D) FSC curves for 3D reconstruction. E) Sharpened aldolase reconstruction at 2.8 Å. F) FSC curve for the final reconstruction.

B.3.3 Making cryoEM data processing education accessible

To facilitate the adoption of cryoEM/ET and to train the next generation of structural biologists, the NIH has

funded both cryoEM/ET data collection centers in addition to cryoEM/ET curricular grants. In order to alleviate the often inhibitory financial burden associated with the acquisition, installation, and operation state-of-the-art cryoEM facilities, several NIH-funded cryoEM centers -- the National Center for CryoEM Access and Training (NCCAT), the Pacific Northwest Center for CryoEM (PNCC), and the Stanford-SLAC CryoEM Center (S2C2) -- were established to provide practitioners with free access to both sample screening and data collection instruments under the supervision of EM experts. To further support users at these national centers, a series of curricular grants (EM-Learning.com, CryoEM 101, CryoEM Principles, and cryoVR) were funded that addressed theoretical aspects of cryoEM in addition to practical details for sample preparation.

Despite these critical investments in cryoEM/ET, there remains a gap in the available curricula to data analysis. Even though new users have access to online educational curricula and on-site training at national centers, users are frequently overwhelmed and often lost when it comes to steps related to data assessment, analysis, and validation. Towards this end, we have started to build an educational platform focused on cryoEM/ET data processing, called 'cryoEDU', that helps users understand, analyze, interpret, and validate cryoEM data and structure determination. The cryoEDU platform is built upon three pillars: 1) self-paced online modular curricula; 2) hands-

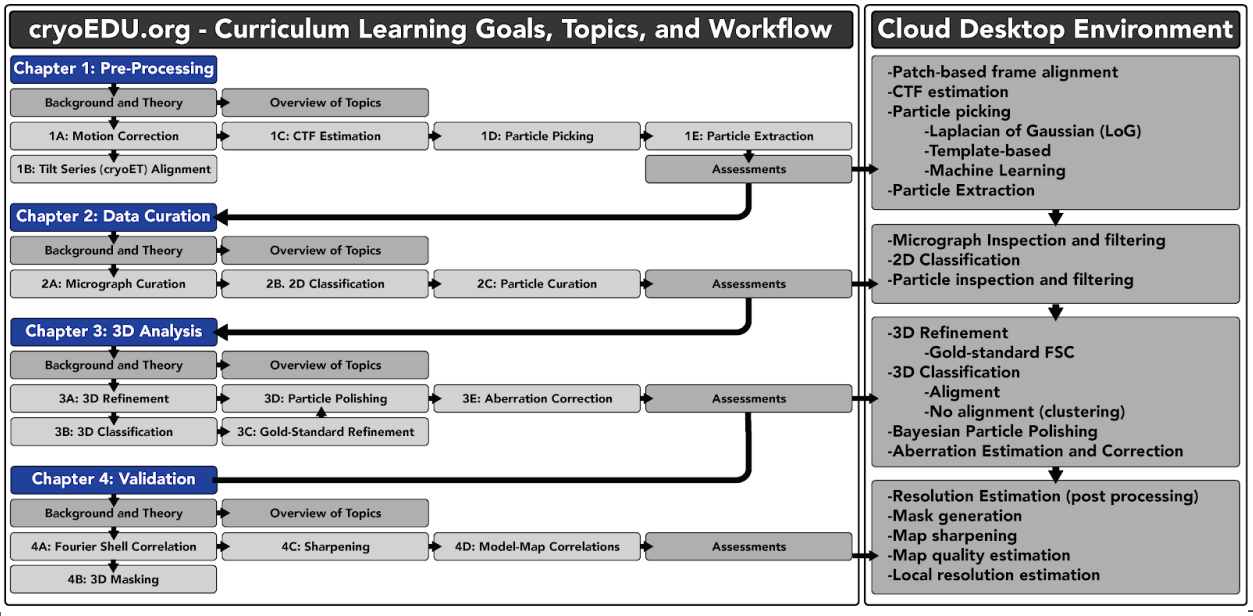

Fig. B3 Overview of cryoEDU Chapter, Modules, and connection to cloud environment. CryoEM/ET data processing is broken down into chapters (blue boxes) that form the basis for the online curriculum. For each Chapter and Module, there will be directly relevant modules and workflows on the cloud environment to provide learners with a hands-on interactive data processing experience.

on data analysis in a cloud desktop environment; and 3) community engagement to facilitate information exchange related to cryoEM/ET data analysis. Our interactive cloud desktop environment will enable hands-on learning for users from all science backgrounds and by integrating our curriculum within the existing learning environment, we will help to train users better to assess, interpret, and analyze cryoEM/ET datasets.

We have acquired the domain name cryoEDU.org and have since transferred hosting services to the Physics Computing Facility at UCSD for maintenance, server operations, and Wordpress support. We have elected to use Wordpress to build out the website infrastructure due to the extensive support for teaching and learning-based plugins, general ease of use and design, as well as the extensive community support. When users first land on cryoEDU.org they will be presented with the mission statement of our curriculum, a preview of the topics covered by our learning modules, and a means to register for a user account for the self-paced curriculum. This will allow each learner to return to cryoEDU.org at a pace suitable for their learning style. From the home page, each Chapter will have a dedicated page with associated Modules, Topics, and Assessments that will be easily accessible through a user-intuitive toolbar (Fig. 3).

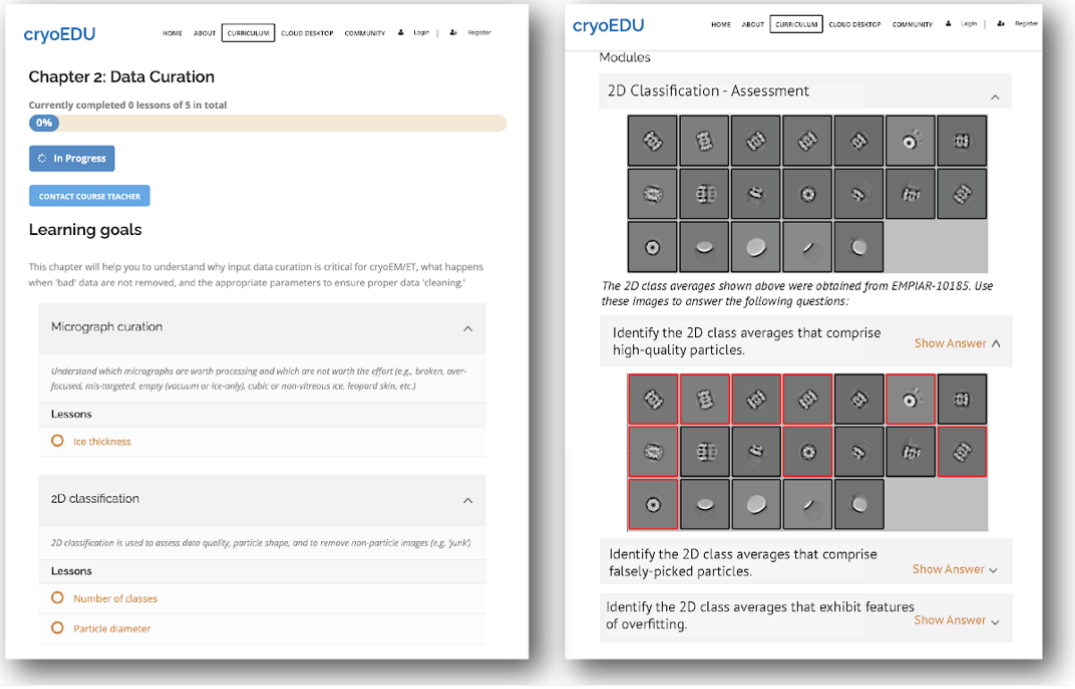

Fig. B4 Example of cryoEDU.org layout for Chapter, Modules, and assessment quiz. Left) Landing page for Chapter 2 highlighting the progress bar, modules, and lessons available. Right) Example assessment quiz related to identifying 'good' vs 'bad' 2D class averages.

In addition to establishing the formal foundation for data processing, the curricula will also draw on real-world data examples to highlight appropriate processing schemes. This coupling to computational frameworks will give learners hands-on experience with data in an environment amenable to learning why data is processed in a certain way. In practice, this will look like a "choose your own adventure" as users go through different processing pathways. To limit the computational load, the data will be pre-calculated so learners going through the processing pathway will be drawing upon already existing data rather than taking the time and resources to recalculate data, much like the "choose your own adventure" book series having a predetermined number of pages and outcomes. Moreover, the total number of combinations will be limited by implementing "dead ends" of data processing, such as too few particles, incorrect CTF parameters, incorrect particle size, etc. where learners will net be able to continue down a processing branch if a high-resolution reconstruction cannot be obtained or another pathological outcome would result.

To provide users with a simulated data processing experience, we selected RELION as the initial software package that we will use for precalculation and the cloud desktop environment. We selected RELION because it's the most common software associated with deposited entries in the EM Data Bank, is open source, is fairly intensive yet GUI-based, and offers developments in cryoET, thus allowing for both single particle analysis in addition to sub-tomogram averaging. cryoEM/ET software, along with the pre-calculated data, will all be hosted on a cloud environment, thus reliving the computational burden in training users to analyze data, in addition to being able to train multiple users at once.

B.4 Discussion

B.4.1 Data quality and resolution increase with beam-tilt correction

The dataset analyzed in this work utilized significant beam-image shift data collection at 200 keV on a Talos-Arctica. This strategy introduced significant microscope aberrations into the raw data and was significant enough to cause objective astigmatism in micrographs due to a large amount of beam tilt (Figure 2A, right). During data collection, we did not perform additional alignments such as those used to set up parallel illumination. We only corrected objective astigmatism and beam-tilt pivot points for automatic focusing. Both of these slight adjustments did not alter imaging abnormalities suggesting aberrations came from altering the beam-image shift during data collection.

By taking advantage of microscope aberration correction in RELION-3.0+ (Zivanov et al., 2020) we were able to improve the resolution of aldolase from 4.9Å to 2.8Å. While previous work demonstrated that aberration refinement allows for resolution improvements for data at both 300 keV (Zivanov et al., 2018) and 200 keV (Zivanov et al., 2020; Wu et al.), all datasets analyzed were collected on relatively well-aligned instruments. With high-quality starting data, the initial reconstructions prior to aberration correction achieved ~3Å (unlike this work which was 4.9Å). Moreover, the data collected at 200 keV (Wu et al.; Herzik et al., 2017) used stage position instead of beam-image shift, further minimizing microscope aberrations in the dataset. Although, it should be noted that the observed difference in resolution between our and previous work could have been a result of ice thickness, and grid or sample preparation in addition to beam-image shift corrections.

Using algorithmic improvements in RELION (Zivanov et al., 2018) in combination with Bayesian particle polishing (Zivanov et al., 2019), we were able to improve the resolution of aldolase to 2.8Å (Figure 4 & 5). Analysis of the measured beam tilts indicates that there was axial beam tilt present on the instrument prior to using beam-image shift (Figure 3E). This confirms that the microscope had axial beam tilt prior to data collection, where better microscope alignments could have minimized this issue. That said, beam tilt correction not only fixes off-axis coma, but also other coma from imperfect alignment.

B.4.2 Quicker collection time means longer data processing time

The main motivation to utilize beam-image shift for data collection instead of stage position is the increased data collection throughput. For the dataset collected here, we were able to obtain a 2.4X increase in throughput for beam-image shift when compared with stage position: 73 movies per hour (beam-image shift) vs. 30 movies per hour (stage position). Considering the cost of instrument time, beam-image shift provides 1,752 movies per 24 hour period vs. 720 movies per 24 hour period for stage position. Indeed, the latest generation of detectors that have faster readout stands to triple this throughput for beam-image shift (Alewijnse et al. 2017; Bromberg et al. 2020).

Based on our analysis of aldolase, there is a significant difference between 200 keV vs. 300 keV beam-image shift data collection (for instances where there is not an optical correction on the microscope). At 300 keV, it is possible to use a comparable beam-image shift as that used

in this study but instead obtain a structure ~3Å (Zivanov et al. 2018). For this dataset at 300 keV, beam-image shift provides high-resolution structures prior to aberration correction. Unlike this previous study, our aldolase structure collected using beam-image shift at 200 keV was limited in resolution due to aberrations to 4.9Å. In order to correct for the aberrations, significant effort was required in order to perform optical grouping and analysis, steps that may be beyond beginning to intermediate RELION users.

With these considerations, we advocate beam-image shift at 200 keV for sample screening. This is because we observed high-quality 2D class averages for aldolase despite significant beam tilt, information well-suited for sample screening (i.e. changing buffers, sample concentrations, etc.). However, this study does indicate that even if a user collected data with significant beam tilt from beam-image shift data, software-based aberration correction is possible to <3Å for well-behaved samples like aldolase.

B.4.3 Accessible education and databases improve the field of cryoEM

Even though our cryoEM education platform, cryoEDU, has not been officially launched yet, we anticipate that many who are new to the field will find it useful. Additionally, we expect that it'll continue to bring the community together to discuss best practices in data processing and structure validation. We believe that cryoEDU is within the same vein and shares the same purpose as the NIH-funded national cryoEM centers which help users collect data.

Beyond the increasing accessibility of microscopes and cryoEM educational content, open data has been a longstanding tradition within the structural biology community (Kearns 2020). For structural biology, the Protein Data Bank (PDB) acts as a preservation steward of structural data following OA FAIR principles (Wilkinson et al., 2016). Established in 1971, the PDB is the first open access digital data resource among all biology and medicine resources. The PDB focuses on biocuration, archive management, data exploration, and outreach, which allows for structural biology data to impact basic and applied research in a wide variety of applications (Burley et al., 2018, 2019). As a database that does more than store data and additionally annotates content, the PDB, along with partner databases like the Electron Microscopy DataBase (EMDB) and Electron Microscopy Public Image Archive (EMPIAR), provides a priceless resource to not only the field of structural biology, but to scientific research as a whole.

Expert validation, along with biocuration of the model, structure factors, and atom coordinates are all deposited into the PDB. Validation provides objective assessments of structure quality, and biocurators validate incoming structures using established parameters and software. Biocurators work to verify or correct structure coordinates, confirm chemical consistency of the 3D coordinates and any bound ligands, and in general make sure that the deposited model checks with the experimental data (Burkhardt et al. 2006). There are many challenges along the way coming from information validation. Despite the careful measures taken by researchers in determining and solving structures, PDB biocurators, and validation metrics, errors still exist. Even during a pandemic, where key structures were solved in a hurry, deposited structures generally haven't seen a decline in validation scores during the pandemic, but nevertheless verifying cryoEM maps and models remains a challenge.

Even though model validation is tricky, the structural biology community constantly discusses and updates validation statistics to keep up with the rapid changes to the field in terms of new technologies and software. For example, Dr. Tristan Croll, a researcher at the University of Cambridge, started to look at the then recently released structure of an CoV-2 RNA polymerase (Fig. 1D), he realized that part of the model did not fit into the electron density map. Using a molecular dynamics-based software, ISOLDE (Croll, 2018), he was able to find that a 31-residue stretch model was shifted out of register by nine residues. Doing some more investigative research, he proposed that this shift in amino acid registry in the CoV-2 structure likely derived from a similar issue in the SARS equivalent (pdb 6nur). Since then, the atomic coordinates have been updated under the original ID and have been used for atomic model building (Hillen et al., 2020). Since then, a whole Coronavirus Structural Task Force, spearheaded by the Thorn Lab, has created a whole pipeline for analyzing CoV-2-related structures.

Method-specific validation task forces determine which experimental data and metadata from data collection should be archived and how these data and the derived models should be verified. For example, since 2012, an annual Electron Microscopy Validation Task Force Meeting concludes with recommendations to increase the impact of electron microscopy in biology and medicine (Henderson et al., 2012) and since then modeling and validation challenges have occurred, the most recent one occurring in 2019 (Lawson et al. 2020). Periodic conversations between experts in the structure field regarding validation statistics create a culture that supports best practices in data curation and accessibility. Combining a myriad of knowledge from software

developers, wet lab researchers, and data curators combines perspectives and expertise to drive the field of structural biology in useful directions. Additionally, it seems structural biologists are willing to adapt to community guidelines, even when they are not mandatory. Being aware that mistakes happen in the rush to go from cryoEM models to maps, a call was made to the community to deposit raw data to EMPIAR. By sharing raw data, there could be a global effort to re-process and re-analyze these data to make sure structures are accurate before biologists and bioinformaticians use them, like the recently deposited data of CoV-2 virions (Turoňová et al., 2020).

As these improvements advance the cryoEM/ET field, I hope that cyroEDU will serve as a platform for continued education and conversation with the community. I very much look forward to staying up-to-date and working on this project as we secure funding and publish our content online.

B.5 Materials & Methods

Sample preparation. Pure aldolase isolated from rabbit muscle was purchased as a lyophilized powder (Sigma Aldrich, 89933139) and solubilized in 20 mM HEPES (pH 7.5), 50 mM NaCl at 1.6 mg/ml. Sample as dispensed on freshly plasma cleaned UltrAuFoil R1.2/1.3 300-mesh grids (Electron Microscopy Services) and applied to grid in the chamber of a Vitrobot (Thermo Fisher) at ~95% relative humidity, 4°C. Sample was blotted for 4 seconds with Whatman No. #1 filter paper immediately prior to plunge freezing in liquid ethane cooled by liquid nitrogen.

Cryo-EM data acquisition and image processing. Proper eucentric height of the specimen was determined using Leginon immediately before starting data collection. Parallel illumination of the beam was achieved earlier in the week by first adjusting the defocus to bring the objective aperture into focus in the front focal plane of the diffraction lens in diffraction mode followed by adjustments of beam intensity to minimize the spread of diffraction. Data were acquired using the Leginon automated data-acquisition program (Suloway et al. 2005). Image pre-processing (frame alignment with MotionCor2 (Zheng et al. 2017) and CTF estimation using CTFFIND4 (Rohou and Grigorieff 2015)) were done using the Appion processing environment (Lander et al. 2009) for real-time feedback during data collection. Images were collected on a Talos Arctica

transmission electron microscope (Thermo Fisher) operating at 200 keV with a gun lens of 6, a spot size of 6, 70 μm C2 aperture and 100 μm objective aperture using beam-image shift. Movies were collected using a K2 direct electron detector (Gatan Inc.) operating in counting mode at 45,000x corresponding to a physical pixel size of 0.91 Å/pixel with a 10 sec exposure using 200 ms per frame. Using an exposure rate of 4.204 e/pix/sec, each movie had a total dose of approximately 42 e/Å^2 for the 2,111 movies over a defocus 0.8-2 μm.

Pre-processing. Movies were aligned using RELION-3.0 (Zivanov et al. 2018) (3.0-beta-2) motion correction with 5 patches in both X & Y directions, a B-Factor of 150Å^2 without binning. Following motion correction, CTF estimation was performed with CTFFIND4 (Rohou and Grigorieff 2015) using exhaustive search for a defocus range of 0.5 to 5.0 μm (0.05 μm step size) and an astigmatism search range of 0.5 μm within a resolution range of 6 and 30Å. The combination of a large astigmatism search with exhaustive searches led to many over-estimates of CTF resolution fits for this dataset. Therefore, in order to remove micrographs automatically, we utilized our recently developed *MicAssess* (Li et al., 2020) program to remove all empty and bad micrographs. This removed 685 micrographs, leaving 1,426 micrographs for particle picking. Particles were picked from aligned micrographs using crYOLO (Wagner et al. 2019) general model PhosaurusNet with an anchor size of 98 x 98 pixels.

Single-particle analysis without aberration correction. For 2D classification, 718,578 particles were extracted with an unbinned box size of 300 pixels and subsequently binned to 2.73Å (box size 100 pixels). Particles were then subjected to 2D classification into 100 classes using RELION-3.0.2 (T=2; Iter=25). After selecting particles from the best classes, 275,487 particles underwent 3D classification into 5 classes using RELION-3.0.2 (T=4; Iter=25) and EMD-8743 (Herzik, Wu, and Lander 2017) as a reference model. Following the selection of the best classes, 186,841 particles were centered and re-extracted at 0.91Å/pixel. This stack was used for 3D refinement to obtain a post-processed structure with a resolution of 4.9Å and a B-Factor of -347Å^2.

Aberration correction and particle polishing. Particles were grouped into optics groups based on beam-image shift values obtained from the Leginon database. In order to group particles into discrete optics groups, the entire file of beam-image shift values were divided into 5x5, 10x10, or

20x20 groups. The first two beam tilt estimation steps (CtfRefine #1 & #2, Figure 4) used RELION-3.0 (3.0-beta-2). Subsequent steps (Bayesian polishing and CtfRefine #3) used RELION-3.1 (version 30001). All steps for aberration correction and polishing are described in Figure 4. Aberration correction and polishing did not improve resolution more than the final 2.8Å aldolase structure. We also tested whether using predicted beam tilts from CtfRefine #1 could improve the resolution of a final reconstruction, however, this did not improve dataset resolution (data not shown).

Model building and refinement. The coordinates for rabbit aldolase (PDB: 5vy5) were docked into each map in PHENIX using phenix.dock_in_map (Adams et al. 2012). Structure refinement and model validation were performed using phenix.real_space_refine (Afonine et al. 2018). The same docking and refinement parameters were used for each map. To make figures showing map density, phenix.map_box was used to restrict the map shown to specific stretches of residues. Root mean square deviation (rmsd) values comparing all atoms between structures were calculated using a Least Squares Fit in Coot (Emsley et al. 2010). The PyMOL Molecular Graphics System (Version 2.1, Schrödinger, LLC) was used to render images showing these structures and ChimeraX for rendering the map images (Goddard et al. 2018; Pettersen et al. 2020).

B.6 References

Adams, P. D., P. V. Afonine, G. Bunkóczi, V. B. Chen, I. W. Davis, N. Echols, J. J. Headd, et al. 2012. "PHENIX: A Comprehensive Python-Based System for Macromolecular Structure Solution." *International Tables for Crystallography*. https://doi.org/10.1107/97809553602060000865.

Afonine, Pavel V., Billy K. Poon, Randy J. Read, Oleg V. Sobolev, Thomas C. Terwilliger, Alexandre Urzhumtsev, and Paul D. Adams. 2018. "Real-Space Refinement in PHENIX for Cryo-EM and Crystallography." *Acta Crystallographica. Section D, Structural Biology* 74 (Pt 6): 531–44.

Alewijnse, Bart, Alun W. Ashton, Melissa G. Chambers, Songye Chen, Anchi Cheng, Mark Ebrahim, Edward T. Eng, et al. 2017. "Best Practices for Managing Large CryoEM Facilities." *Journal of Structural Biology* 199 (3): 225–36.

Bromberg, Raquel, Yirui Guo, Dominika Borek, and Zbyszek Otwinowski. 2020. "High-Resolution Cryo-EM Reconstructions in the Presence of Substantial Aberrations." *IUCrJ* 7 (Pt 3): 445–52.

Cheng, Anchi, Edward T. Eng, Lambertus Alink, William J. Rice, Kelsey D. Jordan, Laura Y. Kim, Clinton S. Potter, and Bridget Carragher. 2018. “High Resolution Single Particle Cryo-Electron Microscopy Using Beam-Image Shift.” *Journal of Structural Biology* 204 (2): 270–75.

Emsley, P., B. Lohkamp, W. G. Scott, and K. Cowtan. 2010. “Features and Development of Coot.” *Acta Crystallographica. Section D, Biological Crystallography* 66 (Pt 4): 486–501.

Glaeser, Robert M., Dieter Typke, Peter C. Tiemeijer, James Pulokas, and Anchi Cheng. 2011. “Precise Beam-Tilt Alignment and Collimation Are Required to Minimize the Phase Error Associated with Coma in High-Resolution Cryo-EM.” *Journal of Structural Biology* 174 (1): 1–10.

Goddard, Thomas D., Conrad C. Huang, Elaine C. Meng, Eric F. Pettersen, Gregory S. Couch, John H. Morris, and Thomas E. Ferrin. 2018. “UCSF ChimeraX: Meeting Modern Challenges in Visualization and Analysis.” *Protein Science: A Publication of the Protein Society* 27 (1): 14–25.

Henderson, R., J. M. Baldwin, K. H. Downing, J. Lepault, and F. Zemlin. 1986. “Structure of Purple Membrane from Halobacterium Halobium: Recording, Measurement and Evaluation of Electron Micrographs at 3.5 Å Resolution.” *Ultramicroscopy*. https://doi.org/10.1016/0304-3991(86)90203-2.

Herzik, Mark A., Jr, Mengyu Wu, and Gabriel C. Lander. 2017. “Achieving Better-than-3-Å Resolution by Single-Particle Cryo-EM at 200 keV.” *Nature Methods* 14 (11): 1075–78.

Kearns, Sarah. 2020. “Structure of the Pandemic.” *Structure* 28 (8): 874–78.

Kim, Laura Y., William J. Rice, Edward T. Eng, Mykhailo Kopylov, Anchi Cheng, Ashleigh M. Raczkowski, Kelsey D. Jordan, Daija Bobe, Clinton S. Potter, and Bridget Carragher. 2018. “Benchmarking Cryo-EM Single Particle Analysis Workflow.” *Frontiers in Molecular Biosciences* 5 (June): 50.

Lander, Gabriel C., Scott M. Stagg, Neil R. Voss, Anchi Cheng, Denis Fellmann, James Pulokas, Craig Yoshioka, et al. 2009. “Appion: An Integrated, Database-Driven Pipeline to Facilitate EM Image Processing.” *Journal of Structural Biology*. https://doi.org/10.1016/j.jsb.2009.01.002.

Lawson, C. L., A. Kryshtafovych, P. D. Adams, and P. Afonine. 2020. “Outcomes of the 2019 EMDataResource Model Challenge: Validation of Cryo-EM Models at near-Atomic Resolution.” *BioRxiv*. https://www.biorxiv.org/content/10.1101/2020.06.12.147033v1.abstract.

Li, Yilai, Jennifer N. Cash, John J. G. Tesmer, and Michael A. Cianfrocco. 2020. “High-Throughput Cryo-EM Enabled by User-Free Preprocessing Routines.” *Structure* https://doi.org/10.1101/2019.12.20.885541.

Pettersen, Eric F., Thomas D. Goddard, Conrad C. Huang, Elaine C. Meng, Gregory S. Couch, Tristan I. Croll, John H. Morris, and Thomas E. Ferrin. 2020. "UCSF ChimeraX: Structure Visualization for Researchers, Educators, and Developers." *Protein Science: A Publication of the Protein Society*, September. https://doi.org/10.1002/pro.3943.

Rohou, Alexis, and Nikolaus Grigorieff. 2015. "CTFFIND4: Fast and Accurate Defocus Estimation from Electron Micrographs." *Journal of Structural Biology* 192 (2): 216–21.

Suloway, Christian, James Pulokas, Denis Fellmann, Anchi Cheng, Francisco Guerra, Joel Quispe, Scott Stagg, Clinton S. Potter, and Bridget Carragher. 2005. "Automated Molecular Microscopy: The New Leginon System." *Journal of Structural Biology* 151 (1): 41–60.

Wagner, Thorsten, Felipe Merino, Markus Stabrin, Toshio Moriya, Claudia Antoni, Amir Apelbaum, Philine Hagel, et al. 2019. "SPHIRE-crYOLO Is a Fast and Accurate Fully Automated Particle Picker for Cryo-EM." *Communications Biology* 2 (June): 218.

Wu, Mengyu, Gabriel C. Lander, and Mark A. Herzik. 2020 "Sub-2 Å Resolution Structure Determination Using Single-Particle Cryo-EM at 200 keV." https://doi.org/10.1101/855643.

Zheng, Shawn Q., Eugene Palovcak, Jean-Paul Armache, Kliment A. Verba, Yifan Cheng, and David A. Agard. 2017. "MotionCor2: Anisotropic Correction of Beam-Induced Motion for Improved Cryo-Electron Microscopy." *Nature Methods* 14 (4): 331–32.

Zivanov, Jasenko, Takanori Nakane, Björn O. Forsberg, Dari Kimanius, Wim Jh Hagen, Erik Lindahl, and Sjors Hw Scheres. 2018. "New Tools for Automated High-Resolution Cryo-EM Structure Determination in RELION-3." *eLife* 7 (November). https://doi.org/10.7554/eLife.42166.

Zivanov, Jasenko, Takanori Nakane, and Sjors H. W. Scheres. 2020. "Estimation of High-Order Aberrations and Anisotropic Magnification from Cryo-EM Data Sets in -3.1." *IUCrJ* 7 (Pt 2): 253–67.